

İTÜ



AIAA

Mars Orbiter Constellation for Hemispheric & Atmospheric Characterization (MOCHA)

A proposal for Mars Exploration Surveyors to Enable
Human Exploration

Elif Fatma Avcılar

Halil Karlıer

Ahmet Ali Çetin

Nurbanu Sarıgül

Sarper Gider

Mehmet Umut Türker

Özge Özarslan

Ahmet Fevzi Akargöl

Ali Rıza Eyi

Sıla Ertürk

Faculty Advisor:

Prof. Dr. Alim Rüstem Aslan

Contents

Executive Summary	7
A Introduction	13
B Mission Overview	14
B.1 Mission Requirements	14
B.2 Concept of Operations.....	15
C Concept of Operations	
D Launch Vehicle Overview	16
E Mission and Trajectory Analysis	18
E.1 Trajectory Requirements	18
E.2 Trajectory Trades.....	18
E. 3 Finalized Mission Operations.....	22
F Mars Orbiter Vehicle	26
F.1 Science Instruments	
F.2 Structures.....	35
F.2.1 Load Cases.....	35
F.2.2 Structural Trades.....	36
F.2.3 Orbiter Structure Driving Stress Analysis.....	39
F.2.4 Orbiter Structural Mass Budget.....	39
F.3 Propulsion.....	40
F.3.1 Orbiter Main Propulsion System Trades.....	40
F.3.2 Orbiter RCS/OMS.....	41
F.3.3 Orbiter Propulsion System Sizing and Design.....	42
F.3.3.1 Orbiter Main propulsion system sizing.....	42
F.3.3.2 Orbiter RCS and OMS sizing.....	44

F.4 Communications and Data Handling.....	47
F.4.1 The Data Budget.....	47
F.4.2 The Link Budget.....	49
F.4.2.1 Transmitter Specifications.....	49
F.4.2.2 Path Losses.....	50
F.4.2.3 DSN Services	52
F.4.2.4 Modulation Scheme.....	53
F.4.3 Trade-Offs.....	54
F.4.3.1 Transceiver Selection.....	54
F.4.3.2 Antenna Selection.....	55
F.4.3.3 Command and Data Handling.....	55
F.4.4 Subsystem Overview	56
F.4.4.1 Communications Architecture.....	56
F.4.4.2 Hardware Properties.....	57
F.5 Attitude Determination and Control.....	59
F.6 Power.....	61
F.6.1 Lander Power Configuration.....	62
F.6.2 Orbiter Power Configuration.....	63
F.7 Thermal Control Systems.....	65
F.7.1 Orbiter Thermal Design.....	65
F.7.1.1 Heat Transfer Load Analysis.....	66
F.7.1.2 Trades.....	67
F.7.1.3 Final Configuration.....	69
F.8 Orbiter Vehicle Overview.....	71
G Constellation Cubesats	72
G.1 Daelion.....	72
G.2 Cosmos.....	74

H Risk Analysis and Mitigation	80
I Cost Estimate and Schedule	81
J Compliance Matrix	82



Sarper Gider
AIAA 1811152



Ahmet Ali Cetin
AIAA 1786353



Özge Özarslan
AIAA 1810321



Halil Karlier
AIAA 1810300



Ali Rıza Eyi
AIAA 1810260



Ahmet Fevzi Akargöl
AIAA 1786352



Mehmet Umut Türker
AIAA 1799203



Nurbanu Sarigül
AIAA 1810304



Sela Ertürk
AIAA 1811270



Elif Fatma Avcılar
AIAA 1810133



Alim Rüstem Aslan
Faculty Advisor
AIAA 338946

Symbol	Meaning	Symbol	Meaning
bps	Bits per Second	km ² /s ²	Kilometers ² per Second ²
m ³	Cubic Meters	kN	Kilonewton
dB	Decibel	kPa	Kilopascal
dBm	Decibel Meter	kW	Kilowatt
dBW	Decibel Watt	kW·h	Kilowatt Hour
°	Degree	L	Liter
°C	Degrees Celsius	Mbps	Megabits per Second
Δv	Delta V	MHz	Megahertz
FPS	Frames per Second	MPa	Megapascal
g's	G-Forces	m	Meter
GB	Gigabyte	m/s	Meters per Second
GHz	Gigahertz	m ²	Meters ²
GPa	Gigapascal	μm	Micron
g	Gram	N	Newton
g/cm ³	Grams per Cubic Centimeter	Pa	Pascal
K	Kelvin	s	Second
kbps	Kilobits per Second	I□□	Specific Impulse
kg	Kilogram	V	Volt
kHz	Kilohertz	W	Watts
km	Kilometer	W/kg	Watts per Kilogram
km/s	Kilometers per Second	W/m ²	Watts per Meter ²

Acronym	Expansion
AIAA	American Institute of Aeronautics and Astronautics
ADCS	Attitude Determination and Control System
AIRS	Atmospheric Infrared Sounder
CDR	Critical Design Review
CL	Lift Coefficient
CMC	Chemical Equilibrium Applications (NASA CEA code)
COSMOS	[Constellation] CubeSat for Martian Ionospheric Studies
CPR	Capsule Parachute Recovery
CRISM	Compact Reconnaissance Imaging Spectrometer for Mars
CYGNSS	Cyclone Global Navigation Satellite System
ΔV	Delta-V (change in velocity)
DICE	Dynamic Ionosphere CubeSat Experiment
DPD	Deep-Space Deployer (ISISpace)
DSN	Deep Space Network
EDL	Entry, Descent, and Landing
EMCS	ExoMars Climate Sounder
EPS	Electrical Power System
FPA	Flight Path Angle
FPP	Floating Potential Probe
GCM	General Circulation Model
HR	Scale Height
IMU	Inertial Measurement Unit
IR	Infrared
ITU	Istanbul Technical University
LOLA	Lunar Orbital Laser Altimeter
MARLI	Mars Direct-Detection Wind and Aerosol Lidar
MAJIS	Moons and Jupiter Imaging Spectrometer
MLI	Multi-Layer Insulation

MOCHA	Mars Orbiting Constellation for Hemispheric & Atmospheric Characterization
MOI	Mars Orbit Insertion
MSU	Mars Science Laboratory Unit
OB	On-Board (as in OBC: On-Board Computer)
OBC	On-Board Computer
PDR	Preliminary Design Review
PPM	Parts Per Million
QARMAN	CubeSat Hypersonic Entry Demonstrator (Flight Experiment)
RN	Nose Radius
RPV	Re-entry Vehicle
RWA	Reaction Wheel Assembly
SEU	Single-Event Upset
SNR	Signal-to-Noise Ratio
SOI	Sphere of Influence
S-Band	2–4 GHz Satellite Band
TBR	To Be Resolved
TMI	Trans-Mars Injection
TMACS	Thermal Management and Control System
TPS	Thermal Protection System
TTI	Time-to-Impact
TWTA	Traveling-Wave Tube Amplifier
UHF	Ultra High Frequency
ULM	Ultra-Lightweight Materials
VHF	Very High Frequency
WFE	Worst-Case Flight Envelope



Executive Summary

The 2024–2025 AIAA Student Spacecraft Design Competition tasks participants with developing a scientific mission concept in support of a future human exploration campaign to Mars. The primary objective is to maximize scientific return by characterizing the Martian atmosphere, regional topography, and subsurface volatiles, while achieving at least 75% planetary coverage by December 31, 2033, by the Request for Proposal (RFP) requirements. The mission timeline starts with a Preliminary Design Review (PDR) and Critical Design Review (CDR), leading to system integration and testing in 2028. The spacecraft is scheduled to launch in January 2029, with science operations continuing through December 2033.

A team of ten undergraduate students from Istanbul Technical University developed the MOCHA mission (Mars Orbiting Constellation for Hemispheric & Atmospheric Characterization). MOCHA is a constellation of orbiting platforms focused on understanding the Martian atmosphere, regional topography, and subsurface volatiles through systematic observations of Mars. The MOCHA constellation comprises 9 spacecraft, including two types of CubeSats, four of each type, and one main orbiter, designed to carry out four investigations. Each of the four investigations is strategically mapped to one of the RFP's three primary objectives—atmosphere, topography, and resources—to maximize scientific return. A constellation of spacecraft is preferred over a single orbiter to enable simultaneous, distributed measurements and to achieve aimed temporal and spatial coverage of the Martian atmosphere and surface. Additionally, the inclusion of multiple CubeSats within the constellation provides inherent redundancy by ensuring the continuity of scientific observations and data return even in the event of partial CubeSat loss. This distributed system architecture significantly improves mission fault tolerance, making it well-suited for high-priority pre-human exploration campaigns.

As a first investigation, the mission aims to characterize the vertical structure and variability of the Martian atmosphere by observing diurnal and seasonal climate dynamics from the surface up to 90 km altitude. This objective will be pursued using orbiter-based remote sensing instruments, specifically an infrared sounder and a direct-detection wind and aerosol lidar system. The goal is to improve the predictive performance of the existing atmospheric model Mars-GRAM, thereby enabling more accurate weather forecasting and enhancing onboard Entry, Descent, and Landing (EDL) guidance for future human missions. The inclusion of an infrared sounder—analogous to the Atmospheric Infrared Sounder (AIRS) employed in Earth observation—is essential for retrieving atmospheric temperature, pressure, composition, water vapor profiles, and aerosol distributions with its spectral band within the range of $0.3 \mu\text{m}$ - $45 \mu\text{m}$. Additionally, a direct-detection lidar system is critical for resolving persistent wind measurement gaps in Mars-GRAM. By using this wind information, the atmospheric density and temperature profiles within the 0–30 km altitude range can be modified, as Mars-GRAM begins to diverge from real entry data within this region because of the wrong wind approximations—an adjustment that is vital for



accurate EDL planning in future missions. This investigation will also be pursued by one of the CubeSat platforms, Daelion, which will conduct in-situ measurements during three mission phases. One of the phases spans the 180 km to 120 km altitude range, where the CubeSat will profile the upper atmosphere. In the second phase, Daelion will characterize the aerothermodynamic effects of atmospheric entry at a shallow flight angle, collecting data on temperature, pressure, and atmospheric composition down to the Martian surface.

The second investigation aims to deliver a comprehensive multi-phase analysis of Martian dust storms and their interaction with the ionosphere, combining orbiter-based remote sensing with in-situ atmospheric measurements. The first objective is to vertically profile dust storms from the surface up to 90 km, looking at temperature fluctuations, dust loading, and the escape of atmospheric gases associated with thermal forcing by using an imaging spectrometer, infrared sounder, and a direct-detection wind and aerosol lidar system. The second objective is to use the Cosmos CubeSat to monitor the electric field, electron density, and electron temperature of dust storms in situ during entry, especially between 90 km and the surface. The third objective discusses the evolution and mapping of dust storms, including the observation of storm start, development, transport, and dissipation, as well as the identification of probable activity routes and zones of generation over the Martian surface. The resulting data will complement and expand the capabilities of currently developed Mars atmospheric models, such as Mars-GRAM, and increase their applicability to EDL phase conditions in future human missions.

The third investigation will focus on identifying, mapping, and measuring minerals on the Martian surface that could be valuable for In Situ Resource Utilization (ISRU). An orbital imaging spectrometer will be used for this purpose. This instrument will analyze the mineralogical composition of the Martian surface to assess the distribution and availability of resources critical to human missions, particularly water ice, hydrated minerals, and other volatiles captured in the regolith. The main objectives of this study are to uncover the potential for local resource utilization in future human Mars missions, optimize mission architectures, reduce the amount of payload to be brought from Earth, and increase sustainability for long-term human presence. The data obtained will enrich existing Mars surface models and resource maps, providing vital information for future landing site selection and surface operations.

The fourth investigation focuses on the characterization of Martian surface topography to support future EDL operations. As missions progress toward crewed exploration, ensuring the safety and precision of landing becomes increasingly critical. One of the key factors in enabling safe and reliable landings is the availability of accurate and up-to-date terrain data, particularly regarding surface elevation and slope distribution. To enhance EDL performance, our mission aims to improve Terrain-Relative Navigation (TRN) systems, which rely on comparing onboard imagery with preloaded surface maps. While TRN has been successfully demonstrated in recent missions, its effectiveness is currently limited by outdated or low-resolution topographic data. In line with the goals of our mission, we will incorporate a surface altimetry system and



select a suitable, feasible instrument capable of producing a refined terrain model. To support the identification of potentially hazardous surface features, such as rocky or uneven regions, that may pose risks to lander stability, a laser altimeter will be utilized. By updating the terrain database with improved elevation and slope information, this investigation will contribute directly to safer landing site selection and more reliable EDL operations. The resulting data will also enhance planning for future surface missions by providing a more accurate understanding of local terrain conditions.

The mission begins with the launch from Cape Canaveral. Cape Canaveral is preferred for Mars missions due to its proximity to the Equator, which provides a launch speed advantage, and its extensive infrastructure and experience in handling space missions. The location also offers multiple launch pads, a safe environment with surrounding oceans, and collaboration opportunities with both NASA and private companies like SpaceX. Mission is using a Falcon Heavy rocket on 16 January 2029, requiring a total delta-v of 7800 m/s. Shortly after, the first and second stage separations occur, followed by the entry into Earth orbit, where system checks and solar panel deployment take place. The second stage then performs the Trans-Mars Injection (TMI) burn with a delta-v of 4200 m/s, setting the spacecraft on its interplanetary trajectory toward Mars. Solar panel deployment and system checks occur after this burn is complete and the spacecraft has separated from the upper stage, ensuring no risk of damage during high-thrust maneuvers. Following this, the spacecraft enters the outbound transit phase, a cruise period lasting 258 days. Upon arrival at Mars's circular science orbit on 30 December 2029, the spacecraft performed a series of orbital maneuvers totaling 2244 m/s in delta-v. Of this, 772 m/s is allocated for the Mars Orbit Insertion (MOI) maneuver to achieve Mars capture and start a highly elliptical orbit. Next, an Apoareion reduction maneuver with a delta-v of 44.7 m/s is performed. Following this, 153.5 m/s is dedicated to an inclination change maneuver, while the remaining 1319 m/s is allocated for the circularization burn to place the orbiter into its final science orbit: a 77-degree inclined circular orbit at 300 km altitude.

From this perspective, the orbiter requires a substantial delta-v budget, totaling 2244 m/s, to perform critical mission maneuvers including capture, inclination change, orbital maintenance, and deorbiting. These maneuvers demand high-thrust capability to be executed impulsively, ensuring that the actual change in velocity corresponds closely to the calculated delta-v values without significant loss due to orbital perturbations. To meet these requirements, hypergolic propellants have been selected due to their extensive Mars mission heritage, high specific impulse, and high density, which together optimize performance and tank volume. For the primary propulsion system, the S400-15 400N Bipropellant Apogee Engine of ArianeGroup has been chosen for its proven capability and low structural mass. This engine enables completion of all major maneuvers within a cumulative burn time, consistent with the operational timelines of prior Mars orbiter capture events. After orbital insertion, initiating the next phase of the mission: the start of scientific operations by the orbiter. This phase is planned to span two years within the mission timeline.



The orbiter ADCS is designed to meet the diverse and demanding pointing needs of its scientific instruments. They range from stable nadir-pointing for instruments like lidar for surface mapping flights, full limb viewing coverage for infrared sounder via continuous slewing, fixed 30° off-nadir pointing for fixed 30° off-nadir pointing for direct-detection wind and atmospheric measurement by aerosol lidar, and agile and high-accuracy slews for imaging spectrometer's targeted spectroscopy. To maintain these pointing conditions throughout the mission, the system must withstand a range of disturbance torques, including external torques like gravity gradient and solar radiation pressure, as well as transient internal torques like propellant slosh. Since Mars lacks a global magnetic field, magnetorquers were excluded from the design, and attitude corrections must be accomplished through active control. From known mass properties of the spacecraft and geometry, inertia values were calculated for each of the axes, allowing the estimation of torques required to maintain pointing errors within mission parameters. These torque requirements drove actuator size and led to the use of reaction wheels. With the reaction wheel's demonstrated performance, high momentum capacity, and good torque resolution, these wheels are well adapted to control nominal and moderate disturbances. For handling momentum accumulation and spasmodic high-torque events outside the wheels' ability, a redundant thruster-based momentum dumping system fills out the design, offering attitude stability and long-term operation robustness.

After two years of scientific data collection by the orbiter, the mission enters the next phase: deployment of the CubeSats. Two different types of CubeSats—Daelion and Cosmos—will be deployed using the spring deployers, enabling the formation of the constellation. Although pursuing different objectives, both CubeSats will follow the same trajectory, transitioning from a 300 km to a 180 km circular orbit using their propulsion systems to perform in-situ measurements in low Mars orbit. To execute this transfer, they are designed to perform a Hohmann transfer with several 28 burns in ~2 days, requiring a total delta-v of ~56.64 m/s. For this maneuver, they are equipped with the MPS-130 green propellant propulsion system, which has a total propellant capacity of 500 grams, consuming approximately ~280 grams of propellant. Once established in their science orbit at 180 km, they begin measurements and continue collecting data as they undergo orbital decay down to an altitude of 120 km at about ~230 days. At their final mission phase, Daelion and Cosmos CubeSats capture data during Mars atmospheric entry to study aerothermodynamic effects. Both use front-mounted P50 cork ablative shields for thermal protection, thinner than Earth-based designs due to Mars' thinner atmosphere. Daelion's sensors are embedded within this shield inside ceramic-lined cavities, enabling precise measurements during controlled ablative erosion, while Cosmos deploys sensors on the rear, protected by advanced thermal materials like Nextel ceramic fabric, Kapton films, and Pyrogel aerogel.

Throughout the mission, the CubeSats encounter Mars orbital conditions including solar irradiance ranging approximately from 550 to 650 W/m², planetary infrared emission between about 100 and 200 W/m², deep space cooling



during eclipse periods with temperatures dropping to roughly 150–160 K, and ionizing radiation levels varying between 200 and 300 μ Gy/day. Below 120 km altitude, convective heating becomes significant, with stagnation point temperatures ranging from approximately 1100°C to 1600°C and heat fluxes spanning from about 40 to 80 W/cm² during atmospheric entry. To withstand these, both employ passive thermal controls: aerogel insulation, 15-layer MLI blankets, and aluminum-titanium radiation shielding. Cosmos uses aerogel collars for rear sensors, while Daelion integrates sensors in the ablative shield with localized insulation. This combined strategy ensures subsystem survival and mission success within CubeSat constraints.

Reliable onboard data handling is a critical enabler for the MOCHA mission. Both the orbiter and the CubeSats must be capable of processing collected science data, managing temporary storage during communication blackouts, and ensuring seamless relay to Earth. For the CubeSats, this means having sufficient onboard capacity to retain mission data across multiple orbits and potential delays in downlink. For the orbiter, it involves handling not only its sensor payloads but also aggregating incoming data from all CubeSats, storing it securely, and transmitting it effectively through the Deep Space Network. Given the interplanetary nature of the mission and extended operation around Mars, system robustness is essential. The onboard computing architecture must offer resilience against radiation-induced faults and support fault-tolerant data handling to maintain data integrity throughout the mission timeline. These capabilities ensure the continuity of scientific return and the overall success of MOCHA's multi-platform architecture.

The communication system is based on a relay structure. Cosmos and Daelion send data to the orbiter, which then forwards all collected data, including its own, to the Deep Space Network (DSN). Cosmos and Daelion use Ultra High Frequency (UHF) and S-band for communication with the Orbiter. UHF is used to receive commands and transmit low-rate data during the orbital drift phase. During the entry phase, UHF can also send data to other Mars orbiters, acting as relay stations. This serves as a backup if a communication window with the primary orbiter is missed. S-band is also used during orbit and entry phases, serving as the main method during entry to reduce blackout duration. During the most data-intensive phases, Cosmos and Daelion transmit data at rates of 390 kbps and 245 kbps, respectively.. The system is designed to function reliably even under harsh Martian atmospheric conditions. All collected data is transmitted to Earth via X-band at a maximum rate of 18 Mbps. The system is expected to generate approximately 17 GB of data daily, and the communication link budget analysis confirms that the system is capable of reliably transmitting this data volume, ensuring robust data collection and relay capabilities.

Reliable power generation, storage, and distribution are critical enablers for MOCHA's multi-platform mission architecture. To ensure uninterrupted operation during eclipse periods and support high-power events such as propulsion and communications, a detailed power budget was constructed for each CubeSat and the orbiter by segmenting the mission into



distinct phases. Solar array sizing was performed using worst-case Mars orbital lighting conditions during the orbiting phases, ensuring sustained energy generation under degraded incidence angles. Instantaneous power draws were extracted from maneuver phases, where propulsion and high-rate communications occur. Battery capacity was determined based on eclipse durations, accounting for system loads and energy autonomy during sunless intervals. For CubeSats, the EDL phase provided the peak power demand profile, driving the final battery sizing to support simultaneous operation of critical subsystems under harsh thermal and entry conditions.

The primary constraints for the MOCHA mission include strict mass and volume limits per spacecraft, especially for the CubeSats, and adherence to the AIAA RFP requirement of achieving 75% planetary coverage by December 2033. Additionally, the mission is constrained by an overall budget limit of \$1 billion, covering development, launch, and operations for all 9 spacecraft. Communication continuity and atmospheric entry survivability for CubeSats also present key technical challenges. To mitigate these risks, MOCHA employs a distributed satellite architecture, enabling redundant science coverage across multiple spacecraft. The orbiter acts as a centralized node for data relay, constellation coordination, and time synchronization, reducing complexity at the CubeSat level.



A. Introduction

In recent decades, Mars has stood as a central focus of scientific investigation and planetary exploration. Its geological and atmospheric similarities to Earth, coupled with its closeness, make it a prime candidate for advancing our understanding of planetary evolution and preparing for human exploration. Despite numerous successful missions—including MRO, MAVEN, and ExoMars TGO—critical knowledge gaps remain in the characterization of the Martian atmosphere, surface, and subsurface resources. These gaps directly impact the reliability of mission-critical operations such as Entry, Descent, and Landing (EDL), which remain among the most challenging phases of Mars exploration due to the planet's thin atmosphere, variable dust loading, unpredictable winds, and rough terrain. Addressing these deficiencies is the foundation of the 2024–2025 AIAA Undergraduate Student Spacecraft Design Competition, which tasks participants with designing a scientific mission in support of future human exploration of Mars. The mission must provide a comprehensive characterization of the Martian atmosphere, surface topography, and potential resources, achieving at least 75% global coverage by the end of 2033. To fulfill this objective, the Istanbul Technical University undergraduate team developed the Mars Orbiting Constellation for Hemispheric & Atmospheric Characterization (MOCHA) mission.

MOCHA is a distributed architecture of one main orbiter and eight 6U CubeSats—designed to deliver integrated atmospheric, topographical, and resource investigations through four primary science objectives. This constellation approach ensures high spatial and temporal resolution and provides redundancy through parallel data acquisition across platforms. The mission strategy leverages both remote sensing and in-situ measurements, enabling direct observation of key phenomena such as vertical wind velocity, diurnal aerosol variation, terrain elevation, and surface mineralogy.

MOCHA's novel integration of previously flight-ready yet unflown payloads, such as the ExoMars Climate Sounder (EMCS) and the MARLI direct-detection wind lidar, allows the mission to achieve unprecedented coverage and atmospheric insight. This is supplemented by in-situ entry data from the CubeSats—Cosmos and Daelion—which will measure electrostatic activity, plasma properties, aerodynamic heating, and density gradients from 180 km down to the Martian surface. In addition to advancing scientific understanding, MOCHA directly supports the design of safer and more efficient human missions to Mars. By refining current atmospheric models like Mars-GRAM, improving Terrain Relative Navigation (TRN) with high-fidelity elevation data, and identifying key in-situ resources, the mission enhances the feasibility of future crewed surface campaigns. In this way, MOCHA aligns with both the scientific and strategic goals of NASA and international partners working toward long-duration human presence on the Red Planet.



B. Mission Overview

B.1. Mission Requirements

The following table summarizes the top-level mission requirements derived from the AIAA Request for Proposal (RFP) and aligned with the MOCHA mission architecture. These high-level objectives are supported by detailed subsystem-level requirements, presented in later sections.

Table 1. Overall Mission Requirements

Req. ID	Requirement Description
REQ-MOCHA-RFP-01	The launch vehicle shall depart Earth by January 2029 and inject the spacecraft into a Mars transfer trajectory.
REQ-MOCHA-RFP-02	The system shall be capable of inserting into Mars orbit and executing all orbital maneuvers required for science.
REQ-MOCHA-RFP-03	Eight 6U CubeSats shall be deployed from the orbiter and conduct targeted atmospheric entry and in-situ measurements.
REQ-MOCHA-RFP-04	The orbiter shall be equipped to perform nadir, limb, and off-nadir pointing with angular accuracy finer than 0.1°.
REQ-MOCHA-RFP-05	The orbital platform shall maintain functional operations for at least two Martian years, ensuring mission longevity.
REQ-MOCHA-RFP-06	CubeSats must sustain atmospheric entry conditions down to altitudes below 120 km and collect data during entry.
REQ-MOCHA-RFP-07	Communications architecture shall ensure sustained Mars-to-Earth downlink at ≥ 244 kbps during nominal operations.
REQ-MOCHA-RFP-08	The total mission cost will remain under \$1 billion (FY24), covering development, hardware, and operations.



B.2. Concept of Operations

The second stage performs the Trans-Mars Injection burn after launch and following first and second stage separation, which leaves the spacecraft in a heliocentric transfer orbit on its way to Mars. The interplanetary cruise to Mars lasts 258.83 days. Early in this phase, essential system checkouts are completed, and solar panels are installed to maintain spacecraft health. A mid-course correction maneuver, requiring approximately 50 m/s of ΔV , is performed during the cruise to ensure optimal targeting for Mars arrival. Upon reaching Mars on October 1, 2029, the spacecraft executed a Mars Orbit Insertion (MOI) burn of 772.1 m/s. This critical maneuver places it into an initial elliptical orbit of $300 \times 180,000$ km with an inclination of 30.35° . Subsequently, to prepare for the primary inclination adjustment, a 44.73 m/s burn transfers the spacecraft into a $300 \times 90,000$ km orbit. This intermediate orbit is selected to facilitate a more time-efficient inclination change towards the science-required 77° . Achieving this target inclination, which involves a 46.65° shift from the initial 30.35° , is accomplished over approximately 57 days. This is done through a series of small burns, totaling 153.5 m/s in ΔV , applied perpendicular to the orbiter's velocity vector at apoareion, where the spacecraft's orbital speed is at its minimum. Following the successful inclination adjustment, the spacecraft performs a series of 20 periareion burns over a period of 35 days. These maneuvers are designed to circularize the orbit to a 300 km altitude and require an additional ~ 1319.0 m/s of ΔV . The target orbit is expected to be reached by March 28, 2030. All major propulsive burns throughout these mission phases are conducted using the onboard S400-15 bipropellant propulsion system.

The orbiter must operate in a 300 km circular orbit at 77° inclination to enable global coverage, full diurnal sampling, and support for nadir, limb, and off-nadir observations. This orbit is essential for satisfying the pointing and coverage needs of all remote sensing instruments.

Following orbit stabilization, the spacecraft has entered its science phase, which is scheduled to continue uninterrupted until December 31, 2033. Scientific operations continue for more than two Martian years. During this phase, the orbiter conducts its remote sensing campaign using four primary instruments: an imaging spectrometer for mineral mapping, an infrared sounder for atmospheric profiling, a lidar for global wind and aerosol observations, and a laser altimeter for mapping surface topography. These instruments operate in coordinated pointing modes—such as nadir, limb, and off-nadir—a capability provided by the spacecraft's 3-axis stabilized attitude control system, which ensures high pointing accuracy and agility. The orbiter's terminal science orbit is maintained by regular station-keeping maneuvers and offers constant diurnal sampling and complete latitudinal coverage. Throughout the mission, MOCHA maximizes data return via distributed in-situ sensing combined with high-resolution remote sensing—facilitating atmospheric modeling, entry system design, and surface resource mapping in support of future human Mars exploration.



In this context, a total of eight CubeSats—four Daelion and four Cosmos models—will be deployed sequentially from the orbiter. The CubeSats will be released in pairs, each pair consisting of one of each of the two different types (Daelion and Cosmos), at 156-day intervals. This phased deployment strategy is designed to maximize the probability of success for the CubeSats in this challenging and unpredictable environment.

Following approximately two years of scientific measurements by the orbiter, the deployment of the CubeSats will commence while the orbiter continues its science operations. This initial orbiter measurement period aims to provide potential calibrations for the CubeSats, which are designed with an approximate 80% fuel margin, and to offer some trajectory flexibility if needed.

All mission phases of each CubeSat will be carefully monitored. Particularly against unforeseen consequences that may be encountered during the CubeSats' atmospheric entry and (if it occurs) impact, necessary calibrations will be performed on the main orbiter, and if required, deemed necessary adjustments, including potential modifications to the CubeSats' orbits, can be implemented. This approach aims to mitigate risks to the CubeSats and ensure that a maximum of four CubeSats are communicating with the orbiter concurrently; the communication architecture has also been specifically designed for this operational strategy.

Following their deployment, each CubeSat will first complete system checkouts in a 300 km altitude orbit, then perform a Hohmann transfer maneuver to a 180 km altitude circular orbit using its onboard propulsion system. From this stage, the satellites will begin their in-situ atmospheric measurements by descending to a 120 km altitude through orbital decay. During this process, critically important data will be collected for modeling the atmospheric entry environment, studying ionospheric activity, and determining surface atmospheric conditions. When the 120 km altitude is reached, the entry phase will begin for the CubeSats; as planned, CubeSats with the necessary thermal protection will enter the atmosphere and continue their in-situ measurements. These satellites are designed to transmit the data they collect to the main orbiter and to other existing satellites operating in Mars orbit. The orbiter also functions as a communication relay. Science data are received on UHF and S-band by the orbiter during CubeSat orbital phases and entry through the atmosphere. The orbiter buffers and relays all science data, including its own, back to Earth through X-band using the Deep Space Network (DSN) with up to 50 Mbps downlink capacity. The communications system is extremely reliable in blackout-prone entry conditions and accommodates an estimated 41 GB per day data volume. The general mission lifetimes and operational phases of the CubeSats are summarized in the table below.

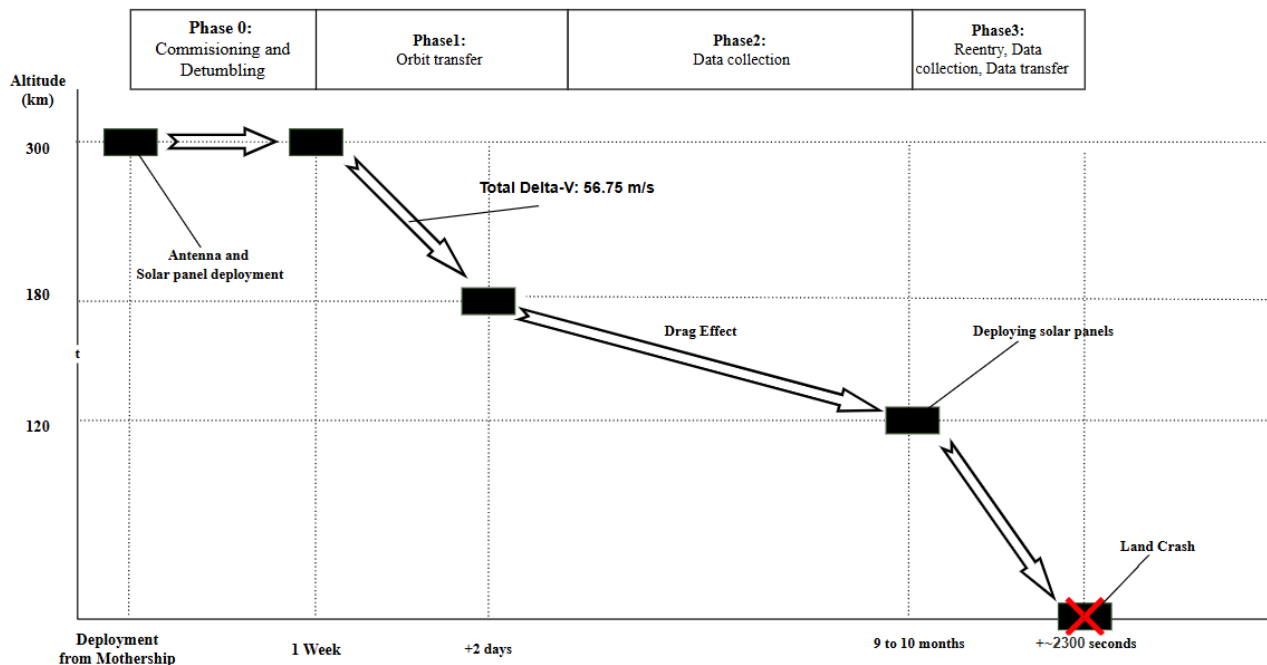
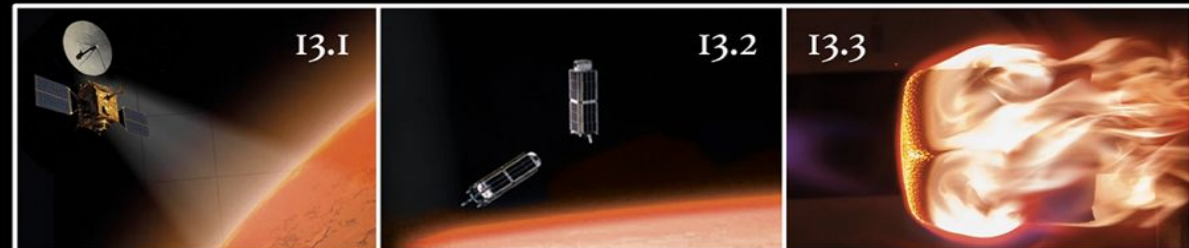


Figure 3. CubeSat Mission Profile: Altitude Transition and Entry Phase

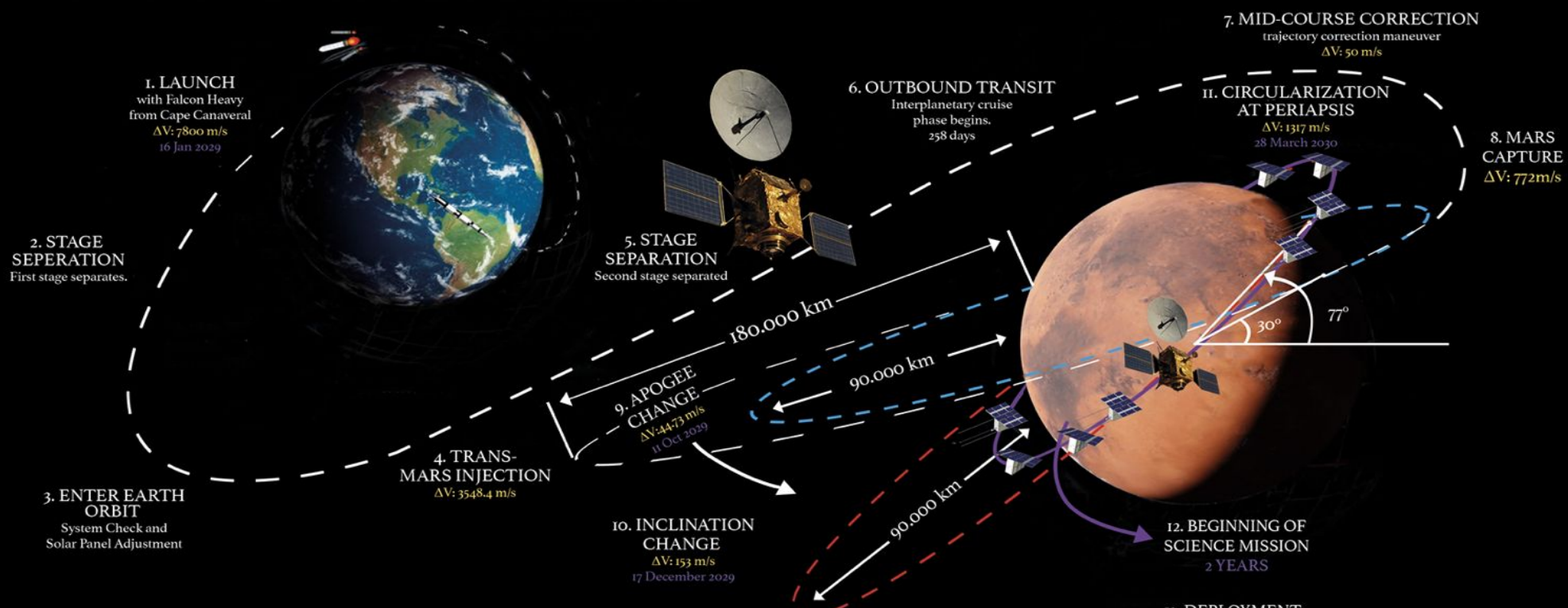
For our constellation mission to Mars, the CubeSats accompanying our spacecraft will be housed and managed by the advanced ISISpace Deep Space Deployer (DSD). This specialized deployment system, an evolution of the flight-proven DuoPack, is specifically engineered to withstand the challenges and unique demands of interplanetary travel. The DSD will ensure the CubeSats' structural integrity during launch and the long transit to Mars and facilitate critical pre-deployment health checks and potential software updates via an umbilical connection even after launch. Its key feature, a low-velocity, staged deployment mechanism, will allow for the precise and gentle release of our CubeSats into their designated Martian orbits, crucial for maintaining the trajectory of both the orbiter and the CubeSats, and enabling the CubeSats to activate their own systems post-separation safely.



C. Concept of Operations of MO



Atmospheric Entry



MOCHA MISSION

Concept of
Operation





D. Launch Vehicle Overview & Trades

The selection of a suitable launch vehicle is a critical step in ensuring the success of the MOCHA Mars orbiter mission. This trade-off analysis evaluates candidate launch vehicles based on payload capacity, reliability, and cost, aligned with the mission's specific requirements: a spacecraft mass of approximately 4600 kilograms, a delta-V insertion capability of 2,794 m/s. The vehicles considered include SpaceX Falcon Heavy, Ariane 6 (64), and China's Long March 5. These vehicles represent a spectrum of heritage, payload capability, and cost structures suitable for interplanetary Mars missions. This trade study is shown in Table 2.

Table 2. Trade Study for Launch Vehicle [32,33,34,35]

Parameter	Weight	SpaceX Falcon Heavy	Ariane 6 (64)	Long March 5
Payload to Mars Orbit (kg)	0.35	16,800	7,400	6,000
Reliability (%) (flights)	0.25	98 (11/11)	92 (2/2)	92.86 (13/14)
Fairing Usable Volume m ³	0.25	145	170	135
Cost (Estimate)	0.15	130	125	70
Overall Score	0.705	0.277	0.225	0.208

The Falcon Heavy was chosen to be the most suitable launch vehicle based on the criteria and weighting used in this analysis. However, the selection process also considers other factors not quantified here, such as launch site availability, integration complexity, political considerations, and specific interface requirements for the MOCHA spacecraft. Changes may be made in the launch vehicle selection, taking into account technological developments until launch time.



E. Mission and Trajectory Analysis

The MOCHA mission follows a carefully optimized interplanetary transfer and Mars orbit insertion strategy to minimize delta-v requirements while achieving its stringent science orbit parameters. After a 258.83-day cruise phase and a minor mid-course correction, the spacecraft arrived at Mars on October 1, 2029. Upon arrival, a 772 m/s Mars Orbit Insertion (MOI) burn captures the vehicle into an initial $300 \times 180,000$ km elliptical orbit inclined at 30.35° . Following this, a 44.7 m/s maneuver is performed to lower the apoareion, transitioning the spacecraft into a $300 \times 90,000$ km transfer orbit. This transfer orbit is selected for its high Apoareion that enables an efficient inclination change maneuver of 153 m/s at Apoareion, in terms of both fuel and time. Subsequently, a 1319 m/s circularization burn lowers the periareion to 300 km, finalizing the target science orbit with 77° inclination—critical for enabling global coverage and repeated local time observations. The total delta-v of 2244 m/s required for orbit insertion and shaping is delivered using a high-thrust bipropellant system based on the S400-15 engine, chosen for its reliability and heritage. The orbiter remains in this low Mars orbit for the duration of the mission, supporting both its own remote sensing payloads and acting as a relay for the deployed CubeSats. These trajectory decisions ensure the platform achieves the spatial and temporal observation cadence needed to meet the mission's atmospheric and topographical science goals.

E.1. Trajectory Requirements

Orbit selection plays a critical role in achieving scientific objectives. The $H=300$ km altitude and $i=77^\circ$ orbital inclination selected for the MOCHA mission enable the laser altimeter and infrared sounder instruments to achieve at least 75% coverage of the Martian surface, while the infrared sounder serves to conduct detailed investigations of the daily atmospheric dynamics, a capability distinct from previous Mars missions. The chosen $i=77^\circ$ orbital inclination, due to the orbital plane precession resulting from Mars's rotation (approximately 12.56 minutes per Martian sol), allows the spacecraft to make observations across all local Martian times within approximately 57.1 sols. This capability is of great importance for understanding short-term and diurnal variations in the atmosphere. Furthermore, the $i=77^\circ$ inclination value allows an instrument like laser altimeter, capable of detailed topographic mapping, to cover the latitude range of $[-77^\circ, +77^\circ]$. This aligns with the objectives of identifying potential landing sites for future human missions and expanding the boundaries of topographic investigation beyond what has been accomplished by previous (e.g., Mars Polar Lander at 76° South latitude) or planned missions. Thus, the MOCHA mission aims to collect more comprehensive data about Mars by making measurements within the $[-77^\circ, +77^\circ]$ latitude range.



CubeSats are initially deployed into the same 300 km orbit, where they perform commissioning before conducting a Hohmann transfer to a 180 km circular orbit. There, they begin in-situ measurements and continue collecting data during orbital decay down to 120 km. These altitude and inclination requirements are driven by the scientific need for coordinated multi-altitude atmospheric profiling and surface interaction studies.

E.2. Trajectory Trades

Among the considerations for choosing the trajectory was the upcoming Earth–Mars launch window in early 2029. With planetary alignment constraints, optimal interplanetary transfer to Mars opportunities occur approximately every 26 months. The launch date of January 16, 2029, selected here coincidentally falls within an opportunity window, enabling a low-energy Hohmann transfer with a departure delta-v of 3548.4 m/s. This timing supports a 258.83-day cruise phase and permits Mars arrival on October 1, 2029, in accordance with mission science obligations and orbital dynamics constraints. By setting this launch date, the mission has a well-timed schedule of preparation, which allows for approximately four years of concurrent development, testing, and verification—from the accomplishment of Preliminary Design Review (PDR) and Critical Design Review (CDR) milestones in 2025. This phase of preparation is critical to the completion of hardware fabrication, flight software integration, environmental testing, and launch campaign dress rehearsals. The fixed launch opportunity also puts aggressive timelines on all of the subsystems with the requirement for close schedule coordination and risk reduction to be flight-ready by late 2028.

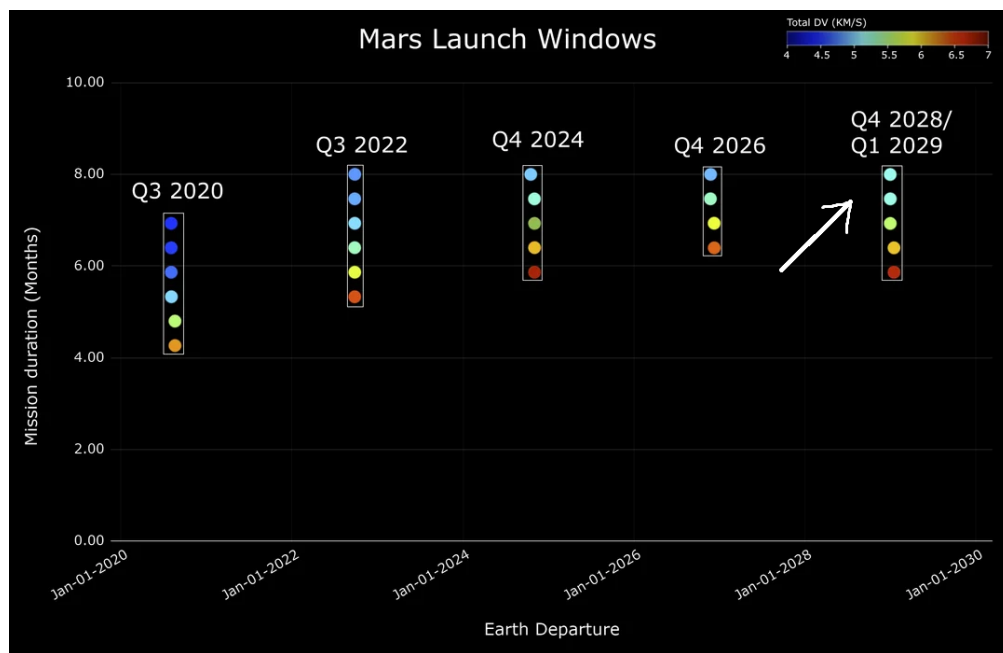


Figure 4. Earth-to-Mars Launch Windows



To achieve the mission's final science orbit of 300 km altitude and 77° inclination, a detailed trade study was conducted to minimize total ΔV while meeting pointing and coverage requirements. Direct insertion into a circular 300 km orbit was quickly ruled out due to the high ΔV cost (6206 m/s) for the required inclination change. Instead, several elliptical capture orbits were analyzed to exploit Apoareion-located inclination changes, where orbital velocity—and thus ΔV cost—is minimized. The trade table below summarizes five trajectory options evaluated based on apoareion altitude, Mars Orbit Insertion (MOI) cost, inclination change, and circularization requirements. Among them, the $300 \times 90,000$ km orbit proved optimal, minimizing total ΔV to 2244 m/s.

Table 3. Delta-V Breakdown for Various Mars Orbit Maneuvers at Different Apoareion Altitudes

Maneuver Type	Apoareion Altitude (km)	Mars Orbital Insertion (m/s)	Inclination Change (m/s)	Circularization (m/s)	Total (m/s)
Elliptic	30,000	925.7	415.0	1165.0	2506.0
Elliptic	60,000	814.0	223.9	1277.0	2315.0
Elliptic	90,000	772.1	153.4	1319.0	2244.0
Circular	300	3407.0	2799.0	0.0	6206.0
SOI	600,000	772.1	2175.0	1317.0	4266.0

Based on this table, an orbit with an apoareion of 90,000 km was decided upon with the most optimal delta-v value. The calculations revealed that the spacecraft needed to make corrections to settle into the circular orbit for a total of 35 days and 1318.81 m/s of delta-v, along with changing inclination in this orbit. During this time, the spacecraft will pass periareion 20 times.

This mission design is an optimal balance of science requirement fulfillment, operational versatility, and propellant utilization. Orbit selection and sequencing were resolved through delta-v minimization and instrument coverage constraints. The result is a technically valid and very resilient trajectory plan that provides full-spectrum atmospheric, mineralogical, and topographical science on orbiter and CubeSat missions. The table containing detailed mission phases, dates, delta-v summary and durations is given below.



Table 4. Chronological Overview of Mission Events and Delta-V Requirements

Mission Phase	Date	ΔV (m/s)	Duration
Launch & TMI Burn	Jan 16, 2029	3548.4	30 min
Mid-Course Correction	Cruise Day 130	50.0	1 day
Mars Orbit Insertion (MOI)	Oct 1, 2029	772.1	30 min
Apoareion Change	Oct 2, 2029	44.73	10 days
Inclination Change	Oct 13, 2029	153.5	56 days
Periareion Burn Sequence	Dec 9, 2029	1319.0	35 days
Final Science Orbit For Orbiter	Jan 13, 2030	Maintenance	1449 days (Until 31 Dec 2033)
8 CubeSat Deployment (Deploying two units every 120 days)	Jan 1, 2032	-	480 days (Deployment of CubeSats with 100 days difference)
CubeSat Orbital Decay & Entry	December 10, 2033 (Calculated crash date for the last 2 CubeSats)	-	-
Extended Mission	Jan 1, 2034	-	-



F. Mars Orbiter Vehicle

F.1 Science Objectives

Over the years, numerous missions, including Mars Reconnaissance Orbiter (MRO), ExoMars Orbiter, and MAVEN, have advanced our understanding of the Martian atmosphere and climate. Despite these advancements, significant gaps remain in our understanding of Mars' atmosphere, especially for the investigation of the during critical phases such as Entry, Descent, and Landing (EDL). As a part of the first and second atmospheric contributions, we aim to characterize the complex Martian environment, where the thin atmosphere, unpredictable winds, variable dust content, and rough terrain make Entry, Descent, and Landing (EDL) particularly challenging [4]. For example, density profiles remain incompletely mapped, yet they are vital for designing efficient EDL systems. It is also notable that more than two-thirds of Mars missions have ended in failure, highlighting the harsh and unpredictable nature of the Red Planet. While the Mars Weather Research and Forecasting (MarsWRF) model offers some predictive insights into EDL profiles, it tends to underestimate temperature and overestimate density at altitudes above 15 km—altitudes where wind behavior critically affects spacecraft navigation. This discrepancy is largely due to inaccuracies in dust loading representations, which significantly influence heating rates and other variables essential for EDL planning [4].

We also aim to investigate diurnal variations because current observations—limited by local time coverage—show significant fluctuations in the amount and vertical distribution of dust, ice aerosols, and water vapor, yet do not fully characterize these variations over the entire diurnal cycle. This leaves considerable gaps in our understanding. Winds play a crucial role in this cycle by transporting water vapor, dust, and ice aerosols, mixing all gaseous constituents throughout the atmosphere.

Therefore, as part of the MOCHA team's first atmospheric contribution, this mission seeks to advance our knowledge of wind and dust dynamics, the CO₂ cycle, aerosol distribution, and temperature and pressure gradients in order to address these gaps. These factors are essential for refining models of Martian atmospheric behavior, particularly during Entry, Descent, and Landing (EDL) operations. Additionally, the mission will gather detailed surface roughness and elevation data to improve landing site predictions for future Mars exploration.

Martian atmospheric dust and its associated dust storms play a critical role in shaping the planet's climate and atmospheric evolution. Our mission aims to investigate key processes such as the vertical transport of dust, its interactions with atmospheric gases, storm life cycles, and the global distribution of airborne particles. Previous missions—including MRO, MAVEN, ExoMars TGO, and Mars Express—have made significant progress in characterizing the distribution of



atmospheric dust, thermal structure, water vapor variability, and the general behavior of dust storms. For instance, studies using the Mars Climate Sounder (MCS) have demonstrated how dust storms heat the atmosphere and enhance the vertical transport of water vapor.[42] However, none of these missions has provided high-resolution, simultaneous measurements of vertical dust profiles alongside gas composition. Moreover, to date, no mission has performed in situ measurements of the electrostatic properties of Martian dust; data regarding plasma behavior and electric field strength are still based solely on theoretical models.[54] While global dust maps have been produced, they generally lack the temporal resolution needed for near-real-time storm monitoring.[42] Although a wide range of measurements has been conducted on Martian dust and dust storms, the MOCHA mission will be the first to acquire simultaneous, multi-parameter observations of most dust and dust storm characteristics. This capability will enable significant improvements in the atmospheric models used for mission planning. Specifically, the mission enhances our ability to resolve the thermodynamic and dynamic structure of the dust-laden atmosphere at both global and local scales. Notably, atmospheric layers below 30 km remain poorly represented in current dust and dust storm models; our mission directly addresses this shortcoming through a combination of orbital remote sensing and in situ measurements acquired during the Entry, Descent, and Landing (EDL) phase.[56] Building on past datasets, the MOCHA mission is uniquely designed to deliver the first high-resolution, simultaneous observations of dust profiles, atmospheric composition, and electrostatic behavior—addressing critical gaps in our understanding of the Martian atmosphere and offering transformative insights into both its steady-state and storm-driven dynamics.

As part of the MOCHA team’s fourth, surface-focused contribution, we aim to enhance Terrain-Relative Navigation (TRN)[7] systems to support safer Entry, Descent, and Landing (EDL) for future crewed and robotic Mars missions. TRN allows real-time position and motion estimation by comparing onboard sensor data to preloaded surface maps. While HiRISE imagery provides high-resolution visual references, existing MOLA-based elevation models lack sufficient spatial fidelity. To address this, we propose updating Mars Digital Elevation Models (DEMs) using a modified LOLA-type altimeter.

Our goal is to improve the mapping of surface slope, roughness, and elevation to better identify hazardous landing zones—especially regions likely to contain rocks around 50 cm in diameter, which pose tipping and mechanical failure risks during landing. While individual rocks of this size cannot be directly resolved using a 10-meter spot-size altimeter, energy return variations can still reveal rough terrain statistically associated with such features. This enables the classification of unsafe landing areas and enhances the robustness of TRN-guided EDL operations.

For In-Situ Resource Utilization (ISRU) on Mars, the primary targets are the presence of water (either as ice or in bound form within hydrated minerals), suitable metal oxides for oxygen extraction, and other raw materials necessary for construction



materials and fuel production. Currently, it has been determined through orbital and surface missions that significant quantities of water ice exist at high latitudes on Mars and in some mid-latitude craters, and that hydrated minerals such as phyllosilicates (clays) and sulfates (like gypsum) are widespread; atmospheric carbon dioxide is also known as an abundant and accessible source of oxygen and carbon. However, for the feasibility and efficiency of ISRU, particularly for crewed missions, a more detailed, high-resolution mapping of the distribution, depth, purity, and volume of near-surface ice, especially at more accessible low and mid-latitudes, as well as the type, water content, processability, and precise locations of hydrated minerals, is required. Furthermore, there is a need for detailed investigation of the geotechnical and mineralogical properties of high-grade metal oxide (primarily hematite and other iron oxides) deposits suitable for oxygen and metal production, and construction materials like regolith and basalt. The absorption features of water ices are (especially around 1.25 μm , 1.5 μm , 2.0 μm , and near 3 μm), the absorption bands of hydrated minerals (phyllosilicates, sulfates, hydrated silicas) arising from metal-OH bonds and water molecules (particularly in the 1.4 μm , 1.9 μm , and 2.2-2.5 μm range), the distinct spectral signatures of iron oxides in the visible and near-infrared (VISNIR, ~0.5-1.0 μm) region, and the absorption features of mafic minerals such as pyroxenes and olivine around 1 μm and 2 μm . Some weaker spectral features of other important minerals like carbonates may also be detectable (especially in the 2.3-2.5 μm and 3-4 μm ranges)[36]. Thereby, spectral measurements in these ranges can provide the necessary information for both the detection and basic characterization of minerals critical for ISRU, helping us to understand the potential of Mars's resources better.

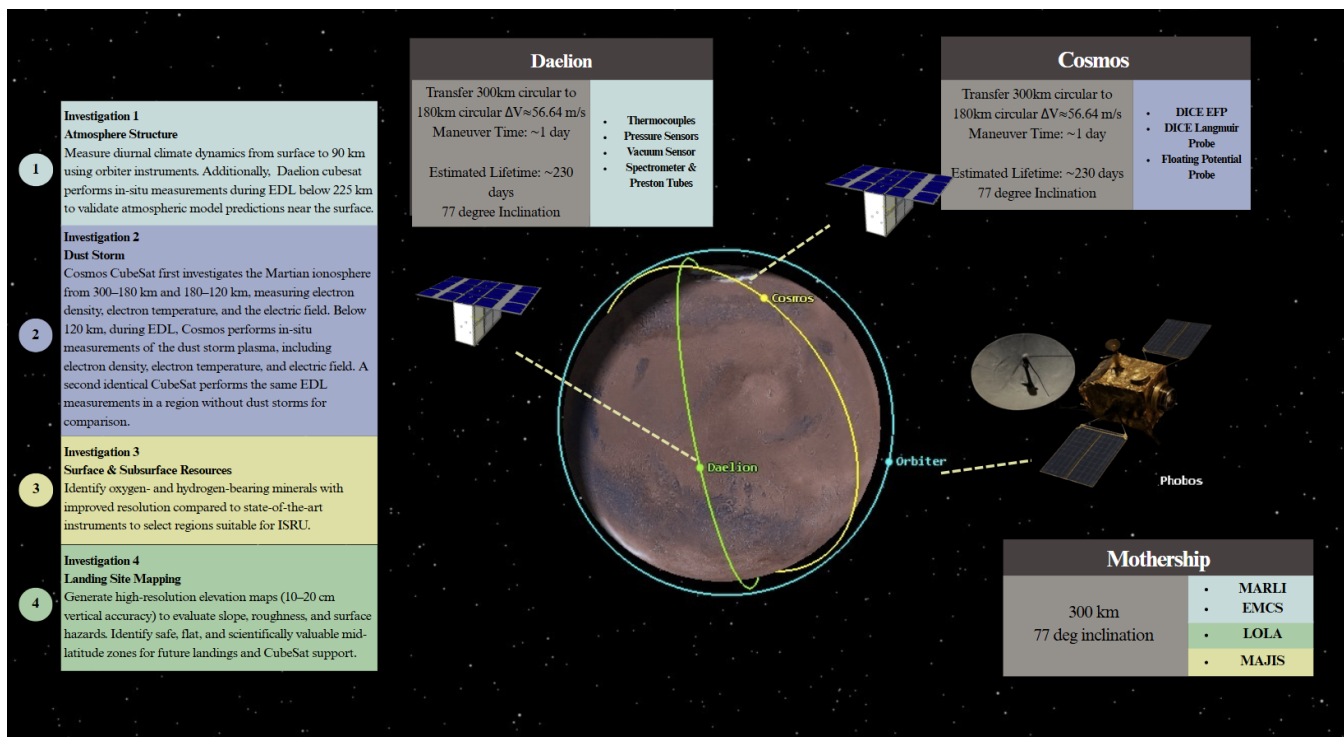


Figure 5. MOCHA Mission Concept



F.2 Science Instruments

As part of the MOCHA mission orbiter, four scientific instruments serve as primary investigators aligned with the three main objectives of the Request for Proposal (RFP). These instruments are the ExoMars Climate Sounder (EMCS), Mars Direct-Detection Wind and Aerosol Lidar (MARLI), Moons and Jupiter Imaging Spectrometer (MAJIS), and the Lunar Orbital Laser Altimeter (LOLA).

The ExoMars Climate Sounder (EMCS) was originally developed for the ExoMars mission to provide high-resolution vertical profiles of temperature, dust, water and CO₂ ices, and water vapor in the Martian atmosphere but not selected for the intended ExoMars mission. It remains a uniquely capable instrument that has never flown, making it ideally suited for the MOCHA mission. With its broad spectral range of 0.3 to 45 μm with 9 channels, EMCS is capable of detecting key atmospheric constituents such as CO₂, N₂, O₂, CO, H₂O (water vapor), CH₄, and O₃ [24]. Additionally, this spectral range enables the retrieval of temperature, pressure, and CO₂ ice extinction profiles from the surface up to 90 km in altitude—an essential capability for improving current atmospheric Mars models, which is known to diverge significantly from in-situ data below 30 km, particularly in terms of density and temperature [4]. EMCS features a 90-degree cross-track scanning capability, enabling it to obtain measurements at multiple local times over the same geographic location. This allows the instrument to detect diurnal atmospheric changes by revisiting the same region at least twice per sol, typically with a ±3 hour time offset. Currently, the Mars Climate Sounder (MCS) is the only operational sounder on Mars, presenting a limitation in atmospheric observation and model validation. EMCS adopts a similar approach to that of AIRS on Earth, aiming to enhance atmospheric visualization and improve weather prediction models—critical for the design of future onboard entry systems. With its planned 77° inclination and 57-day orbital cycle, EMCS is capable of providing daily, global, pole-to-pole coverage across all local times within the 57 -day orbital cycle. The resulting profiles are intended to be assimilated into Mars General Circulation Models (MGCMs), producing global interpolated fields of key parameters such as temperature, aerosol content, water vapor, and winds. These measurements will support characterization of diurnal, day-to-day, and seasonal variations in atmospheric structure and composition, providing essential insights into global temperature, pressure, aerosol and water vapor distribution, as well as aerosol latitudinal transport processes.

As part of our surface analysis contribution, the MOCHA mission team proposes the utilization of a modified version of the Lunar Orbiter Laser Altimeter (LOLA) to support and enhance Terrain-Relative Navigation (TRN) systems. Originally flown on NASA's Lunar Reconnaissance Orbiter, LOLA was instrumental in generating the lunar global Digital Elevation Model (DEM) and serves as a heritage-proven design for orbital laser altimetry.



The baseline LOLA instrument has a mass of 14.6 kg and operates nominally at 26.8 W, with an initial power draw of up to 29.9 W during activation. It features a five-beam diamond configuration with a beam divergence of 0.1 milliradians and a beam separation angle of 0.5 milliradians. Operating at a pulse rate of 28 Hz [3], LOLA was originally designed for a 50 km lunar orbit. When scaled to our mission's 300 km Martian orbit, these parameters result in a ~30 m spot size, ~150 m center-to-center beam spacing, and approximately 120 m along-track displacement due to orbital motion.

However, to effectively support EDL hazard detection and TRN performance, a spot size on the order of 10 meters is required. Achieving this resolution at 300 km altitude necessitates a reduction in beam divergence to approximately 0.03 milliradians. Although such divergence levels were beyond the capabilities of LOLA's original era, advancements in laser optics have made 0.03 milliradian divergence a common standard as of 2025. Instruments like GALA and ATLAS have already demonstrated this level of optical performance in interplanetary and Earth-observing missions.

Building upon these technological developments, the MOCHA team proposes the integration of an improved LOLA configuration featuring upgraded optics with a 0.03 milliradian beam divergence. This modification will substantially reduce spot size, enhancing the resolution and fidelity of the generated topographic dataset.

Although simulation-based modeling was initially considered to estimate surface coverage and resolution over a four-year mission lifetime, the relatively narrow scanning swath of the LOLA instrument limited the validity of synthetic simulation results. Consequently, the team conducted a comparative analysis using historical performance data from LOLA and MOLA. Based on this empirical assessment, it was determined that over the planned four-year mission duration, the enhanced LOLA will enable a reduction in the global DEM resolution used by TRN systems from the legacy 435 meters to approximately 100 meters. This resolution improvement represents a significant advancement in safe landing site selection and autonomous navigation accuracy for future Mars missions.

As a complementary instrument to the ExoMars Climate Sounder (EMCS), MARLI is designed to provide direct wind velocity measurements and detailed aerosol profiling in the Martian atmosphere. Its operation is based on emitting laser pulses at a wavelength of approximately $1.57 \mu\text{m}$ into the atmosphere [25]. When these pulses encounter atmospheric particles such as dust, aerosols, and gas molecules, a portion of the light is scattered back toward the instrument. By detecting the Doppler shift—the slight change in frequency of the returned laser light caused by the motion of scattering particles relative to the spacecraft—MARLI can determine the line-of-sight wind velocity with high vertical resolution. Additionally, the intensity of the backscattered signal provides critical information about aerosol density and distribution, enabling detailed profiling of dust and aerosol layers. This capability is essential because, to date, no Mars instrument has directly measured



wind; existing instruments infer wind indirectly through temperature and pressure measurements. This lack of direct wind data is believed to contribute significantly to divergences in current atmospheric models, making MARLI's measurements vital for improving the accuracy of Martian atmospheric simulations. Accurate wind velocity data provide sensitive input and validation for Global Circulation Models (GCMs) and are crucial for the safety and precision of spacecraft Entry, Descent, and Landing (EDL) operations. Furthermore, accurate Mars weather and wind predictions are critical because dust storms and high winds affect surface mission operations by impacting visibility and solar power availability.

Finally, MARLI is designed to operate from a spacecraft in a circular polar orbit at a nominal altitude of 400 km, at 300 km in the science orbit of the MOCHA mission, its resolution significantly increases. Also, it will be pointed 30° off-nadir in the cross-track direction, allowing for retrieval of cross-track wind profiles [37]. With this cross-track capability and the spacecraft's 77° inclination orbit, MARLI can measure winds up to approximately 82° latitude, a region where dust storms become less frequent after this latitude.

Together with EMCS, MARLI aims to significantly improve current atmospheric models, enhancing our understanding of Mars' atmospheric dynamics and supporting safer, more precise mission planning.

The Moons And Jupiter Imaging Spectrometer (MAJIS) was developed for the ESA JUICE (JUpiter ICy Moons Explorer) mission to conduct detailed studies of the Jupiter system, particularly its moons Ganymede, Callisto and Europa. Operating in a wide spectral range from 0.5 μm to 5.55 μm, MAJIS covers this range with two separate channels: VISNIR (Visible and Near Infrared, 0.5-2.35 μm) and IR (Infrared, 2.25-5.56 μm).[38] This spectral range is critical for detecting key components of the Martian atmosphere and surface. It will be used to detect and map a variety of minerals on the Martian surface, such as olivine, pyroxenes, sulphates, hydrated minerals, chlorides and carbonates, as well as water ice and CO ice. Atmospherically, the presence of major aerosols such as water vapor, carbon dioxide, ice and dust, and potential trace gases such as methane and ozone will be investigated. In addition, this broad spectral capability allows for surface temperatures (especially from the long-wavelength IR channel) and atmospheric temperature, pressure and aerosol/ice distribution profiles (especially from nadir and limb observations) to be obtained – a key capability to improve current Mars atmospheric models, which are known to differ significantly from in situ data below 30 km, particularly in terms of density and temperature. Collaborative operation of two sensors with different capabilities, MAJIS and the ExoMars Climate Sounder (EMCS), in Mars orbit could provide complementary and highly valuable information for understanding both the Martian atmosphere and surface. How different surface compositions and thermal properties affect local atmospheric conditions (temperature, humidity, aerosol load) can be directly investigated. The sublimation and condensation cycles of surface ice (especially seasonal CO and H₂O ice), their



exchange with the atmosphere, and their effects on local weather patterns can be better understood. A link can be established between the source regions of dust storms (surface type determined by MAJIS) and the vertical structure and propagation of these storms (monitored by EMCS).

To satisfy the RFP-mandated requirement of achieving at least 75% surface coverage of Mars by the end of the mission, a coordinated sensing strategy utilizing four onboard instruments—LOLA, MARLI, EMCS, and MAJIS—was implemented. Among these, EMCS and MAJIS employ wide-swath observational methods, enabling rapid surface mapping across large areas. In contrast, LOLA and MARLI operate as spot-sampling altimeters and are therefore unable to provide full global coverage instantaneously. However, their cumulative scanning approach enables the resolution of terrain data to improve steadily over time, with expected spot densities becoming sufficient for landing site analysis and hazard mapping by the end of the four-year mission. To estimate the resolution and the coverage our team used the previous missions of our instruments and the similar instruments used in Mars missions such as MOLA. A mid-fidelity simulation was conducted to assess the global coverage potential of EMCS and MAJIS, assuming an operational inclination of 77°, realistic duty cycles, and swath widths of approximately 18 km and 21 km, respectively. The results indicate that 75% planetary coverage can be achieved in approximately 34 sols, although this figure remains sensitive to calibration drift, operational gaps, and attitude uncertainties. While this estimate may be conservative, it confirms that the sensing system architecture, when operated over the full mission duration, is well-positioned to fulfill the mission's topographic and terrain characterization objectives.

F.2. Structures

The 4 requirements taken into account in the structural design process are as listed below.

Table 5. Structure Requirements

Req. ID	Requirement Description
REQ-MOCHA-STR-01	The structure shall withstand all quasi-static, dynamic (sinusoidal and random vibration), acoustic and shock loads encountered during launch and ascent on the Falcon Heavy launch vehicle, as specified in the Falcon Heavy User Manual [Ref: Falcon Heavy User Manual, Final Version], with specified safety factors.
REQ-MOCHA-STR-02	The orbiter's static and dynamic envelope will fit into the Falcon Heavy payload fairing (assumed to be a 5.2 m diameter extended fairing), including all openings required for launch and separation events.
REQ-MOCHA-STR-03	The structure will maintain its integrity and performance when exposed to the Mars orbital environment, including Thermal cycling: Temperatures ranging from approximately -120°C to +120°C Radiation: Total ionizing dose and single event effects relevant to the Martian environment.



REQ-MOCHA-STR-04

The total mass of the structural subsystem, including all primary and secondary structures, mechanisms and fasteners, should not exceed 20% of the dry mass.

The structural design of the mission was based on maximum load carrying capacity with minimum weight of the prime mover and fasteners used in the mission. The bus was designed with skin and several stringers. Since the main load-carrying elements are stringers, structural analysis is based on the stringers.

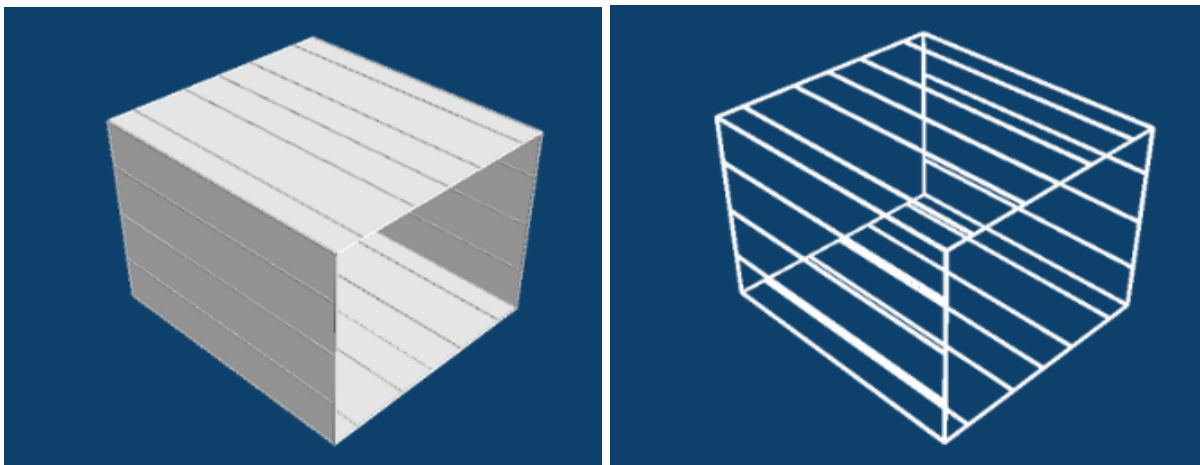


Figure 6. Structural Design of the Orbiter Bus

The choice of materials was chosen to be suitable for space and the Martian environment. Al-7075 aluminum alloy was used in the Orbiter bus due to its low density, high strength, and ability to resist radiation and corrosion. The mass of the orbiter bus is 300 kg. Ti6Al4 alloy was used for fuel, oxidizer and pressure tanks due to its high strength. The material properties is like below:

Table 6. The Material Properties of Al-7075 Aluminum and Ti6Al4 Alloy

Property	Al 7075-T6	Ti6Al-4V (Grade 5)
Density	2810 kg/m ³	4430 kg/m ³
Elastic Modulus	71.7 GPa	113.8 GPa
Poisson's Ratio	0.33	0.34
Ultimate Strength	572 MPa	900 MPa



F.2.1 Load Cases and Structural Analysis

The skeletal structure of our orbiter bus consisting of stringers was subjected to structural analysis in Abaqus Cae software.

This analysis was made by taking into account the loads created by Falcon Heavy during launch.

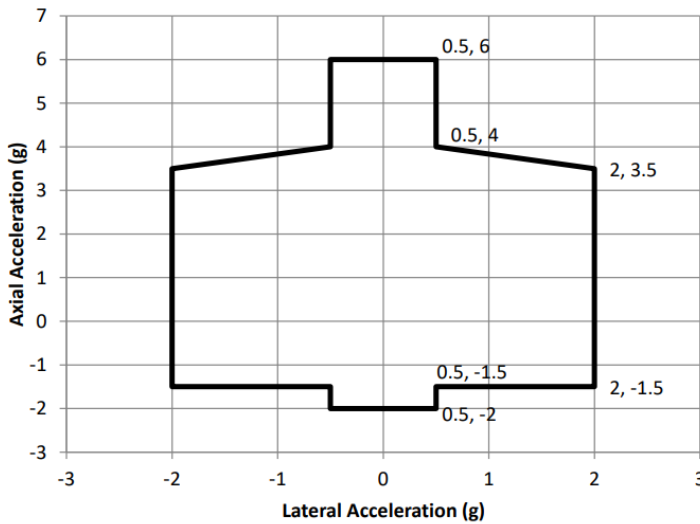


Figure 7. Falcon 9 and Falcon Heavy flight limit load factors for “standard” mass payloads (over 4,000 Ib)

Two analyses were performed on the structure. One for axial 6 g, lateral 0.5 g case and the other for axial 3.5 g, lateral 2 g case. These casings were chosen because they form the two ends of the launch payloads. The structure that can withstand these two loads can maintain its strength within the entire load envelope.

For case 1, the analysis results are as in the following two images:

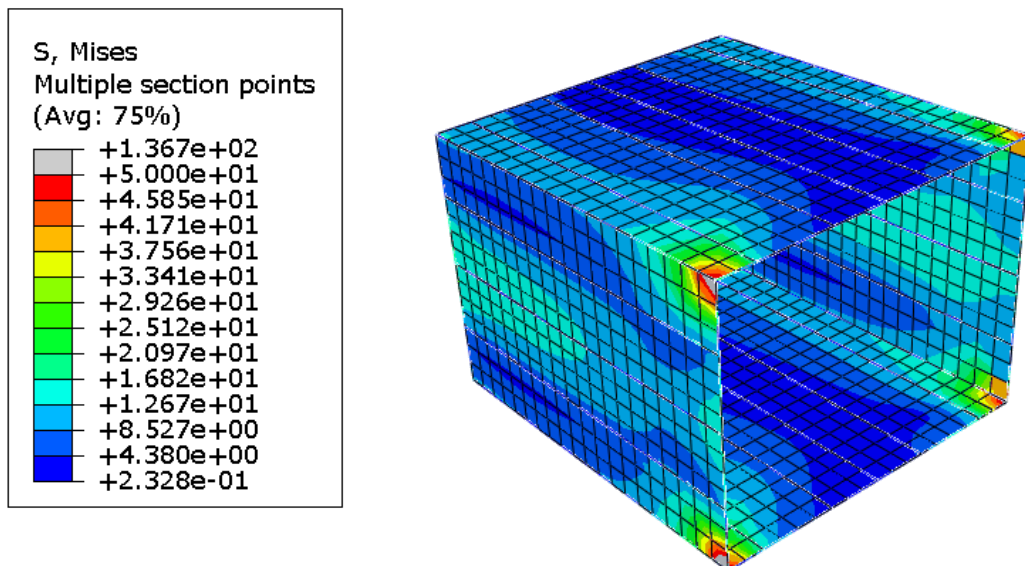


Figure 8. Von Mises stress distribution of the structural enclosure under axial 6 g and lateral 0.5 g loading

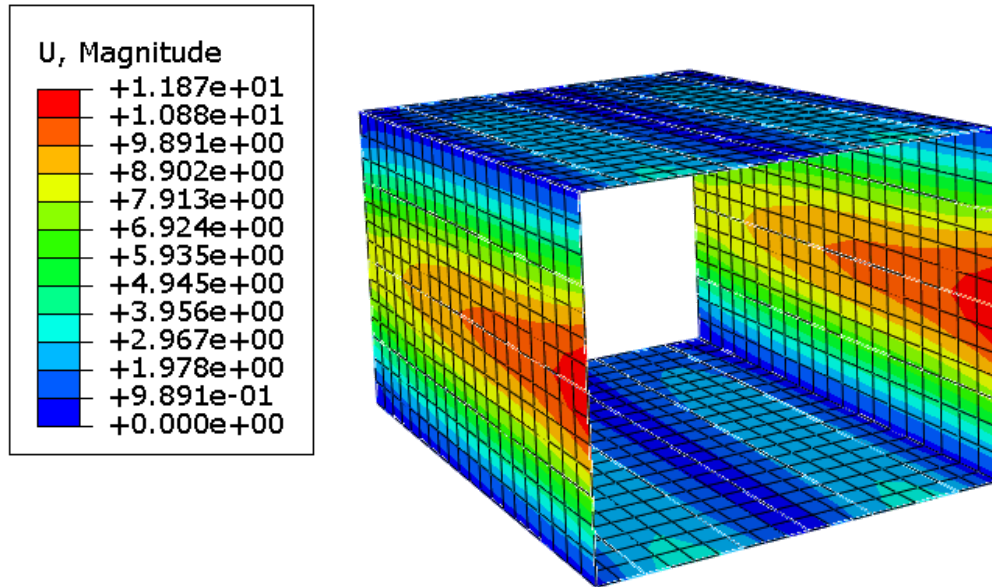


Figure 9. Displacement magnitude of the structural enclosure under axial 6 g and lateral 0.5 g loading

The max stress value was found to be 137.6MPa. In this case, where the yield strength of the material is 572MPa, the Factor of Safety comes as 3.7, which is more than enough margin to prove the strength of the structure.

For case 2, the analysis results are as in the following two images:

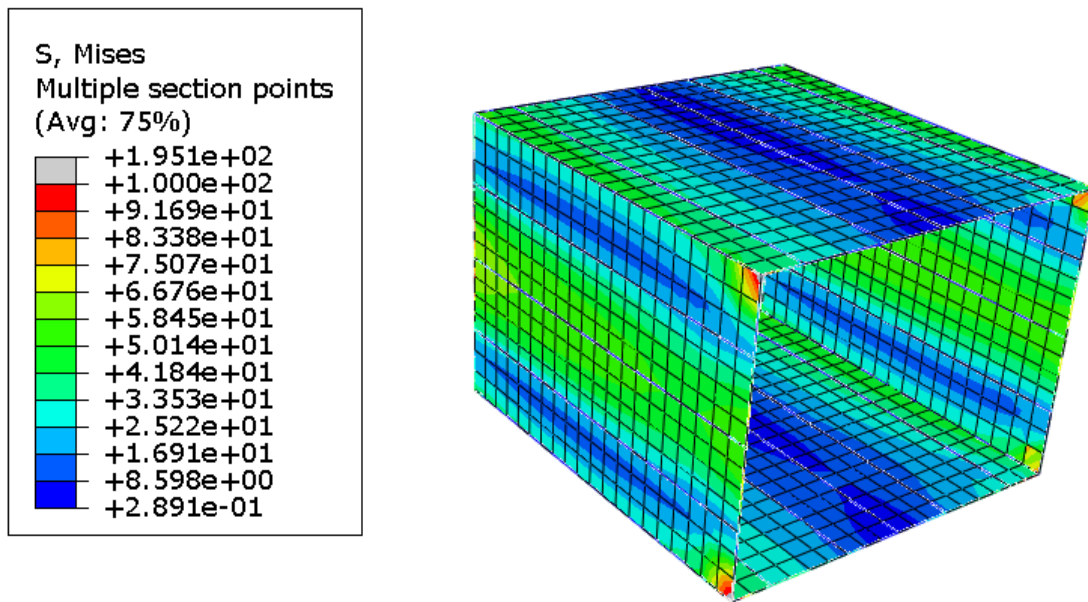


Figure 10. Von Mises stress distribution of the structural enclosure under axial 3.5 g and lateral 2 g loading

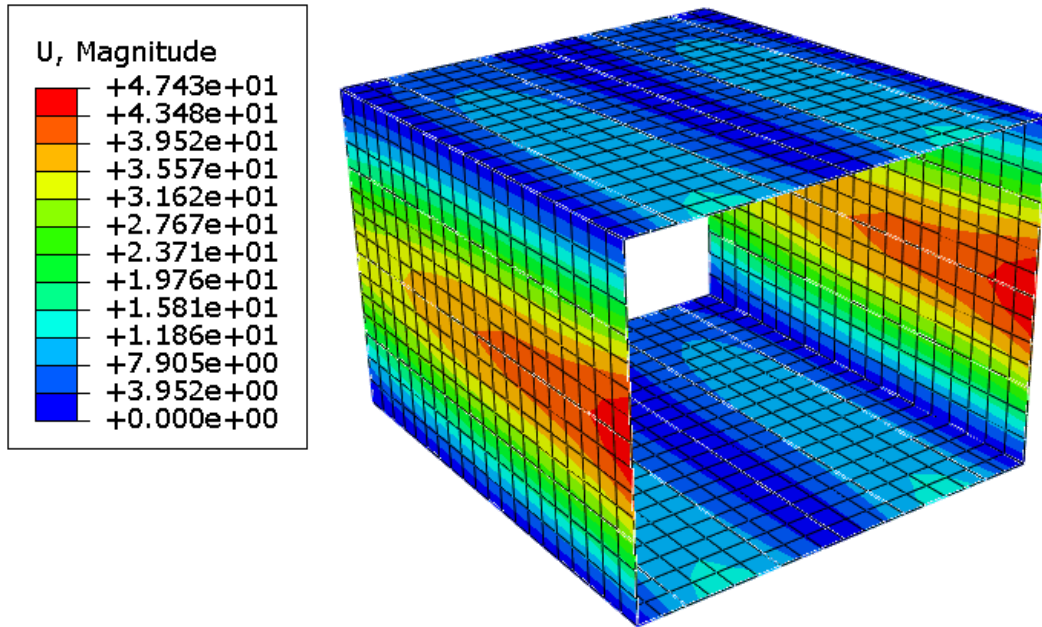


Figure 11. Displacement magnitude of the structural enclosure under axial 3.5 g and lateral 2 g loading

The max stress value was found to be 195.1MPa. In this case, where the yield strength of the material is 572MPa, the Factor of Safety comes as 2.58, which is more than enough margin to prove the strength of the structure.

F.2.2. Orbiter Design

The exterior and interior images of the orbiter are as follows. Orbiter bus dimensions are 2700mm x 2100mm x 3000mm.

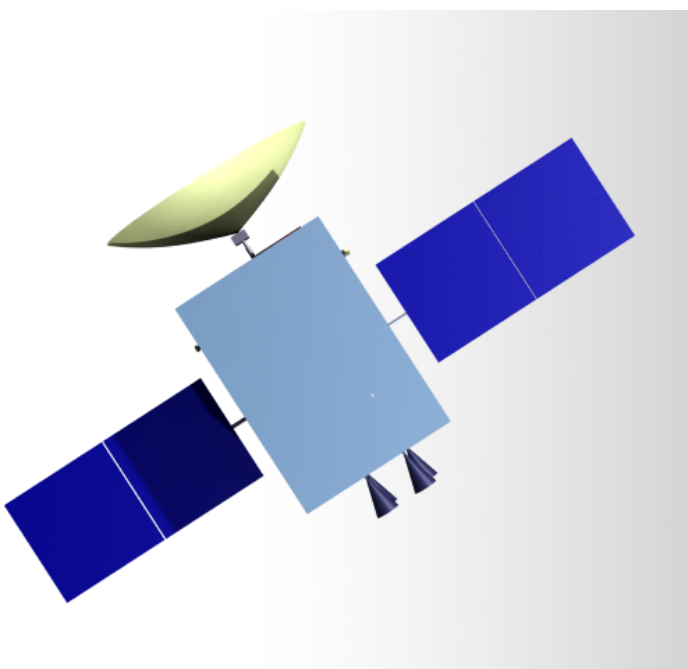


Figure 12. Exterior view of the orbiter bus

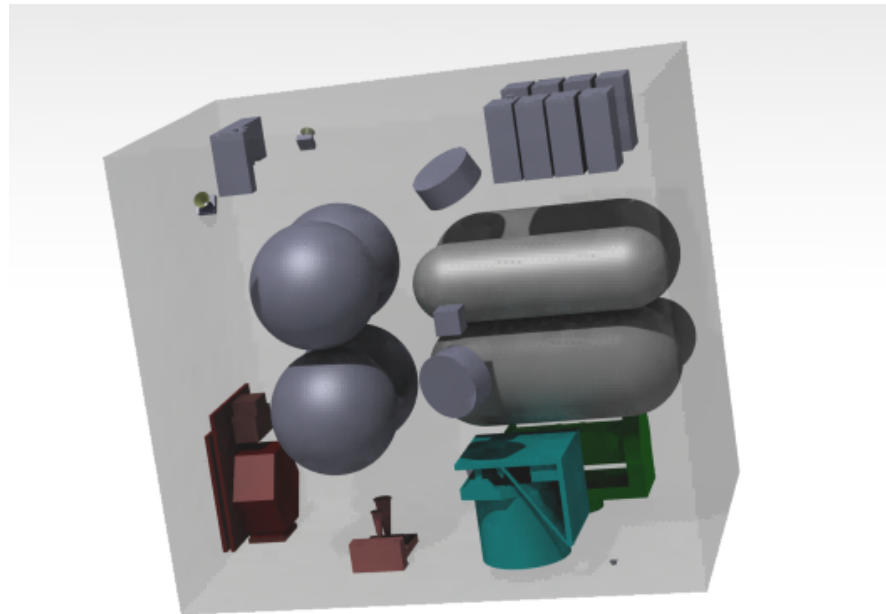


Figure 13. Interior view of the orbiter bus



Figure 14. Interior view of payload fairing stage of Falcon Heavy with MOCHA



F.3. Propulsion

In the context of the mothership orbiter's onboard propulsion system, the Mars Capture maneuver and the subsequent inclination change maneuver with Apoareion Change—both necessary to achieve the designated science orbit—are planned to occur. The launch from Earth and the insertion into the Martian parking orbit will be managed by the selected launch vehicle. Consequently, the requirements of the main propulsion system are summarized in Table 7 below.

Table 7. Propulsion Requirements

Req. ID	Requirement Description
REQ-MOCHA-PROP-01	Upon Mars arrival, the orbiter must be able to achieve orbital capture via a Mars Capture maneuver, requiring a delta-v of 772 m/s.
REQ-MOCHA-PROP-02	To satisfy the science requirement of achieving greater than 75% planetary coverage, the orbiter must be placed into a high-inclination orbit of 77 degrees. Therefore, a dedicated inclination change maneuver and circularization at periareion are required with a delta-v 153.5 m/s and 1319 m/s delta-v following the Mars Capture to transition from the initial capture orbit to the designated science orbit.
REQ-MOCHA-PROP-03	To maintain long-term coverage requirements through nodal precession, the propulsion system should support station-keeping and minor trajectory corrections requiring a delta-v of 10 m/s per year.
REQ-MOCHA-PROP-04	The propulsion system is required to be restartable to support multiple critical maneuvers throughout the mission, including Mars Capture, inclination change, orbit maintenance, and potential end-of-life disposal burns.

F.3.1 Method of Propulsion

In accordance with the listed mission requirements of the mothership orbiter, a chemical propulsion system has been selected for this part of the system due to its high reliability, high thrust capability, and reduced maneuver execution time factors that are critical given the mission's strict time constraints.

F.3.2 Fuel

Among the monopropellant and bipropellant options—including hypergolic and cryogenic propellant combinations hypergolic bipropellants have been identified as the most suitable choice for the MOCHA mission based on multiple performance and operational criteria. First of all, although monopropellant systems offer benefits such as simplicity and reduced system complexity, they are limited by lower specific impulse and thrust performance. In contrast, hypergolic bipropellants provide significantly higher specific impulse and overall efficiency, both of which are essential for meeting the



delta-v requirements specified under MOCHA PROP-001 and MOCHA PROP-002. Furthermore, hypergolic propellants are preferred over cryogenic options due to the impracticalities associated with cryogenic fluid storage in deep space. Cryogenic systems require complex thermal management, extensive insulation, and active cooling to prevent boil-off—factors that add risk and mass to the spacecraft design. Additionally, cryogenic propellants typically have lower densities, resulting in larger tank volumes and increased structural mass. In contrast, hypergolic propellants are easy to store and offer higher propellant densities, reducing overall tank volume. Furthermore, their inherent start and restart capability [49] makes them particularly well-suited for MOCHA-PROP-005. These characteristics make hypergolic systems a practical and mission-aligned solution for this mission.

To assess propellant suitability, a trade study was conducted using the NASA Chemical Equilibrium Applications (CEA) code [48] and nitrogen tetroxide (NTO) as the theoretical oxidizer. To compare the Isp, a theoretical engine was used with a chamber pressure of 68.94 bars and expansion ratio of 400 comparing commonly used hypergolic bipropellants with a representative cryogenic propellant, liquid methane (CH_4). As presented in Table 8 monomethylhydrazine (MMH) was selected as the most appropriate fuel due to its extensive Mars mission heritage, high specific impulse, superior density compared to other hypergolics, and more manageable thermal requirements relative to cryogenic options.

Table 8. Propellant Trade Study

Parameter	MMH	UDMH	CH_4
Specific Impulse (Isp)	348	338.5	360
Density (g/m ³)	874	792	423.9
Freezing Point	-52.5 °C	-57.2 °C	-183 °C
Mars Heritage	Extensive	Moderate	Low
Total	4.34	4.19	3.38

F.3.3 Oxidizer

To operate with the selected MMH fuel, variations of dinitrogen tetroxide (N_2O_4) have been investigated for oxidizer selection. The corresponding oxidizer candidates, listed in Table 9 from [3], are based on N_2O_4 with varying amounts of nitric oxide (NO) added, forming Mixed Oxides of Nitrogen (MON) formulations. In the oxidizer selection process, key performance criteria include high specific impulse (Isp), low freezing point, and high propellant density, the latter being particularly important to minimize tank volume and overall system mass.

While the addition of NO to N_2O_4 decreases the freezing point—thereby improving thermal stability—the associated reduction in Isp occurs. Given the thermal capacity of the MOCHA spacecraft and the relatively short eclipse durations



experienced in Mars orbit, the slightly lower freezing point of MON-3, compared to pure N₂O₄, remains thermally manageable. In addition, MON-3 offers a slightly higher density than pure N₂O₄, which contributes to improved tank volume efficiency. Therefore, MON-3 has been selected as the oxidizer for the mothership orbiter.

Table 9. Oxidizer Trade Study

Parameter	N ₂ O ₄	MON 1.3	MON 3	MON 25
Specific Impulse (Isp)	348	347.7	347.2	341.2
Density (g/m ³)	1430	1430	1450	1450
Freezing Point	-11.2 °C	-11.6 °C	-15 °C	-54 °C
Material Compatibility	High	Moderate	Moderate	Low
Mars Heritage	Extensive	Moderate	Moderate	Moderate
Total	6.95	6.8	6.6	7

F.3.4 Main Engine

To execute critical maneuvers, such as the Mars Capture and inclination change maneuver, the propulsion system must include a main thruster capable of delivering high thrust with reliable restartability for multiple burns. Therefore, the 400 N Bipropellant Apogee Engine from ArianeGroup has been selected, configured with four thrusters with characteristic properties as Table 10. This engine is compatible with the chosen propellants and provides a favorable balance between high thrust output and low structural mass [21].

Table 10. Apogee Motor Characteristics

400N Bipropellant Apogee Motor Characteristics	
Thrust Range	340 - 440N
Mass per Thruster	4.30 kg
Specific Impulse	321 s
Oxidizer to Fuel ratio (O/F)	1.65
Chamber Pressure	10 bar
Flow Rate Range	110 - 142 g/s

With the given delta-v requirement the propellant mass has been calculated for every maneuver by using Tsiolkovsky rocket equation since the wet mass changes after every maneuver as Equation (F.3.4.1):

$$\Delta V = I_{sp} \times g_0 \times \ln(m_o/m_f) \quad (\text{F.3.4.1})$$



With a mass flow rate of 0.142 kg/s per engine, the propulsion system—configured with four engines—is capable of executing the Mars capture maneuver within 1800 seconds and the circularization maneuver within 220 sec as follows:

Table 11. Mission Propulsion Overview: Mars Capture to Deorbiting Phase

Parameter	Delta-v Requirement	Propellant Mass	Burn Time
Mars Capture (Elliptic at Periareion)	772 m/s	1000.31 kg	1800 sec
Apoareion Change	44.73 m/s	50.75 kg	91.30 sec
Inclination Change (at Apoareion)	153.49 m/s	168.77 kg	20 sec
Circularization at Periareion	1319 m/s	1155.20 kg	220 sec
Orbital Maintenance	30 m/s	21.37 kg	Not Impulsive Maneuver
Deorbiting	55 m/s	38.65 kg	1 minute
Margin %15	420.58 m/s	282.78 kg	Not Impulsive Maneuver
Total	2794.8	2717.83 kg	



Figure 15. Model No S400-15 apogee motor

F.3.5 Tank Sizing

By considering the engine's oxidizer-to-fuel mixing ratio of 1.65, the corresponding oxidizer and fuel masses and volumes have been calculated for each phase of the delta-v budget. The mass calculations account for the effects of trapped propellant, system outage, loading error, and an applied mass margin as stated in Table 12. Additionally, the volume calculations accounting for the influence of %10 ullage has been considered for accurate volume estimation. As a result, the required oxidizer volume is calculated to be 0.876 m³, while the corresponding fuel volume is 2.409 m³.

Table 12. Mass Allocation of Oxidizer and Fuel with Operational Margins

Propellant	Oxidizer Mass (kg)	Fuel Mass (kg)
Usable Propellant	1013.324879	1671.986051
Trapped Propellant (%3)	30.39974637	50.15958152
Outage (%1)	10.13324879	16.71986051
Loading Error (0.5%)	30.12	8



Margin (%10)	101.3324879	167
Loaded Propellant	1155.190362	1914.424028

Cylindrical tanks with hemispherical ends were selected due to their ability to minimize stress concentrations by evenly distributing internal pressure, which allows for thinner walls and reduced structural mass. The tank sizing was performed based on aspect ratio constraints. Accordingly, the design adopts a maximum aspect ratio of 3.5 to ensure structural integrity and propellant stability under varying thermal and pressure conditions.

Table 13. Physical Parameters of Storage Tanks

Fluid	Number of Tanks	Total Volume	Radius (m)	Aspect Ratio	Total Height (m)
MMH	2	2.409 m ³	0.308	1.367	1.458
N ₂ O ₄	2	0.876 m ³	0.217	2.36	1.458
He	5	0.22	0.374	1	-

F.4. Communications and Data Handling

The orbiter communication system must be designed to maintain communication with all CubeSats even under worst-case scenarios. Within this scope, the orbiter should collect the data generated by the CubeSats during orbital drift, orbit phase, and entry, and transmit it to Earth. The orbiter must also transmit its own generated data to Earth. The requirements for the orbiter communication subsystem are as follows:

Table 14. Orbiter Communication Requirements

Req. ID	Requirement Description
REQ-MOCHA-COMM-01	Orbiter shall communicate with Earth DSN and transmit the total 17 GB data at least once a day.
REQ-MOCHA-COMM-02	Orbiter shall maintain continuous two-way communication with ground control throughout the specified mission duration.

To meet these requirements, several critical factors were considered during the calculations and selection process. Hardware selection prioritized compatibility with the required data size, power output, and antenna gain. Atmospheric losses caused by both Earth and Mars, as well as pointing requirements that could negatively impact communication, were incorporated into the calculations. The system was also designed to maintain data reception capability even when multiple CubeSats simultaneously enter the communication window. Additionally, a robust communication system was developed to operate effectively across various scenarios, accounting for the varying distance between Earth and Mars and its impact on data transmission.



F.4.1. The Data Budget

The data handling subsystem of the orbiter has been designed to meet two major requirements: it must be capable of processing and managing data originating from the orbiter's own payloads, including ADCS sensors and housekeeping telemetry, as well as the high-volume data transmissions expected from eight accompanying CubeSats. In addition to this multi-source processing requirement, the subsystem must also support extended onboard storage, enabling data retention over long communication blackouts—defined in our mission as lasting up to one month due to limited communication windows with Earth.

Table 15. Orbiter Data Budget

Orbiter	Quantity	Sampling Frequency (Hz)	Total Data Rate (kbps)
LOLA	1	28	27
Majis	1	1	10000
MARLI	1	250	50
EMCS	1	1	2.15
Data From 8 CubeSats			49.34
Total(%50 Margin)			15192.73

Although the orbiter operates under a single continuous mission phase, the subsystem must be prepared to handle peak loads during the CubeSats' entry sequences, when large volumes of critical data are transmitted in a short time. Meaning processing data up to 15Mbps and storing. But since MAJIS only works %12.5 of the orbit it causes 17GB of data from all sources in one day. However, the choice of onboard computer and storage system was not based solely on data throughput and capacity. Given the mission's extended duration of approximately five years and its interplanetary operational environment, radiation tolerance became a defining selection criterion. Unlike LEO missions, interplanetary missions are subject to increased radiation exposure from galactic cosmic rays and solar particle events, necessitating robust fault-tolerant architecture.

F.4.2. The Link Budget

The link budget evaluates the connection between the receiver and transmitter by considering all influencing factors. Ensuring that communication between the orbiter and DSN operates at the desired distance, capacity, and error rate is only possible through accurate link budget analysis. Therefore, taking all relevant factors into account, the link budget was calculated using the equation provided below [2]:

$$\frac{E_b}{N_0} = \frac{P_t \cdot G_t \cdot L_p \cdot G_r}{k \cdot T_s \cdot B} \quad (\text{F.4.2.1})$$



In this equation, $\frac{E_b}{N_0}$ is the energy per bit to noise power spectral density ratio, commonly referred to as the signal-to-noise ratio (SNR) and expressed in decibels (dB). The parameter P_t is the output power at the transmitter in dB, while G_t and G_r are the transmitting and receiving antenna gains in dBi. The term L_p denotes the total path loss, accounting for signal attenuation in dB. k is the Boltzmann constant, representing thermal noise power per degree of temperature, and T_s is the system noise temperature in kelvin. B defines the signal bandwidth in hertz.

Table 16. Orbiter Link Budgets

Parameter	Orbiter to DSN (Closest)	Orbiter to DSN (Farthest)	DSN to Orbiter	Unit
Eb/No (required)	9	9	9	dB
Data Rate	18000000	350000	100000	bps
Transmit Power	53	53	73	dBm
Transmit Antenna Gain	46.58	46.58	68	dBi
Carrier Frequency	8.42	8.42	7.2	GHz
Range	55000000	400000000	400000000	km
FREE SPACE Path Loss	265.8	283.0	281.6	dB
Atmospheric Loss	1.77	1.77	1.77	dB
Pointing loss	1.44	1.44	1.23	dB
Receive Antenna Gain	68	68	44.49	dBi
Received Signal Power	-101.4	-118.6	-99.1	dBm
kTB	-113.50	-130.61	-137.10	dB
Eb/No (achieved)	12.1	12.0	38.0	dB
Link Margin	3.1	3	29.0	dB

F.4.2.1. Transmitter Specifications

The orbiter uses a parabolic reflector antenna to focus transmitted signals in a specific direction. The antenna gain is calculated by assessing the effective aperture area, which is the physical area adjusted for efficiency. The operating wavelength, determined by dividing the speed of light by the frequency, is then used to calculate the isotropic radiator area.

The gain is the ratio of the effective aperture to the isotropic area and is expressed in decibels (dBi) as [2]:



$$G_{dBi} = 10 \log_{10} \left(\frac{A_e}{A_{iso}} \right) \quad (\text{F.4.2.1.1})$$

where A_e is the effective aperture area and A_{iso} is the isotropic radiator area. This expression quantifies how much more power the parabolic antenna directs compared to an ideal isotropic radiator. For the orbiter's 3-meter parabolic antenna with 0.65 efficiency and an operating frequency of 8.42 GHz, the gain is calculated as 46.58 dBi.

The transceiver power output P_t represents the RF power in watts, which can be converted to dBm using [2]:

$$P_{t(dBm)} = 10 \log_{10} (P_{t(W)} \times 1000) \quad (\text{F.4.2.1.2})$$

Here, $P_{t(W)}$ is the power in watts, and the factor of 1000 converts watts to milliwatts before taking the logarithm. The $P_{t(dBm)}$ of the Orbiter TWTA with a 200 W RF output was found to be 53 dBm.

F.4.2.2. Path Losses

Path loss in the communication link between the orbiter and Earth is determined by considering three primary components: free space loss, atmospheric loss, and pointing loss. Free space loss L_{FS} accounts for the spreading of the radio wave as it propagates over distance and is calculated using the standard equation [5]:

$$L_{FS} = 20 \log_{10} \left(\frac{4\pi d}{\lambda} \right) \quad (\text{F.4.2.2.1})$$

where d is the distance between the transmitter and receiver, and λ is the signal wavelength. As the distance between Mars and Earth can reach up to 400 million km, the free space loss can exceed 283 dB in the X-band. Atmospheric loss L_{atm} includes attenuation due to both Earth's and Mars' atmospheres. At X-Band, the vertical atmospheric loss on Mars is 1.15 dB (worst case), while on Earth, it is considered as 0.05 dB under standard conditions [5]. Pointing loss L_{point} arises from antenna misalignment and depends on the half-power beamwidth δ and the pointing error θ . The half-power beamwidth is calculated as:

$$\delta = \frac{21}{fD} \quad (\text{F.4.2.2.2})$$

where f is the frequency in GHz and D is the antenna diameter in meters. The pointing loss in decibels is then given by:

$$L_{point} = 12 \left(\frac{\theta}{\delta} \right) \quad (\text{F.4.2.2.3})$$

The pointing accuracy is defined as 0.1 degrees, resulting in a maximum pointing loss of approximately 1.44 dB. The total



path loss is expressed as the sum of these components:

$$L_p = L_{FS} + L_{atm} + L_{point} \quad (\text{F.4.2.2.4})$$

All components are expressed in decibels (dB) to maintain consistency in link budget calculations, ensuring accurate assessment of signal attenuation under various mission conditions. Under these conditions, the total path loss at the closest distance to Earth (55 million km) is approximately 269 dB, while at the maximum distance of 400 million km, it increases to 286.2 dB. This significant variation in path loss substantially impacts the achievable data rate, necessitating strategic planning of data transmission based on the spacecraft's position relative to Earth.

F.4.2.3. DSN Services

DSN provides multiple receiver options for its users. When conducting a link budget analysis, it is essential to know the gain, noise temperature, G/T ratio, and data rate range of the selected receiver. This information is obtained from the most recent service catalogs published by DSN [8]. For the link budget calculations, the 34-meter Beam Waveguide (BWG) X-Band antenna was used as the baseline. According to the DSN catalog, the key specifications for the 34-m BWG X-Band antenna are as follows:

Table 17. Comparison of DSN Antenna Performance

Antenna	Frequency Band	Gain (dBi)	Noise Temperature (K)	G/T (dB)	Data Rate (Mbps)
34-m BWG	S	56.8	36.8	41.1	1–2
	X	68.0	33.0	52.9	10–50
	Ka	78.5	31.0	63.6	100
34-m HEF	S	56.0	38.0	40.2	1–2
	X	68.1	19.8	55.1	20–50
70-m	S	63.4	22.0	50.0	1–2
	X	74.4	20.6	61.3	10–20

F.4.2.4. Modulation Scheme

Determining the Bit Error Rate (BER) is essential for establishing the required Signal-to-Noise Ratio (SNR). After completing the link budget analysis, the SNR value obtained must be evaluated to ensure it provides adequate data accuracy based on the modulation scheme. For communication between the orbiter and the DSN, Quadrature Phase Shift Keying



(QPSK) was selected as the modulation scheme. QPSK effectively reduces bandwidth usage by transmitting two bits per symbol. For the communication links, the minimum acceptable BER was set to 10^{-5} , which can be achieved with approximately 9 dB SNR under ideal conditions as shown in figure 4. However, to account for potential uncertainties and signal degradation, a 3 dB link margin was added, resulting in a target SNR of at least 12 dB to ensure reliable data transmission [12].

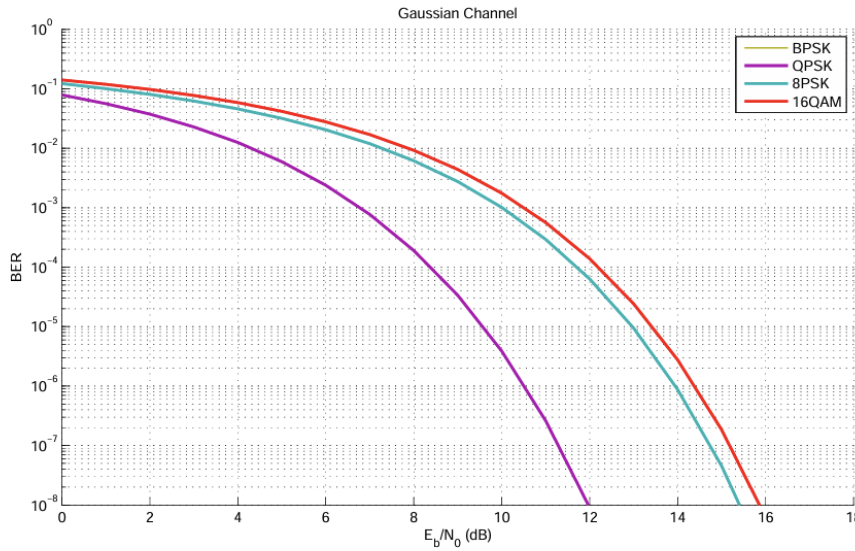


Figure 16. BER over AWGN channel for BPSK, QPSK, 8PSK and 16QAM [12]

F.4.3. Trade-Offs

The main component selections for the systems were made based on the specified requirements and operational constraints.

F.4.3.1. Command and Data Handling

Considering three mission-critical needs—high computational capability, extended data storage, and radiation hardness—the Space Micro ProtonX-Box onboard computer was selected, supported by 1 Tb of storage. The ProtonX-Box can process data up to 20-25 Mbps depending on the data type and can hold up to 1 TB of data[18] This On-Board Computer has demonstrated flight heritage on prior interplanetary missions and offers a high level of reliability, featuring Triple Modular Redundancy (TMR) to mitigate single-event upsets. It is rated for 100 krad TID, meeting the expected cumulative dose over the mission lifetime. Even with a 50% data processing margin, the system can comfortably manage the data flows from both the orbiter and CubeSats. The selected storage system, meanwhile, exceeds the 15-day requirement and is capable of retaining mission data even under extended blackout scenarios of up to 15 days or more without data loss. As a result, the orbiter's data handling architecture ensures resilient, fault-tolerant operations in a high-radiation, long-duration deep space environment, supporting uninterrupted data integrity from all nine spacecraft sources.



F.4.3.2. Transceiver Selection

Since the orbiter must communicate with both Earth and CubeSats, it requires transceivers operating at different frequency bands. Using the DSN for Earth communication is more cost-effective and operationally efficient than building a dedicated ground station, which would have limited coverage. DSN's global network eliminates this constraint. The orbiter must operate on one of DSN's allocated bands S-Band, X-Band, or Ka-Band. X-Band was selected because S-Band could not support the required data rates, and Ka-Band, while offering higher data rates, incurs greater path loss, demanding larger antennas or higher power output, both impractical for the orbiter. Thus, X-Band provides the optimal balance between data rate and path loss. To support this link, the L3Harris C/TT-600 X-Band transceiver was chosen. As a deep space-compatible SDR, it offers adjustable data rates and efficient power management. Its architecture allows simultaneous communication with multiple CubeSats by independently processing different frequency channels, preventing data loss during overlapping communication windows. For CubeSat communication, the C/TT-600 S-Band and UHF transceivers were also included to maintain consistency and meet mission requirements. Specific use cases for these bands are discussed in the CubeSat Communication section, with hardware specifications detailed in the Hardware Properties section **Table 16**.

F.4.3.3. Antenna Selection

Antenna selection for the orbiter focused on ensuring compatibility with the transceivers and maximizing communication efficiency. For Earth communication, a 3-meter directional parabolic antenna was chosen for X-Band, capable of pointing with 0.1° accuracy. While this introduces ADCS requirements, alternative antennas would significantly reduce gain, compromising data transmission efficiency. To maintain basic communication during critical phases such as launch, Mars Orbit Insertion (MOI), and safe mode, two low-gain antennas (LGAs) were added, similar to the Mars Reconnaissance Orbiter configuration [18]. These LGAs support low-rate communication when the primary antenna is not aligned with Earth. For CubeSat communication, four omnidirectional antennas were integrated: two MA-WO-UWB S-Band and two UHF. This setup allows data exchange without precise pointing, preventing data loss when CubeSats temporarily halt transmission to conserve power. Additional hardware specifications are detailed in the Hardware Properties section **Table 16**.

F.4.4. Communications Subsystem Overview

The overall communication subsystem was established based on the link budget analyses, trade studies, and selected hardware components.



F.4.4.1. Communications Architecture

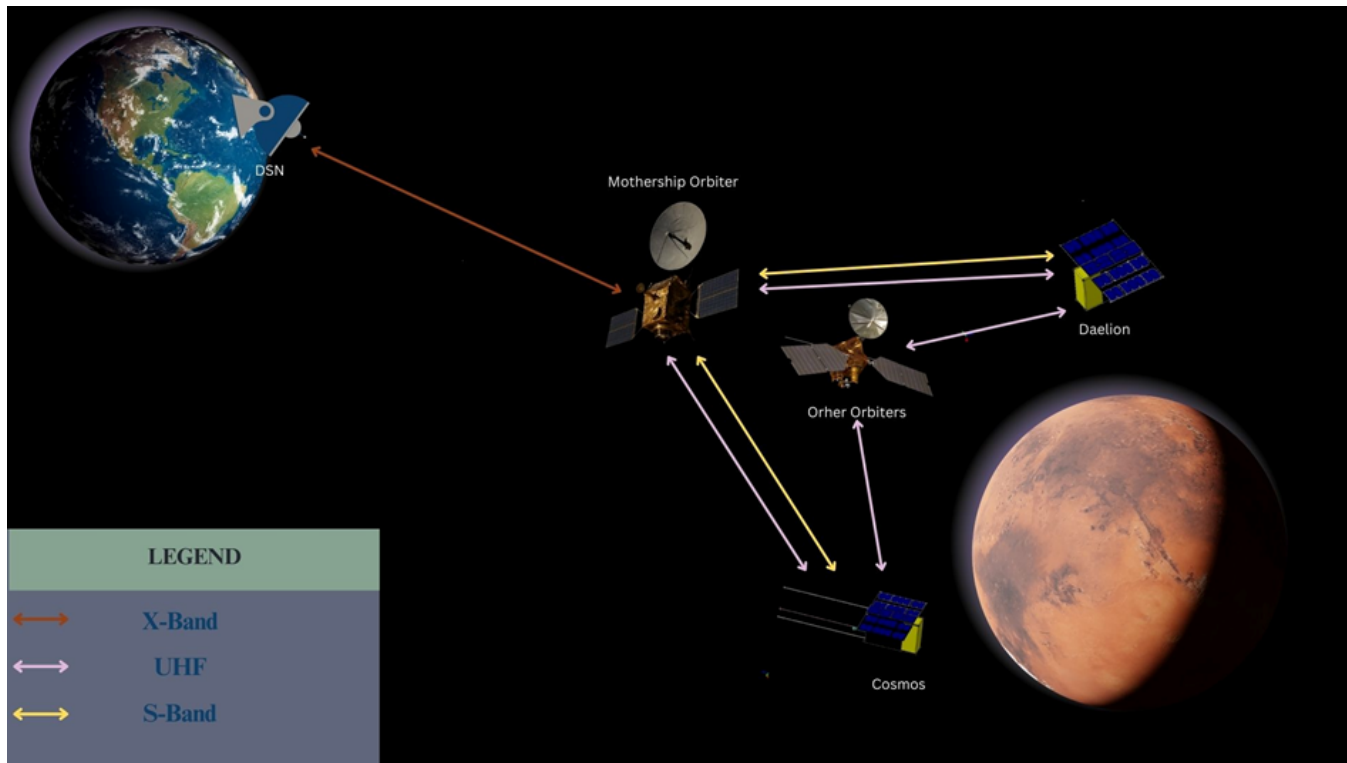


Figure 17. Communications Architecture

The orbiter transmits data to Earth using X-Band, with data rates varying based on its distance from Earth. At the closest approach, the data rate reaches 18 Mbps, allowing the orbiter to transmit up to 17 GB of data in 2 hours. However, at the maximum distance of 400 million km, the data rate drops to 350 kbps, which is insufficient to handle the full data load generated by MAJIS. Therefore, during this phase, MAJIS will remain inactive, reducing the daily data volume to approximately 1.5 GB, making it manageable within the limited data rate. Even under these conditions, critical CubeSat data can still be transmitted at 350 kbps with a 1.5-hour daily communication window, ensuring essential data is relayed under worst-case scenarios. The orbiter is also equipped with multiple receivers operating at different frequencies, allowing it to receive data from up to four CubeSats simultaneously, preventing data loss from overlapping communication windows. This multi-frequency architecture positions the orbiter as a potential relay asset for future manned missions, capable of moving to designated orbits and serving as a communication node with its remaining fuel capacity.



F.4.4.2. Hardwares Properties

Table 18. Orbiter Communication Subsystem Hardwares[18] [19]

Type	Name	Quantity	Mass (kg)	Power Consumption Rx (W)	Power Consumption Tx (W)
Transceiver	C/TT-600 UHF	1	3.2	5	10
	C/TT-600 S-Band	1	3.2	5	17
	C/TT-600 X-Band	1	4.1	15	30
Type	Name	Quantity	Mass (kg)	Power Consumption (W)	Gain (dB)
Antenna	X Band Parabolic Antenna	1	15	-	46.58
	MA-WO-UWB S band	2	0.7	-	8
	MA-WO-UWB UHF	2	0.7	-	5
TWTA	X-band TWTA	1	4	340	53.01
Type	Name	Quantity	Mass (kg)	Power Consumption (W)	Storage
OCB-Storage	Space Micro ProtonX-Box	1	1.91	12.7 Max	1TB
Total Mass (kg)			32.81		

F.5. Attitude Determination and Control

In Table 19, address critical attitude control functions necessary for the spacecraft's operation. These requirements ensure precise attitude stabilization, support for various mission phases, and the ability to meet specific instrument needs. The system must enable stable pointing for instruments like LOLA, MARLI, and MAJIS, as well as handle momentum unloading and autonomous mode transitions. Additionally, the requirements specify the need for jitter mitigation to maintain stable pointing for high-precision instruments. These functionalities are essential for ensuring the orbiter's ability to collect accurate data, perform various science operations, and maintain long-term operational efficiency.

Table 19. ADCS Requirements

Req. ID	Requirement Description
REQ-MOCHA-ADCS-01	The orbiter shall provide 3-axis, zero-momentum attitude stabilization to support diverse instrument requirements.
REQ-MOCHA-ADCS-02	The ADCS shall enable full 360° limb viewing coverage for EMCS via coordinated spacecraft slewing as needed.



REQ-MOCHA-ADCS-03	The ADCS shall maintain nadir-pointing orientation for LOLA
REQ-MOCHA-ADCS-04	The orbiter shall support off-nadir pointing at fixed 30° angles for MARLI observations.
REQ-MOCHA-ADCS-05	The ADCS shall enable off-nadir pointing with variable articulation angles for MAJIS, including targeted slews.
REQ-MOCHA-ADCS-06	The orbiter shall perform momentum unloading using thrusters when angular momentum exceeds mission-defined thresholds.
REQ-MOCHA-ADCS-07	The ADCS shall autonomously manage mode transitions between science, slew, and safe modes.
REQ-MOCHA-ADCS-08	The ADCS shall support jitter mitigation strategies to ensure stable pointing for high-precision instruments.

The table X shows the environmental disturbances to which the orbiter is subjected. As expected, the magnetic disturbance is zero.

Table 20. Maximum Expected Torques from External and Internal Sources

Torque Type	Torque Source	Maximum Magnitude (Nm)
External	Solar Radiation Pressure	9.44E-06
External	Atmospheric Drag	2.38E-04
External	Magnetic Disturbance	3.22E-29 ≈ 0
External	Gravity Gradient	0.0186
Internal	Slosh (Nominal Estimate)	2.24

The mothership-orbiter's attitude control system is designed to support various control modes dedicated to specific payload operations and mission needs. During Nominal Science Operations, the LOLA instrument operates in nadir-only mode and requires a pointing accuracy of $\leq 0.1^\circ$ and a maximum slew rate of $\leq 0.05^\circ/\text{s}$. In Limb Scanning mode, the EMCS system utilizes 360° limb access via azimuth and elevation articulation, with the same $\leq 0.1^\circ$ accuracy but accommodating slews of up to 1°/s. For Fixed Off-Nadir Science, the MARLI instrument is in a 30° orientation with an extremely strict pointing requirement of $\leq 0.01^\circ$ and slew capability is not pertinent. Targeted Imaging Slew enable the MAJIS instrument to perform multi-angle spectral imaging with $\leq 0.1^\circ$ accuracy and high slew rates of 2°/s. Standby is entered by all instruments with a loose pointing requirement of $\leq 5^\circ$ in Safe Mode, and slew rate is not critical. Momentum Dumping is performed with all payloads turned off, where accuracy and slew requirements are relaxed. Lastly, under Fallback Operations that rely solely on the sun sensor, all instruments are in degraded mode with a pointing accuracy of $\leq 2^\circ$ and a very slow slew rate of $\leq 0.01^\circ/\text{s}$.



After the requirements were determined, the orbiter's moments of inertia were determined. Then, using the angles and accuracies obtained from the requirements, the torque amounts required for the spacecraft were calculated. At the same time, Table 20 was used for the disturbances. The formulas used to calculate the environmental disturbances are given in the appendix. In addition, while calculating the disturbance for slosh, it was assumed that 10% of the fuel amount was moving based on information obtained from the literature [ref]. As a result of the calculations, it was concluded that the L3Harris RWA-15 model reaction wheels, which can produce 0.5 N torque, could meet the spacecraft's needs, however, since passive momentum discharge was not possible, momentum discharge could be made using Busek BGT-X5 model thrusters. For attitude determination 2 Terma T1 Star Trackers, 2 Honeywell HG9900 RLG IMUs, 16 NewSpace NFSS-411 Sun Sensors will be used.

F.6. Power

The power system design of the orbiter is driven by three main considerations: energy generation, storage, and distribution, each evaluated under worst-case operational scenarios to ensure continuous functionality. The mission profile is divided into four critical phases—maneuver, nominal orbit, eclipse, and entry—each of which imposes unique demands on the power system. Solar array sizing was determined by analyzing the orbit and eclipse phases in detail.

Table 21. Phase-Wise Power Consumption of Orbiter Systems During Orbit, Eclipse, and Entry

Orbiter	Orbit(5564.6s)	Eclipse(1257.41s)	Entry(2400s)
Payload	180.2 W	180.2 W	180.2 W
ADCS Sensor	7.4 W	7.4 W	7.4 W
ADCS Actuator	208 W	208 W	208 W
Comms Rx	5 W(220s)	5 W(220s)	10 W
Comms Tx	370 W(700s)	370 W(700s)	400 W(700s)
Data	10 W	10 W	10 W
Thermal	50 W	50 W	50 W
Total(%20 Margin)	1000 W	1000 W	1040 W

One of the reasons for our very high payload power consumption is that our most power consumption instrument MAJIS includes its thermal protection systems. Operating at an altitude of approximately 300 km around Mars in a Sun-synchronous, high-inclination orbit (77 degrees), the orbiter experiences eclipse durations that vary depending on seasonal and geometric factors with 2514.82 seconds of worst case of eclipse and 0 seconds of best case of eclipse. For sizing purposes, an average eclipse duration of 1257.41 seconds and a corresponding Sunlit period of 5564.6 seconds per orbit were used.



The required solar panel area was calculated using a standard energy balance equation that accounts for power demand during both eclipse and daylight, the solar flux at Mars (590 W/m²), a pointing loss factor of 0.75 due to body-mounted fixed arrays with near polar orbits and X_e and X_d values of 0.65 and 0.85[11]. Triple-junction Gallium Arsenide (GaAs) solar cells with a 29.5% efficiency were selected for their heritage and performance in interplanetary missions with %2.75 degradation per year.[12]

$$\frac{\frac{T_d * P_d}{X_d} + \frac{T_e * P_e}{X_e}}{T_d} = W_{needed} \quad (\text{F.6.1})$$

Using this equation we find the W values for our cells. And since the orbiter will be using its solar panels for 4 years. We can find the necessary area;

$$P_{EOL} = \mu_{cell} * \mu_{pointing} * S_{Mars} \quad (\text{F.6.2})$$

$$P_{EOL} = P_{BOL} * (1 - degradation)^{\text{Mission Time}} \quad (\text{F.6.3})$$

The total required solar array area was found to be 8.94 m² to supply the orbiter's nominal 1000W power demand, both calculated %20 margin. Since this area cannot be stowed within the orbiter's launch configuration, a deployable solar panel system was adopted. The system we are using is similar to ESA's TGO mission and utilizes Two-Panel (Bi-fold) Wing[13] and its estimated mass, including deployment mechanisms and structural support, was calculated based on comparable commercial systems to be 28.6 kg.

Energy storage requirements were evaluated using the combined eclipse and entry phases, during which no solar power is available. For these conditions, a worst-case blackout duration of 2514.82 seconds was assumed. Accounting for a 90% battery efficiency and a Depth of Discharge (DoD) of 50%, the resulting energy storage requirement was calculated to be 1135 Wh. A battery and EPS solution from AAC Clyde Space STARBUCK-Mini EPS and EnerSys / ABSL 8s16p Li-ion Battery Pack was selected, capable of operating at a 28 V nominal bus voltage and delivering 1668Wh within acceptable mass and volume constraints[15].

Furthermore, the EPS unit supports high discharge rates, which are critical for the orbiter's maneuver phase, where peak power draws may reach 1200 W. In particular, the propulsion system draws 10.4 A at 27 V, and the selected EPS configuration is rated to sustain 10+A at 28V, ensuring reliable operation during propulsion maneuvers without compromising energy availability for other subsystems. Since this activation lasts 30 minutes it only has an effect of 200Wh our EPS can withstand this activation of the propulsion systems.



F.7. Thermal Control Systems

The thermal control system is designed to ensure that all spacecraft subsystems operate within their designated temperature ranges across all mission phases, including cruise, orbit, and eclipse. All the requirements have been added to Table 22. The operational temperature limits are derived from the functional and survival requirements of each component including electronics, scientific instruments, propellant tanks and battery. To achieve this, Multi Layer Insulation (MLI) has been used to minimize radiative heat loss and protect components from extreme temperature fluctuations in the space environment as a passive thermal control solution on the mothership orbiter. The multilayer material selection was carried out following the strategy outlined in reference [30], employing a layered configuration starting with an outer layer to protect the MLI from Mars atmospheric degradation, followed by a reflective layer, a separator layer to maintain spacing and reduce conductive heat transfer, and finally an inner layer that provides structural support and electrical isolation. For the outer layer, Aluminized Beta Cloth has been selected to protect the orbiter's structure from Martian atmospheric degradation due to its resistance to ultraviolet (UV) radiation. The reflective layer employs Aluminized Kapton, chosen for its low infrared emittance of 0.05 and absorptance of 0.14 [30], effectively reflecting thermal radiation to maintain thermal balance. To minimize conductive heat transfer between layers, Dacron netting is implemented as the separator layer, maintaining consistent spacing between reflective films. Finally, the inner layer utilizes Kapton film, providing mechanical support and electrical insulation within the multilayer insulation (MLI) system. With this insulation system, the internal temperature of the spacecraft is maintained within the desired operational range.

Table 22. Thermal Requirements

Requirement ID	Requirement Description
REQ-MOCHA-THERMAL-01	The thermal control system shall maintain corresponding scientific instrument and batteries within -20°C to $+40^{\circ}\text{C}$ throughout all mission phases, including cruise, orbit, and eclipse periods.
REQ-MOCHA-THERMAL-02	The MAJIS imaging spectrometer requires special cryogenic operating temperatures for its Optical Head (-143°C) and detectors (IR FPA -183°C , VISNIR FPA -143°C).
REQ-MOCHA-THERMAL-03	Scientific sensors require precise temperature stability especially $\pm 0.5^{\circ}\text{C}$ for MAJIS IR FPA to prevent drift or noise.
REQ-MOCHA-THERMAL-04	The heat generated by the electronics, including that from sensors, batteries, and onboard systems, must be rejected through thermal radiation to maintain component temperatures within their operational limits.
REQ-MOCHA-THERMAL-05	The thermal control system must manage eclipse periods by using pre-eclipse heating to prevent rapid temperature drops in critical components.
REQ-MOCHA-THERMAL-06	The propellant tanks must be maintained above the freezing points of the selected propellants to ensure proper flow and combustion performance throughout the mission. For the chosen bipropellant combination, Monomethylhydrazine (MMH) has a freezing point of -52°C , while MON-3 (Mixed Oxides of Nitrogen) freezes at approximately -15°C .



Specifically for the scientific instruments, for the MAJIS instrument, the thermal management solution is designed to enable the instrument to perform precise scientific measurements at the highest level. The Optical Head (OH) and Visible/Near-Infrared (VISNIR) detector must be maintained at approximately 130K (-143°C), and the Infrared (IR) detector at 90K (-183°C) with high stability ($\pm 0.5\text{K}$ for the IR Focal Plane Array, FPA) [39]. To achieve this, a robust passive thermal design is essential with two different methods. Firstly, high-performance Multi-Layer Insulation (MLI) is selected to isolate the instrument from other heat sources on the spacecraft. Secondly, Two custom-designed, high-efficiency passive radiators that are integrated with MAJIS provide us to reach and maintain these cryogenic temperatures for accurate measurement. As shown in the figure, the two radiators serve distinct detectors: the hot radiator is used for the Visible/Near-Infrared (VISNIR) detector, while the cold radiator provides the necessary cryogenic temperature for the Infrared (IR) detector, ensuring optimal sensor performance. These radiators must be positioned to continuously face cold space and remain unrestrained by Mars and the Sun. To manage thermal loads from Mars and the Sun in a 300 km low Mars orbit, the radiators have been carefully positioned on the MOCHA orbiter to ensure they are shielded from both Mars and the Sun, while maximizing exposure to cold space. Also, to minimize conductive heat transfer from the surrounding to the instrument, thermal insulation interfaces using CFRP/titanium bipods will be used as part of the passive thermal system.

For the EMCS instrument, which inherits design elements from the Mars Climate Sounder on the Mars Reconnaissance Orbiter, the aluminum camera housing presents a critical thermal constraint to ensure proper measurement. Due to aluminum's high thermal conductivity, the housing must not exceed a maximum allowable temperature of 40 °C [2]. To maintain this limit, a thermal margin must be applied, necessitating effective thermal insulation around the EMCS. Therefore, Multi-Layer Insulation (MLI) must be implemented to reduce radiative heat loss and minimize temperature gradients between daytime and eclipse conditions, thus preserving measurement accuracy. Additionally, Kapton heaters are installed on both the housing and the sensor electronics to maintain temperatures within the desired operational range. The thermal control system employs a heater control loop that activates heating when temperatures approach minimum thresholds during eclipses, and deactivates heaters when internal heating, especially during daylight time, is sufficient to prevent overheating. Temperature sensors continuously monitor system conditions to ensure thermal stability within operational limits.

For MARLI, the fused silica etalon, a part of the receiver's optical subsystem, requires strict thermal stability. This is because the temperature-dependent index of refraction of fused silica causes the passband frequency to shift by 355 MHz per 1°C [37]. To prevent this shift, the fused silica etalon must be temperature-stabilized. As a result, MARLI is equipped with its own thermal control system, which includes a conductively mounted etalon held within a precisely controlled oven. The system maintains the temperature within $\pm 5\text{ mK}$ using precision heaters and Cernox RTDs for active control.[3]



LOLA requires temperature stabilization within a range of $\pm 1\text{--}2^\circ\text{C}$, specifically between -20°C and $+20^\circ\text{C}$. The same temperature control strategy used for EMCS will be implemented for this sensor as well for the temperature stabilization across eclipse and daytime period of the orbiter.

For our propulsion system, it is a polished aluminum heat shield strategically placed to protect the valve and surrounding critical elements from thermal loads. Polished aluminum is an excellent choice for this application due to its high reflectivity, which effectively minimizes heat transfer through radiation, and its relatively low mass, which is crucial for spacecraft design. By using this proven thermal protection method, we ensure the reliable operation and longevity of the propulsion system's sensitive parts in the extreme temperature variations encountered during operation. Furthermore, for our tank system, the MLI (Multi-Layer Insulation) solution also used in the orbiter's external system has been chosen, and in the section connecting to the orbiter, CFRP (Carbon Fiber Reinforced Polymer) connectors with low conductivity have been selected.

F.8. Orbiter Overview

Table 23. Orbiter Subsystem Mass and Power Budget

Orbiter	Mass (kg)	Power (W)
Payload	116.6	180.2
EMCS	11.2	18.4
MARLI	40	90
MAJIS	50.8	45
LOLA	14.6	26.8
Structures	300	-
Power	37.9	-
Battery	7.8	-
Solar Panel	26.8	-
EPS	3.3	-
Thermal	5	50
ADCS	72.5	280.2
Honeywell HG9900 IMU	5.44	20
NewSpace NFSS-411 Sun Sensor	0.56	2.4
Terma T1 Star Tracker	1.52	5
L3Harris RWA-15 Reaction Wheels	56	68
Busek BGT-X5 RCS Thruster	9	120



COMM&DH	30.9	420
Transceivers	10.5	80
Antennas	16.4	-
TWTA	4	340
Propulsion	1841.2	280
Thruster	17.2	280
Propellant	1824	0
CubeSats	73.24	0
Total	2477	1210.4

Table 24. Cosmos CubeSat Subsystem Mass and Power Budget

Cosmos	Mass (kg)	Power (W)
Payload	2.1525	0.435
Structures	2	-
Power	1.395	-
Thermal	0	1.4
ADCS	0.976	3.925
COMM&DH	0.707	24.4
Propulsion	2.1	40
Total	9.33	70.16

Table 25. Daelion CubeSat Subsystem Mass and Power Budget

Daelion	Mass (kg)	Power (W)
Payload	1.3076	6.28
Structures	2	-
Power	1.695	-
Thermal	0	1.4
ADCS	0.976	3.96
COMM&DH	0.707	24.4
Propulsion	2.1	40
Total	8.98	76.04



G. Constellation Cubesats

Within the scope of the MOCHA mission, two types of CubeSats are deployed, with four of them of each type. Although they pursue different scientific objectives, both CubeSat types share similar subsystem designs; therefore, their subsequent design descriptions will be approached from a unified perspective.

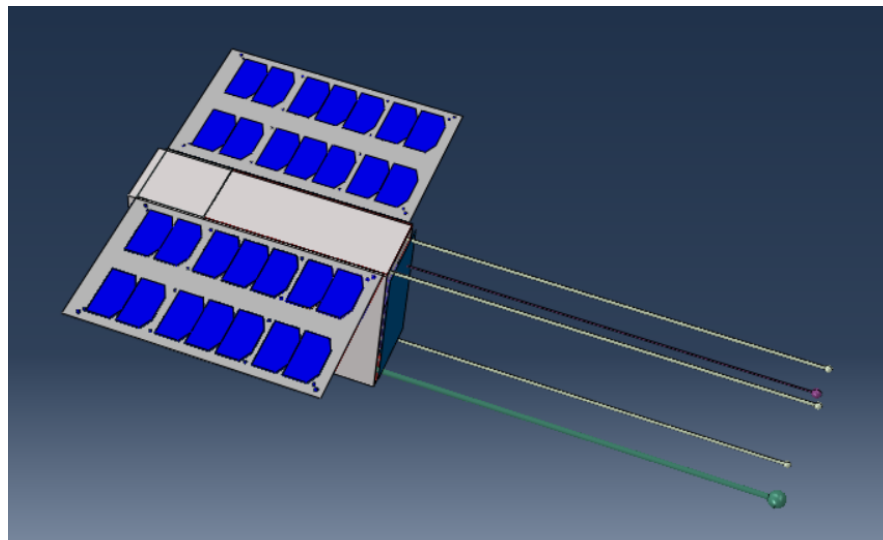


Figure 18. Oblique view of the Cosmos CubeSat with deployed solar panels and sensor booms.

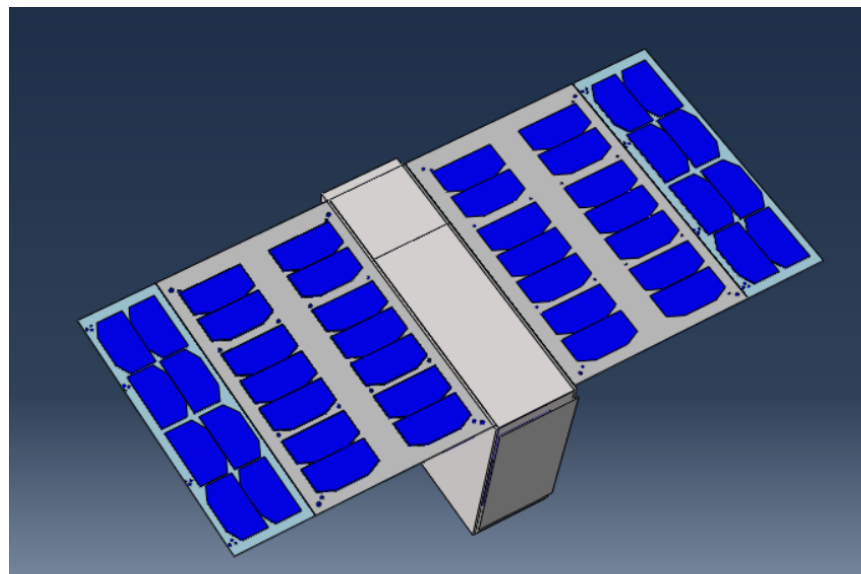


Figure 19. Exterior view of the Daelion CubeSat with deployed solar panels



G.1. Daelion Payload

The primary objective of the Daelion CubeSat is to collect in-situ measurements of temperature, density, and pressure from low Mars orbit down to the surface. To achieve this, Daelion operates in three mission phases: the Orbital Maneuver Phase, the Orbital Data Collection Phase, and the Entry Phase. The Orbital Drift Phase begins with deployment from the mothership orbiter into a 300 km circular orbit with a 77° inclination. Using its onboard propulsion system, Daelion performs a Hohmann transfer to lower its altitude to a 180 km circular orbit. Upon reaching this orbit, the Orbital Data Collection Phase begins. During this phase, the vacuum pressure sensor and accelerometer initiate in-situ sampling to measure atmospheric pressure and density. The extremely low pressure levels at altitudes between 180 km and 120 km impose strict constraints on the selection of suitable vacuum pressure sensors. The sensor requirements have been determined based on pressure data from these altitudes as provided by the Mars Climate Database. At this measurement range, sampling capability must drop to approximately 10^{-7} Pa. The selected vacuum sensor for this task due to its operational range of 1.3×10^{-7} Pa to 6.7 Pa, making it well-suited for the Martian upper atmosphere environment. The Orbital Data Collection Phase continues as the satellite's orbit is gradually lowered from 180 km to 120 km altitude, with the increasing effect of atmospheric drag.

As aerodynamic heating intensifies—particularly below 125 km altitude—the Entry Phase officially begins for Daelion. Achieving the entry phase requires the spacecraft to endure the harsh conditions encountered during atmospheric entry, despite the thin Martian atmosphere, approximately 1/100th the pressure of Earth's atmosphere. During this phase, Daelion's mission focuses on investigating one of the most critical challenges of atmospheric entry: the intense aerodynamic heating and the exothermic chemical reactions resulting from gas-surface interactions at hypersonic freestream velocities because for Mars entry missions, the design of thermal protection systems (TPS) has largely depended on numerical simulations. Daelion therefore aims to expand current understanding of entry dynamics by providing new data on aerodynamic heating and energy exchange processes, which differ significantly from those on Earth due to the polyatomic nature of carbon dioxide by combining the system used in MEDLI and QARMAN CubeSat missions at this phase. This phase aims to minimize both overdesign and underdesign of Mars entry vehicles, ensuring more accurate and optimized designs for future human exploration missions.

The instruments XPL01, XPL02, XPL03, XPL04, XPL05 and XPL06 will start sampling in Table 26 in the Entry Phase. To investigate the effects of atmospheric entry into the Martian atmosphere, a set of sensors—type K thermocouples and pressure sensors—have been strategically selected and placed at various critical locations on the spacecraft. These include placements on the forebody (stagnation point) and on the side panels of the spacecraft. This method mirrors the



sensor selections used in NASA's Mars Science Laboratory (MSL) entry system. The XPL01 sensors -thermocouples -are positioned at the front of Daelion are designed to monitor thermal loads at the stagnation point, enabling accurate heat flux measurements during peak heating as the ablative material in front of it melts. To accurately measure the extreme temperatures encountered during atmospheric entry, Type K thermocouples have been selected for Daelion. These sensors are capable of withstanding temperatures up to 1645 K, providing sufficient margin above the 1100 K maximum temperature recorded by MEDLI during its atmospheric entry.

Table 26. Overview of Scientific Sensors for Aerothermal, Stability, and Pressure Measurements

Sensor	Observed Quantity	Sampling Location	Required	Range	Sampling Altitude	Working Phase
XPL01	Amount of Heating with Thermocouples	Front of Object (2*5+4=14)	-200-1200C	up to 1645K	0-120 km	Only Entry
XPL02	Total pressure in the stagnation region,	Front of Object (3)	0 to 50 kPa	up 200 kPa	0-120 km	Only Entry
XPL03	Vehicle Stability	Side Panel (4)	0 to 50 kPa	up 200 kPa	0-120 km	Only Entry
XPL04	Laminar to Turbulence Transition	Side Panel (2)	-200-1200C	up to 1645K	0-120 km	Only Entry
XPL05	Amount of Heating with Thermocouples	Side Panel (2)	-200-1200C	up to 1645K	0-300 km	Only Entry
XPL06	Spectrally Resolved Data	Front of Object			0-300 km	Critical Altitudes & Entry Phase
Vacuum Sensor	Upper Atmospheric Pressure	Side Panel (2)	minimum 10^{-9}	1.3×10^{-7} to 6.7 Pa	100-300 km	Orbital & Entry Phase
Accelerometer	Velocity (via integrated acceleration) (internal)	Side Panel (2)				Orbital & Entry Phase



Figure 20. Interior view of the Daelion CubeSat

G.2. Cosmos

The COSMOS CubeSat mission is designed to perform in situ measurements of the electrostatic and plasma characteristics of Martian dust storms. Its primary goal is to enhance understanding of the Martian atmospheric electrical environment, which is critical for developing effective mitigation strategies against electrical hazards during future crewed landing and surface operations. COSMOS operates as part of a constellation alongside the Daelion CubeSat, with both spacecraft launched approximately every 120 days to provide complementary and simultaneous datasets that improve the overall scientific return.

The mission is divided into three distinct phases to optimize operational efficiency and data acquisition. In the Orbital Maneuver Phase, COSMOS is deployed from the mothership orbiter into a 300 km circular orbit with a 77° inclination. It then executes a number of burns over ~1 day to lower its orbit to 180 km. Scientific instruments remain inactive during this phase as the spacecraft prepares for scientific operations.

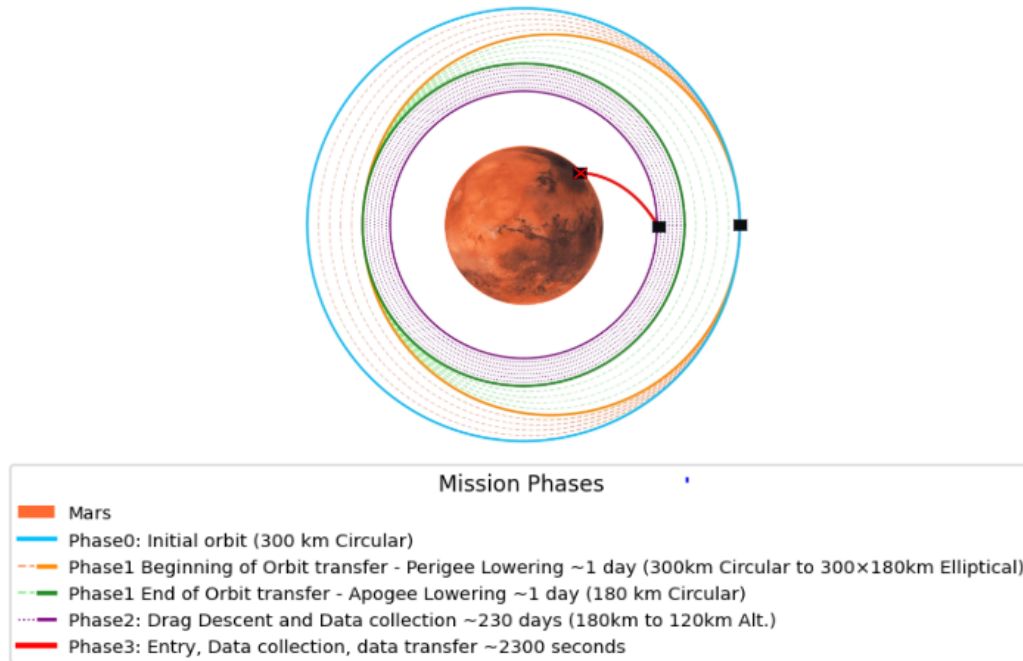


Figure 21. MOCHA Mission Phases

Upon reaching its operational orbit, COSMOS begins the Orbital Data Collection Phase, slowly descending from approximately 180 km to 120 km within the Martian ionosphere. This descent occurs due to atmospheric drag, Eq.(G.2.1), using average density values from the Mars Climate Database. As seen in Figure 22. The Langmuir Probe (LP) measures electron densities typically ranging from 2×10^4 to 5×10^5 cm⁻³ and electron temperatures between 1750 K and 2250 K, focusing especially near the main ionospheric peak around 130–140 km. The Electric Field Probes (EFPs) target the ambipolar electric fields characteristic of this region, which typically measure 1–2 µV/m and can rise up to 3 µV/m. Although the nominal sensitivity of the EFPs is 0.1 mV/m, advanced signal processing techniques enhance their effective sensitivity to detect these subtle fields. Concurrently, the Floating Potential Probe (FPP) monitors the spacecraft's floating potential relative to the plasma environment, providing essential data for correcting the electric field measurements and understanding spacecraft charging phenomena.

$$\Delta a_{rev} = -2\pi \left(\frac{C_D A}{m}\right) \rho a^2 \quad (\text{G.2.1})$$

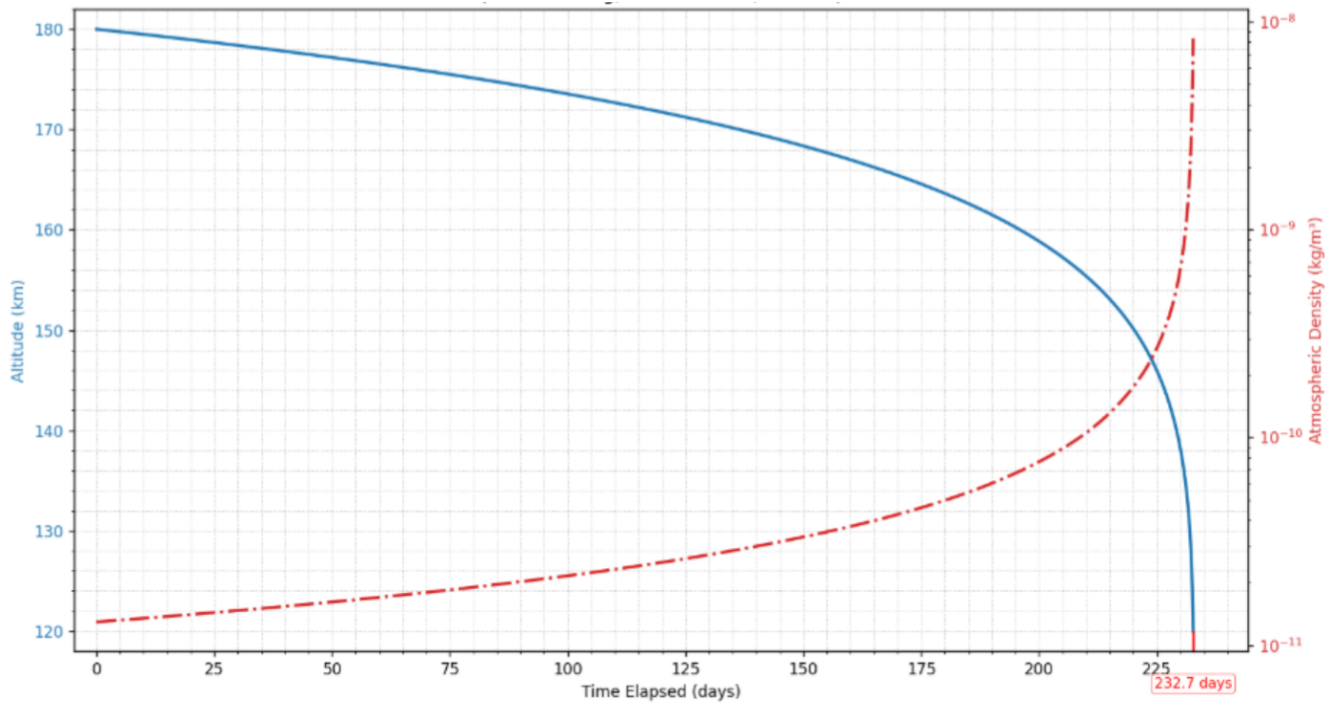


Figure 22. Langmuir Probe electron density and temperature profiles during descent.

As the spacecraft continues to descend, it enters the Entry Phase below 120 km altitude. From this point, impact with the surface is expected to occur in approximately ~ 2400 seconds. During this phase, as COSMOS descends towards the Martian surface due to atmospheric drag, it does so in a passively stabilized manner (entry descend) as a result of the strategic positioning of its center of mass and center of pressure. During this phase, the Langmuir Probe detects electron densities that can drop to as low as 10 cm^{-3} due to electron scavenging by dust particles in intense dust storms, employing optimized slow voltage sweeps and signal averaging to extend sensitivity beyond its nominal limit of about $2 \times 10^3 \text{ cm}^{-3}$. The probe also characterizes transient electron temperatures reaching $\sim 25,000 \text{ K}$ associated with electrical discharges. The Electric Field Probes measure strong triboelectric electric fields within dust clouds and dust devils, which models predict to range between 8 and 34 kV/m. A voltage divider extends the EFPs' measurable range up to $\sim 25 \text{ kV/m}$, enabling quantitative assessment of electric fields approaching Mars' dielectric breakdown limits. Throughout this phase, the Floating Potential Probe continuously records spacecraft potential variations, critical for interpreting the electrical environment in dusty, highly charged regions.

COSMOS's sensor suite, adapted from NASA's Dynamic Ionosphere CubeSat Experiment (DICE), comprises three Electric Field Probes, one Floating Potential Probe, and one Langmuir Probe. Significant design optimizations were necessary to accommodate COSMOS's compact platform constraints. The boom lengths were reduced from the original 5 meters to 1.2 meters for the EFPs and 0.8 meters for the FPP, while electrode diameters remained 15 mm for EFPs, 12 mm



for FPP, and 16 mm for the Langmuir Probe. These design choices balance measurement sensitivity and accuracy with spacecraft attitude control capabilities by minimizing interference from the spacecraft wake region, which extends roughly three times the spacecraft diameter. Deployment is managed via motorized spiral mechanisms with mechanical guides for precise and stable boom extension. The sensors are thermally protected by advanced materials such as 3M Nextel AF62 ceramic fabric, DuPont Kapton films, and Aspen Aerogels' Pyrogel XTE aerogel to withstand Mars's harsh thermal and mechanical environment. The Langmuir Probe is strategically mounted on the spacecraft's rear, offset laterally and angled to avoid contamination from the propulsion exhaust plume.

Collectively, these sophisticated sensor technologies and careful engineering ensure COSMOS can reliably capture the complex electrodynamic environment of Martian dust storms across a broad range of altitudes and conditions. The unprecedented vertical profiles and real-time measurements obtained will significantly advance the understanding of Martian atmospheric electricity and plasma physics. This knowledge is essential for designing safer and more efficient future human exploration missions on Mars, helping to mitigate risks associated with atmospheric electricity and dust storm phenomena.

Table 27. Cosmos Payloads

Sensor	Observed Quantity	Required	Range	Sampling Altitude
DICE Langmuir Probe	Electron density & temperature (via I–V curve)	10^3 – 10^{10} particles/m ³	Ion density range: 1×10^{10} to 2×10^{13} particles/m ³	130–140 (nominal); to 80–30 during descent
DICE EFP	Quasi-static & AC electric fields	± 0.01 – 10 V/m (DC); Frequency range: 0.05 Hz – 2048 Hz (AC)	± 0.1 mV/m to 5 kV/m typical Mars dust storm range	<120 (nominal); <80 during EDL
Floating Potential Probe	Spacecraft charging potential	± 1 to ± 10 V	Ion density range: 2×10^9 all altitudes but optimal to 2×10^{13} particles/m ³	at <120
ADIS16470 IMU	Velocity (via integrated acceleration)	-	Gyroscope Range: $\pm 2000^\circ/\text{s}$ Accelerometer Range: ± 40 g	not affected by altitude

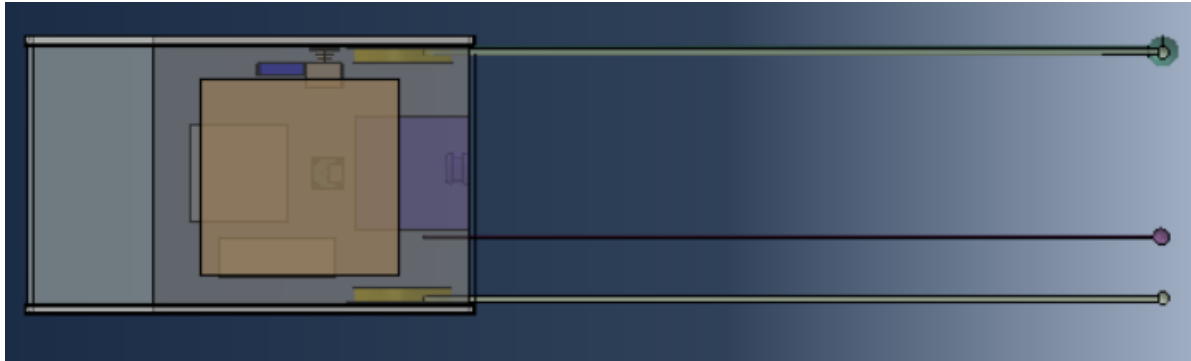


Figure 23. Top-down view of the Cosmos CubeSat

G.1.2. Propulsion System of CubeSats

Table 28. Cosmos Propulsion Requirements

Req. ID	Requirement Description
REQ-COSMOS-PROP-01	The propulsion system shall fit within the allocated spacecraft volume and mass constraints of cubesat
REQ-COSMOS-PROP-02	The selected propulsion system must have a power consumption compatible with the capabilities of CubeSat.
REQ-COSMOS-PROP-03	Cosmos shall perform a retropropulsion maneuver, applying approximately 56.64 m/s of delta-v to lower its periareion and achieve a 180 km circular orbit altitude from a 300 km circular orbit altitude.
REQ-COSMOS-PROP-04	The propulsion system must be capable of desaturating all external torques acting on the CubeSat throughout its mission lifetime from the ADCS

Cosmos is powered by the Aerojet Rocketdyne MPS-130 green monopropellant propulsion system, using AF-M315E. This propulsion system enables Cosmos to perform a single, essential Hohmann transfer maneuver from its initial 300 km deployment orbit down to a 180 km circular orbit. The propulsion architecture features four thrusters, each capable of delivering thrust within a range of 0.25 to 1.25 newtons. It operates with a specific impulse between 206 and 235 seconds and provides a total system impulse of 6000 N·s. The full wet mass of the propulsion system is 1.66 kg, with a dry mass of 1.06 kg and 0.5 kg of usable monopropellant.

The transfer of the spacecraft, with an initial mass of 11.00 kg, from a 300 km circular orbit ($i=77^\circ$) to a 180 km circular orbit ($i=77^\circ$) around Mars will be achieved through a gradual sequence of multiple short burns. This approach is used to prevent undesirable orbital disturbances that a single, long-duration burn might cause. The total delta-v applied during this orbit transfer, which will last for a total of 49.94 hours (2.08 days) (including time in orbit and burn durations), will be 56.64 m/s. These maneuvers will be efficiently applied at apoareion and periareion, and are expected to consume 0.2800 kg of



propellant from the 0.50 kg of available propellant. Before each burn sequence, the catalyst beds of all four (4) nozzles connected to the fuel system will be heated; these four nozzles collectively provide a total thrust of 5 Newtons. Once this heating is complete, the burns will proceed as planned. To lower the orbit's periareion to an altitude of 180 km, a series of short retropropulsion burns, each lasting approximately 5 seconds, will be applied near apoareion. Subsequently, to circularize the orbit at a 180 km altitude ($i=77^\circ$), another series of short retropropulsion burns, each lasting approximately 5 seconds, will be applied near periareion. As a result of these maneuvers, the remaining usable propellant will be 0.2200 kg, and the final mass of the spacecraft is calculated to be 10.743 kg.

The propulsion system is also capable of desaturating the reaction wheels as needed, counteracting torque accumulated from external disturbances such as aerodynamic forces, gravity gradient, and solar radiation. Throughout the CubeSat's ~230-day lifetime, it will deliver a total desaturation performance equivalent to ~6 m/s.

G.1.3. Propulsion System Down-Selection

Previously, electric propulsion systems were primarily considered for CubeSats. While the high Isp values and high total delta-v capabilities of electric propulsion systems can provide significant maneuverability, they were not chosen due to their high power requirements and the considerable extension of maneuver durations. Particularly for Mars, where solar irradiance is much lower compared to Earth, the use of an electric propulsion system is not very realistic.

G.4. Communications and Data Handling

The CubeSats' communication system must be capable of maintaining a link with the orbiter during the communication window, even under worst-case conditions. In this context, CubeSats are expected to transmit data collected by scientific instruments during orbital drift, orbital phase, and entry to the orbiter. Additionally, as a backup during entry, they must also relay data to existing orbiters around Mars. The communication subsystem requirements for the CubeSats are as follows:

Table 29. CubeSats Communication Requirements

Req. ID	Requirement Description
REQ-MOCHA-COMM-03	CubeSats will maintain communication with the orbiter and transmit data at a maximum rate of 400 kbps within the allocated communication window.
REQ-MOCHA-COMM-04	CubeSats shall transfer the data acquired during the entry phase following the conclusion of the blackout period therein.



REQ-MOCHA-COMM-05

CubeSats shall possess the capability to perform relay communication by transmitting data to vehicles orbiting Mars as a backup method.

G.4.1. The Data Budget

In the data handling subsystem design of our CubeSat platforms, two primary requirements were defined: the onboard computer must possess sufficient processing capability to handle data streams originating from the payloads, housekeeping system, and main operating system; and the data storage unit must be capable of retaining the accumulated mission data during prolonged blackout periods.

Table 30. Daelion Data Budget

Daelion	Quantity	Sampling Frequency (Hz)	Data Size	Total Data Rate(kbps)
IGM400 Hornet	2	1	64	0,128
ADIS 16740 IMU	2	4	96	0,768
Total (%50 Margin)				1,3446
XPL-01	14	8	16	1,792
XPL-02	3	8	16	0,384
XPL-03	4	8	16	0,512
XPL-04	2	16	16	0,512
XPL-05	2	8	16	0,256
XPL-06	1	4	512	2,048
IGM400 Hornet	2	2	64	0,256
ADIS 16740 IMU	2	16	96	3,072
Total (%50 Margin)				13,248

Since Daelion CubeSat has two different phases we need different data budgets for the best selection of the best On-Board Computer and storage combination.

Table 31. Cosmos Data Budget

Cosmos	Quantity	Sampling Frequency (Hz)	Total Data Rate(kbps)
m-LNP	1	35	0,56
DICE EFP	1	35	0,56
FPP	1	35	0,56
ADIS 16740 IMU	1	2	0,192
Total(%50 margin)			2.8082



Cosmos actually has two modes but since our sweep mode is rarely used and has less data rate we need to only calculate the nominal modes data rate.

As shown in the table above, the highest data load is expected during the entry phase, due to simultaneous operation of payload instruments and constant housekeeping telemetry. The worst-case total data rate in this phase was determined to be approximately 13,248 kbps by the Daelion CubeSat at the entry phase.. Given the communication constraints and potential delays, a blackout duration of 15 days was defined as the sizing requirement for storage capacity. Over this period, a continuous 13,248 kbps data rate results in a required storage capacity of approximately 2GB. Which is not needed since our entry phase will last only 2400 seconds.

G.4.2. The Link Budget

The link budgets were calculated based on the formulas provided in the Orbiter Communications section, considering the specifications of the selected hardware and accounting for worst-case scenarios. The range was calculated using geometric analysis to determine the maximum distance at which the CubeSats and the orbiter can maintain line-of-sight communication within Mars orbit.

Table 32. CubeSats Link Budgets

Parameter	CubeSats to Orbiter (S-band)	CubeSats to Orbiter (UHF)	Orbiter to CubesSats	Unit
Eb/No (required)	9	9	9	dB
Data Rate	400000	200000	100000	bps
Transmit Antenna Gain	0	2	5	dBi
Carrier Frequency	2.2	0.42	0.42	GHz
Range	1950	1950	1950	km
FREE SPACE Path Loss	165.1	150.7	150.7	dB
Atmospheric Loss	0.64	0.71	0.71	dB
Receive Antenna Gain	8	5	2	dBi
Received Signal Power	-120.7	-107.4	-114.4	dBm



Eb/No (achieved)	16.8	36.1	36.1	dB
Link Margin	7.8	27.1	27.1	dB

According to the link budget calculations, all communication links between the CubeSats and the Orbiter can be maintained with a sufficiently strong signal strength.

G.4.3. Blackout

During atmospheric entry, communication blackout occurs when the ion frequency of the plasma sheath surrounding the spacecraft exceeds the communication frequency, leading to severe signal attenuation or complete signal loss. This phenomenon poses a significant challenge for CubeSats entering Mars, as they are intended to impact the surface and will not survive to retransmit data. Therefore, maintaining a continuous data flow throughout the entry phase is crucial to prevent data loss. The severity and duration of the blackout are influenced by factors such as antenna orientation and orbital positioning. Additionally, employing multiple communication links with existing Mars orbiters can mitigate the effects of the blackout, ensuring that critical data is relayed despite temporary communication disruptions. Here are the critical plasma densities for various communication frequencies during entry:

Table 33. Critical Plasma Densities and Communication Frequencies [5]

Signal Frequency	UHF 381 MHz	S-band 2.295 GHz	X-band 8.43 GHz	Ka-band 32 GHz
Plasma Density	$1.8 \times 10^9 \text{ cm}^{-3}$	$6.5 \times 10^{10} \text{ cm}^{-3}$	$8.8 \times 10^{11} \text{ cm}^{-3}$	$1.27 \times 10^{13} \text{ cm}^{-3}$

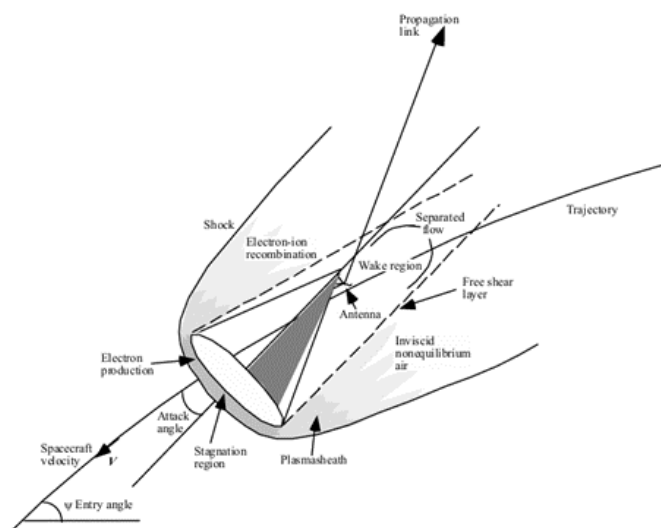


Figure 24. Diagrammed View of Spacecraft Entering the Martian Atmosphere [5]



Based on the entry analysis conducted for the CubeSats, the plasma density profile as a function of altitude was determined as follows:

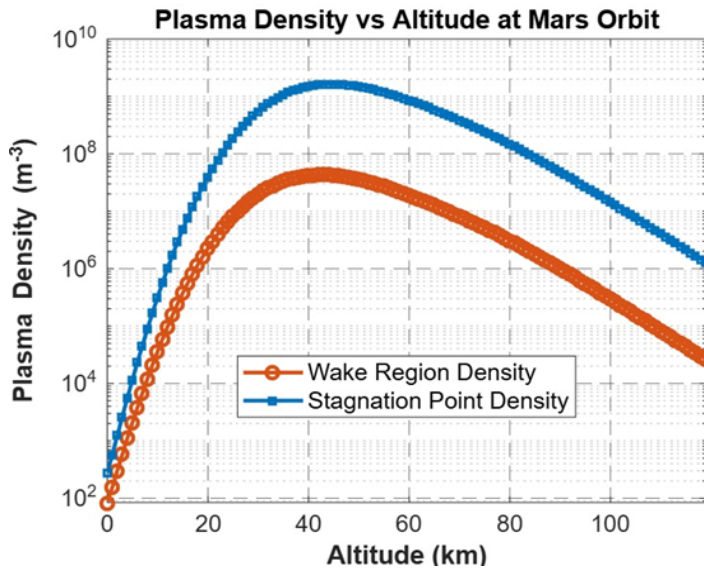


Figure 25. Plasma Density vs Altitude at Mars Orbit

G.4.4. Trade-Offs

The primary system components were selected according to defined requirements and operational limitations.

G.4.4.1. Command and Data Handling

Considering these requirements, the selected onboard computer, IMT CubeSat OBC, was chosen for its processing performance since it can reach a maximum data rate of 500kbps. The unit supports sufficient computational throughput to handle all expected mission data, even under a 50% margin scenario. offering a capacity significantly above the 2GB requirement, with the ability to store mission data up to 8 GB under worst-case blackout conditions[17]

The selected storage unit is rated for 20 krad TID, and although this level of radiation tolerance is limited for interplanetary missions, the relatively short mission duration and the small form factor of the CubeSats allow for localized radiation shielding to mitigate risks. Additionally, both the onboard computer and storage subsystem incorporate TMR (Triple Modular Redundancy) architecture, providing robust protection against bit-flips and other single-event upsets (SEUs), thereby ensuring reliable processing and data integrity throughout the mission.

G.4.4.2. Transceiver and Antenna Selection

CubeSats transmit data in three phases, each with distinct communication needs. During orbital drift, data rates are low,



making UHF preferable due to its lower power consumption. In the orbit phase, data volume increases, making S-Band more suitable for higher data rates. In the entry phase, communication strategy is determined by blackout risk and orbiter visibility. While the entry plan aims to maintain line-of-sight with the orbiter, UHF is necessary for relaying data to existing Mars orbiters if visibility is lost. However, due to its lower frequency, UHF experiences blackouts at 30-60 km altitude, while S-Band remains more reliable, as indicated in **figure 11** based on the critical density values in **Table 28**. Thus, using both bands during entry improves data transmission reliability. CubeSats also require a UHF receiver for occasional commands from the orbiter, given the low data rate requirements. To meet these communication needs, they are equipped with the NANOLink-boost-dp Gen2 and Margas The UHF Transceiver. The NANOLink-boost-dp Gen2's diplexer allows both antennas to function as transmitters and receivers, creating a near-omni configuration through multiple antenna placements. For UHF, an omnidirectional antenna mitigates potential ADCS pointing issues. Details of these hardware components, are provided in the Hardware Properties section **Table 29**.

G.4.5. Communications Subsystem Overview

The maximum data rates generated by the CubeSats 244 kbps and 386 kbps are within link capacity, ensuring successful data transmission to the orbiter even under worst-case scenarios. These rates were calculated based on orbital analysis, accounting for the maximum contact gap and the average communication window. At 180 km altitude, the average communication window for CubeSats is 630 seconds, while the maximum duration without contact is approximately 126,000 seconds. During the window, the S-Band transceiver can transmit data at up to 1.2 Mbps, providing sufficient bandwidth for data transfer. To buffer data during extended contact gaps, each CubeSat is equipped with 8 GB of onboard storage. In the orbit phase, Daelion and Cosmos generate 12.96 MB and 24.8 MB of data per day, respectively, which can be effectively managed within the specified storage capacity until the next communication window.

G.4.5.1 Hardwares Properties

Table 34. CubeSats Communication Subsystem Hardwares [26] [27] [28] [29]

Type	Name	Quantity	Mass (kg)	Power Consumption Rx (W)	Power Consumption Tx (W)
Transceiver	NANOLink-boost-dp Gen2	1	0.385	0.62	24
	Margas The UHF / VHF Transceiver	1	0.025	0.13	3.3



Type	Name	Quantity	Mass (kg)	Power Consumption (W)	Gain (dB)
Antenna	Anywaves-S-Band-TT&C-Antenna	2	0.272	-	6.5 / 4.5 / 0
	AAC ANT-100	1	0.025	-	2
Type	Name	Quantity	Mass (kg)	Power Consumption (W)	Storage(GB)
OBC-Storage	IMT CubeSat OBC	1	0.038	0.3	8
Total			0.745	1.05	

G.1.4. Attitude Determination and Control

In Table X, a certain thrust vector control in orbit transfer mode gives accurate propulsion, proper trajectory, and fuel efficiency. For orbital drifting mode, $\pm 0.478^\circ$ accuracy is to be ensured for maximum power and operationally best solar panel orientation. For entry mode, hypersonic stability is required for preventing structural deformation, safe reentry, and to enable the Cosmos to endure extreme atmospheric conditions during making scientific measurements.

Table 35. Attitude Stability and Accuracy Needs for Different Mission Phases

Mission Phase	Required Attitude	Accuracy Requirement	Duration
Orbit Transfer Phase	Correct attitude for thrust	Thrust vector: $< 1^\circ$	~ 1 day
Orbital Drifting Data Collection Phase	Solar panels facing the Sun	Sun angle $< 45^\circ$	When sunlight is available
Orbital Drifting Data Collection Phase	Solar panels angle of attack $\alpha < 0.478^\circ$ to reduce drag	Solar panel angle of attack pointing accuracy: approx. $\pm 0.478^\circ$	Continuous
Entry Phase	Correct attitude for thrust, Maintain stability of CubeSat at hypersonic velocity during atmospheric reentry	Thrust vector: $< 1^\circ$	Entry duration (< 10 min)

Our satellite has a constant drag area. As depicted in the visual, with the Probes remaining on the -x axis, the +x direction, as



seen in Figure 26, will always face the ablative material section. The reference area will be constant at 0.02m^2 . To ensure our drag area can be managed with a precision of 0.001, there is a risk that the solar panels, as shown, could increase the effective area. To manage this situation, the solar panels' angle of attack (α) has a pointing accuracy value corresponding to an error margin based on our specified precision, with movement within the range of $-0.4774^\circ \leq \alpha \leq 0.4774^\circ$.

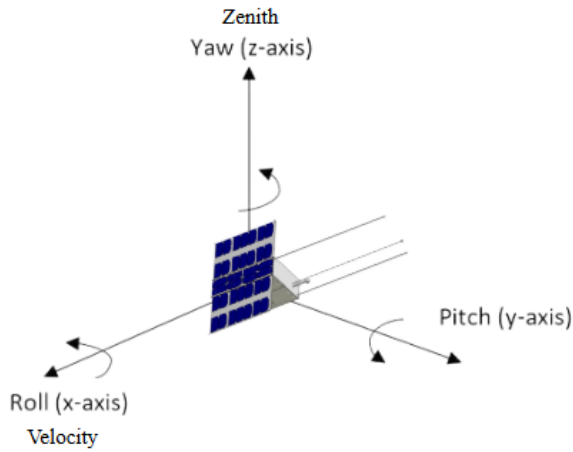


Figure 26. Satellite body-fixed coordinate axes: x-axis (roll), y-axis (pitch), z-axis (yaw), and velocity vector.

A similar approach was applied with calculations made after the Orbiter's ADCS requirements.. The CubeSat's moments of inertia are calculated to determine its resistance to rotational movement along each axis. Using these values, the required angular acceleration is computed based on the desired orientation change and maneuver duration. Subsequently, the torque necessary to achieve the angular acceleration is determined. The AAC Clyde Space RW222 reaction wheel was selected based on these calculations, as it provides sufficient momentum storage and torque capacity to meet the CubeSat's attitude control requirements. For the sensors, 1 AAC Clyde Space ST200 star tracker, 1 Honeywell HG4930 IMU, 6 NSS CubeSat Sun Sensors and 2 CubeSpace CubeSense horizon sensors were selected. When selecting sensors, their ability to determine altitude with the desired accuracy and their durability in the Mars environment (in terms of radiation and temperature) were taken into account.

G.1.5. Power

For our CubeSats the same categorization and phase categories were used for power system design. Since the calculations for the panel size are the same we can easily find the needed solar panel area. The only difference is that our CubeSat's mission time is about 1 year rather than our orbiter's 4 year usage of solar panels.



Table 36. CubeSat Power Budget

Cosmos	Orbit/Eclipse	Entry(2400s)	Daelion	Orbit/Eclipse	Entry(2400s)
Payload	0.435 W	0.435 W	Payload	3 W	6.28 W
ADCS Sensor	3.325 W	3.325 W	ADCS Sensor	3.36 W	3.36 W
ADCS Actuator	0.6 W	0.6 W	ADCS Actuator	0.6 W	0.6 W
Comms Rx	0.13 W	24W Total	Comms Rx	0.13 W	24 W Total
Comms Tx	17 W (65.83s active)		Comms Tx	17 W (65.83s active)	
Data	0.4 W	0.4 W	Data	0.4 W	0.4 W
Thermal	1.4 W	1.4 W	Thermal	1.4 W	1.4 W
Total(%20 Margin)	28 W	36 W	Total(%20 Margin)	31 W	43 W

To determine the solar array sizing, the orbit and eclipse phases were analyzed in detail. Since these CubeSats orbit around Mars between 180km and 120km until entry, We used the worst case orbit to calculate the eclipse times. At 120 km orbit we have a worst case of eclipse of 2615,18 seconds and best case of 0 seconds so for our solar array calculations we used the average value of 1307,84 seconds of eclipse and the remaining case of 5021,92 seconds of orbit time. Using the calculated sunlight and eclipse durations in our orbit, we calculated the required energy production of the solar panels.

The solar panel cell selection is the same with the orbiter and based on the same parameters, the required solar panel area was calculated, and the optimal configurations were determined. Our solar panel size requirements are $0,1134\text{m}^2$ and $0,1580\text{m}^2$. Meaning that we need to use 6U and 9U solar panels for Cosmos and Daelion. For the Cosmos, panels from DHV-6U Series body-mounted solar panels have been selected with two 3U solar panels, while the Daelion will utilize an enhanced configuration with three panels of the same model using a three-fold mechanism. The estimated mass of the solar panel systems is 600 g for the 6U configuration and 900 g for the 9U configuration [9].

The second major design focus is energy storage, particularly battery capacity. To address the worst-case scenario, we considered the combined eclipse and entry phases, during which no power is generated from solar panels. Therefore, all required power must be supplied by the onboard batteries. Then calculated by the time of the eclipse but this time not the average but the actual 2615.18 seconds worst case of eclipse and the entry with relative power consumptions. We used a 0.9 efficiency of batteries and a DoD value of 0.5. Based on this analysis, the required energy storage was found to be 60.51 Wh for the Cosmos and 79.32 Wh for the Daelion. As a result, the EPS and battery system DHV MicroEPS power system configured with one Motherboard (MB) and one Daughterboard (DB), providing a total capacity of 100 Wh has been selected to meet these storage demands efficiently within size and weight constraints [10]. This selection's weight is 795 g.



Finally, in the maneuver phase, the system must support the instantaneous power demand of the onboard propulsion unit. While this phase is short in duration and does not significantly impact overall energy storage requirements (0,22Wh), it introduces high peak power demands that must be handled by the EPS. The propulsion system draws 3.3 A at 12 V, and our selected EPS/battery configuration is capable of supporting this load reliably since it can support 5 A at 12 V and the power load since it can support around 60W of power [23].

G.1.6. Thermal Control Systems

Table 37. COSMOS and Daelion's Thermal Requirements

Req. ID	Requirement Description
REQ-COSMOS-TPS-01 REQ-Daelion-TPS-01	The internal electronics shall be protected to maintain operational temperatures within -20°C to $+60^{\circ}\text{C}$. The protection must prevent thermal drift and failure during both the entry thermal pulse and orbital eclipse/day cycles.
REQ-COSMOS-TPS-02 REQ-Daelion-TPS-02	The CubeSat shall be protected from aerodynamic heating and thermal shock during reentry, with temperatures exceeding 1100°C at the stagnation point. The TPS must prevent damage to sensitive components.
REQ-COSMOS-TPS-03 REQ-Daelion-TPS-03	The CubeSat shall be shielded from solar radiation, orbital thermal cycling, and temperature fluctuations during the orbital phase. The spacecraft must also survive eclipse conditions, where external temperatures can drop significantly, which may lead to cold-soaking of the internal components.
REQ-COSMOS-TPS-04 REQ-Daelion-TPS-04	The CubeSat shall protect antennas and solar panels from thermal stress and structural damage during reentry and orbital conditions.
REQ-COSMOS-TPS-05 REQ-Daelion-TPS-05	The CubeSat's side panels shall prevent thermal conduction during reentry and orbital phases to avoid overheating of internal systems.
REQ-COSMOS-TPS-06 REQ-Daelion-TPS-06	Internal sensor electronics (e.g., spectrometer, vacuum sensor, IMU) shall be thermally isolated to remain within $0\text{--}60^{\circ}\text{C}$ throughout orbit and descent phases.
REQ-COSMOS-TPS-07	The CubeSat's boom-mounted sensors shall be protected from extreme thermal exposure during entry and orbit to avoid thermal degradation.
REQ-Daelion-TPS-07	The front-facing sensors (XPL01, XPL02, XPL05, XPL06) shall withstand temperature peaks of up to 1100°C , as required by the XPL01/XPL04 thermocouple locations.
REQ-Daelion-TPS-08	Materials on side panels housing XPL03, XPL05, IGM400, and IMU shall resist thermal gradients and possible plasma flow exposure during EDL down to 90 km altitude.

G.1.6.1. Thermal Analysis

Thermal balance analysis of a 6U CubeSat orbiting Mars at an altitude of 300 km was modeled. The analysis aims to determine the equilibrium temperatures of the CubeSat in direct sunlight and during an eclipse. In the space environment



there are only heat sources by the means of radiation. They can be grouped as solar radiation, planet infrared radiation and albedo radiation.

The Sun is the biggest source of heat in Mars orbiting satellites, which are not in eclipse. It can be modeled like a blackbody with 5762 K temperature. This means, on Mars, a solar constant is 589 W/m². This radiation flux will meet spacecraft surfaces. Heat flux from sun on a spacecraft surface can be calculated as

$$q_{solar} = \alpha G_s A_{surface} \cos\theta \quad (\text{G.1.6.1.1})$$

where, α is solar absorbance, G_s is solar constant, $A_{surface}$ is the surface area subjected to solar constant, θ is the angle between surface normal and solar rays.

Just like the sun, Mars can also be modeled like a blackbody. Equivalent blackbody temperature is 209.8K for Mars's radiation.[41]

$$q_{planetay} = \varepsilon A_{surface} \cos\theta F \sigma T_{planet}^4 \quad (\text{G.1.6.1.2})$$

ε is infrared emissivity, $A_{surface}$ is the surface area of spacecraft that can see Mars's radiation rays, θ is the angle between surface normal and Mars's center, σ is Stefan-Boltzmann constant, T_{planet} is planet temperature. F is the view factor (also called shape factor and angle factor). Basic approaches that can be used for preliminary analysis.

$$F = (R_{Mars} / R_{orbit})^2 \quad (\text{G.1.6.1.3})$$

Albedo is the radiation, which actually originated from the sun but reaches the satellite by reflecting from a planet. For preliminary analysis an average value of 0.25 can be used.

$$q_{albedo} = \alpha G_s F a \cos\phi k \quad (\text{G.1.6.1.4})$$

a is albedo coefficient, G_s is solar constant, F is view factor, α is solar absorbance, ϕ is solar zenith angle, k is a dimensionless factor, which accounts for the reflection of collimated incoming solar energy off a spherical Mars and calculated as

$$k = 0.657 + 0.54(R_{Mars} / R_{orbit}) - 0.196(R_{Mars} / R_{orbit})^2 \quad (\text{G.1.6.1.5})$$

Thermal Balance Analysis

Preliminary thermal analysis can be done by energy balance between heat received and radiated. Then the following equation is obtained.

$$q_{in} = q_{out} \quad (\text{G.1.6.1.6})$$

Sun light condition :



$$q_{solar} + q_{planetary} + q_{albedo} = q_{radiated} \quad (\text{G.1.6.1.7})$$

$q_{radiated}$ is the radiated energy by spacecraft to deep space. It depends on optical properties of surface and surface temperature.

$$q_{radiated} = q_{emitted\ rad} = \varepsilon A_{surface} \sigma (T_{surface})^4 \quad (\text{G.1.6.1.8})$$

Since each surface of the satellite has different temperatures, it must be calculated separately for each surface and then added together.

Eclipse condition

In eclipse conditions, the only heat source is planetary radiation. And only one surface is subjected to planetary radiation but all surfaces will radiate to deep space.

$$q_{planetary} = q_{radiated} \quad (\text{G.1.6.1.9})$$

$$\varepsilon A_{surface} (\cos\theta) F \sigma (T_{Mars})^4 = \varepsilon A_{surface} \sigma (T_{surface})^4 \quad (\text{G.1.6.1.10})$$

As a result of the calculations, it has been determined that the equilibrium temperature of the CubeSat is 316.47 K (43.32 °C) when it is directly exposed to solar radiation and receives both infrared radiation emitted by the planet and reflected solar radiation from the planet's albedo. This temperature corresponds to the equilibrium reached when the maximum energy input from the Sun-facing surface of the satellite is balanced by the radiation emitted from all its surfaces.

During the eclipse period, when the CubeSat enters Mars' shadow, the direct and reflected (albedo) heat inputs from the Sun disappear. Under these conditions, only the infrared radiation originating from the planet's intrinsic temperature is considered as heat input. In this case, the equilibrium temperature of the CubeSat is calculated to significantly decrease to 145.32 K (-129.83 °C). These two extreme temperature values define the thermal range that the CubeSat will experience along its orbit, playing a critical role in developing the necessary thermal control strategies to ensure that the satellite's subsystems and components can operate safely within this temperature range. [40]

G.1.6.2. Thermal Control Systems

The thermal protection subsystem (TPS) of the Daelion and Cosmos CubeSats is meticulously designed to maintain all spacecraft subsystems within their specified operational temperature limits throughout the mission. This mission involves maintaining circular orbits from 300 km down to 120 km altitude around Mars, followed by atmospheric entry below 120 km. This exposes the spacecraft to a broad spectrum of thermal stresses requiring a comprehensive passive thermal control system optimized for CubeSat constraints and power limitations.



The thermal environment between 300 km and 120 km orbit is highly dynamic, influenced by Mars' elliptical orbit and seasonal variations, causing solar irradiance levels to fluctuate approximately between 550 and 650 W/m². Additionally, Mars' surface reflects solar radiation with an albedo of about 0.25, contributing an extra radiative load of 50 to 150 W/m² at orbital altitude, which varies depending on local terrain and dust conditions. The planet also emits infrared radiation in the range of 100 to 130 W/m², increasing as the spacecraft approaches the surface. These factors cause cyclical heating and cooling of the spacecraft surfaces, further intensified by periodic eclipses lasting 15 to 20 minutes. These rapid transitions impose thermal shock risks to sensitive electronic and mechanical systems. Below approximately 180 km altitude, increased atmospheric density leads to slight aerodynamic drag heating, although this effect is minor compared to radiative heating.

Each subsystem is designed to operate reliably within specific temperature limits under these challenging environmental conditions. The power subsystem—which includes the battery and the Electrical Power System (EPS)—requires careful thermal management. The battery functions safely between -40°C and +70°C, with optimal charging conditions between +10°C and +45°C. The EPS electronics maintain functionality between -40°C and +85°C. Within the 300–120 km orbital range, the battery is particularly vulnerable to freezing, risking capacity loss and damage. To mitigate these thermal risks, both the battery and EPS electronics are housed within a Survival Unit featuring 5 to 10 mm of Pyrogel aerogel insulation, which provides an exceptionally low thermal conductivity barrier (~0.02 W/m·K). A 3 mm aluminum heat spreader distributes internally generated heat evenly, preventing cold spots. The assembly is further insulated by a 15-layer Multi-Layer Insulation (MLI) blanket made of aluminized Kapton films separated by Dacron mesh spacers, approximately 5 mm thick and weighing about 100 grams. The MLI's white thermal control coating reduces solar absorptivity to approximately 0.2 and maintains infrared emissivity near 0.7, minimizing radiative heat loss during eclipses and reducing heat gain during sunlit periods. This passive system preserves the battery and EPS within operational temperatures without the need for active heating, thus conserving onboard power.[41]

On-Board Computer (OBC) faces the dual challenge of potential overheating during extended sunlit exposure and thermal shock during rapid transitions into Mars' shadow. The OBC operates between -20°C and +70°C and is sensitive to these temperature extremes. It is enclosed within the same Survival Unit and benefits from the Pyrogel insulation and aluminum heat spreader. Additionally, thermal spreaders composed of graphite or aluminum composites are installed beneath the OBC's printed circuit boards to ensure uniform heat distribution and prevent localized hotspots. The OBC is further insulated with a localized MLI blanket consisting of 12 to 15 layers of aluminized Kapton films with a total thickness of about 7 mm, reducing radiative thermal cycling during orbit and atmospheric entry.



Attitude Determination and Control System (ADCS) components, operating between -20°C and $+50^{\circ}\text{C}$, are sensitive to increased mechanical friction and sensor noise at low temperatures. To reduce heat conduction to the spacecraft bus, ADCS elements are mounted with low thermal conductivity materials such as PEEK or Vespel. They are additionally wrapped in localized MLI blankets made of 10 to 12 aluminized Kapton layers separated by polyester spacers, with thicknesses of 3 to 5 mm. These blankets are coated with white thermal control paint to reduce solar absorptivity (~ 0.2) and increase infrared emissivity (~ 0.7), stabilizing the temperature environment during thermal cycling. This passive insulation dampens the thermal cycling effects experienced during orbital eclipse and sunlight phases, maintaining ADCS functionality without power-consuming active heaters [30].

Communications subsystems encompass transceivers that operate in temperature ranges from -40°C to $+85^{\circ}\text{C}$ and antennas that tolerate from -120°C to $+120^{\circ}\text{C}$ or -40°C to $+80^{\circ}\text{C}$ depending on the model. Transceivers are housed within the Survival Unit or covered with dedicated MLI blankets (5 to 7 mm thick) to protect against thermal fluctuations. Antennas, however, are mounted externally on deployable solar panels and thus are not covered with MLI to avoid deployment complications. Instead, these external surfaces receive a matte white paint and fluorinated ethylene propylene (FEP) coating, providing low solar absorptivity (~ 0.2), high infrared emissivity ($\sim 0.85\text{--}0.90$), and strong resistance against UV radiation and dust abrasion. This coating system's flexibility accommodates thermal cycling and mechanical motion without degradation.

The propulsion system requires operation between $+5^{\circ}\text{C}$ and $+60^{\circ}\text{C}$ to prevent propellant freezing and valve malfunction. It remains outside the Survival Unit and is passively protected by localized MLI blankets of 3 to 5 mm thickness and thermally isolating mounts, supplemented by thermal mass elements to buffer temperature variations. This configuration ensures readiness for maneuvers during orbit without active thermal control.

The spacecraft's most extreme thermal threat occurs during atmospheric entry, where stagnation point heating ranges approximately between 1100°C and 2000°C , depending on entry velocity and atmospheric density. It is important to note that Earth's atmosphere is significantly denser than Mars', leading to higher aerodynamic drag and consequently higher thermal loads during Earth reentry missions. Inspired by the successful QARMAN CubeSat mission, which employed a P50 cork ablative shield with proven thermal protection and extensive testing, Daelion adopted the same material for its ablative heat shield. The key difference lies in the thickness of the P50 cork layer: because Mars' atmosphere is much thinner, the ablative shield for Daelion is designed to be thinner than that used in QARMAN's Earth reentry.[43]

Ablative thermal protection materials, specifically P50 cork, are employed in Daelion and Cosmos CubeSats to withstand the extreme temperatures encountered during atmospheric entry, which can range approximately from 1100°C to 2000°C .



depending on entry velocity and atmospheric density. Mars' atmosphere is significantly less dense than Earth's, resulting in lower aerodynamic drag forces and consequently reduced stagnation point heating during entry. This fundamental difference allows for a thinner ablative layer on Mars compared to Earth.

Inspired by the QARMAN CubeSat mission—which successfully utilized P50 cork as its ablative shield and validated its thermal performance through extensive testing—Daelion adopts the same material while customizing the shield dimensions to a 2U volume to meet mission-specific constraints. Crucially, Daelion incorporates sensors identical to those employed on QARMAN embedded within the ablative layer to record thermal and pressure data during entry. For these sensors to perform accurate measurements, the ablative cork must erode sufficiently during entry, exposing the sensor surfaces. Since Mars entry temperatures are lower than those encountered in Earth reentry, the ablative layer thickness is reduced relative to QARMAN's Earth configuration to ensure appropriate erosion timing and sensor exposure.[43]

This integrated passive thermal protection system, consisting of ablative shielding, Pyrogel aerogel insulation, Multi-Layer Insulation blankets, low-conductivity mounting materials, thermal spreaders, and matte white paint with FEP coating, collectively ensures that all subsystems maintain thermal stability during Mars orbital operations and atmospheric entry. It prevents freezing, overheating, and thermal shocks, adhering to CubeSat mass and power constraints, thereby safeguarding mission success.

G.1.7. Structural Subsystem Overview

G.1.7.1. Cubesat Structure

For our Cubesat structures, GomSpace's 6U size structure frame was preferred. This choice was based on high reliability, proven design in space missions and compliance with standards. The GomSpace 6U structure has been optimized both in terms of mechanical durability and thermal management, as it has demonstrated and demonstrated that it meets the test requirements. It also features a modular design that allows efficient use of internal volume. It facilitates the integration of subsystems such as scientific instruments, power systems and communication units, and is designed to be compatible with various launch systems.

For our Cubesat structures, GomSpace's 6U size structure frame was preferred. This choice was based on high reliability, proven design in space missions and compliance with standards. Made of aluminum 7075-T7351, it offers high mechanical strength despite its low mass. The mounting rings allow flexible placement of the internal hardware, allowing the integration



of PC104 stacks in different orientations. In addition, four kill switches provide safety for automatic activation after disconnection. The large surface area makes it suitable for external mounting of solar panels, antenna systems and scientific loads. All connection holes use a helicoil as a screw locking system, which ensures robustness and safety in long-term duty. In addition, the GomSpace 6U structure, which has clearly demonstrated that it meets the test requirements, is optimized both in terms of mechanical durability and thermal management.

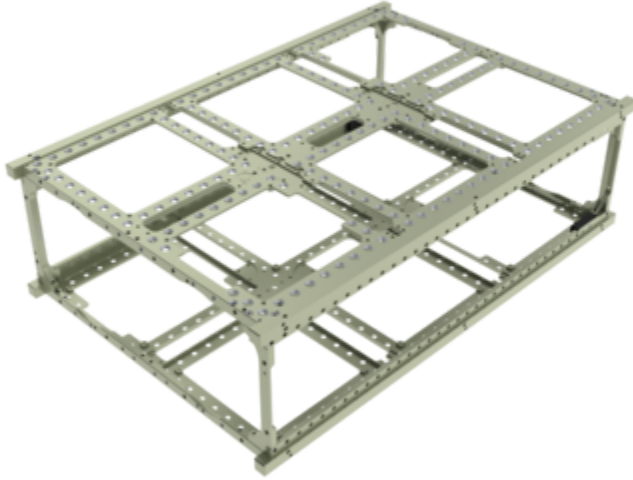


Figure 27. GomSpace's 6U size structure frame



H. Risk Analysis and Mitigation

Data-Based Risk Mitigation

The mission faces two major data-related risks: long-duration communication blackouts that may lead to data overflow, and radiation-induced Single Event Upsets (SEUs) affecting onboard data handling. To address the first, the Orbiter includes 1 TB of solid-state storage with lossless compression and priority-based data queuing to ensure critical data retention during up to 30 days of downlink delays. For SEU mitigation, all key computers and memory units are radiation-hardened and supported by EDAC, watchdog resets, and a Triple Modular Redundancy (TMR) architecture on both the Orbiter and the CubeSats. These measures collectively safeguard data integrity and operational continuity across both the Orbiter and CubeSats.

Structural Risk – Deployment Failures

Multiple mission elements rely on successful mechanical deployment, including the Orbiter’s solar arrays and the release mechanisms for the eight CubeSats. Failure in these systems may result in total mission loss (power shortage or inactive payloads). To mitigate these structural risks, all deployable units utilize redundant spring-loaded actuators and pre-flight vibration and thermal cycling tests. The CubeSat deployment modules are equipped with dual-trigger release mechanisms, while critical deployments on the Orbiter—such as solar panels—include feedback sensors for real-time confirmation. Mechanical latching systems are also tested under Mars-relevant thermal stress profiles to ensure reliability in orbit.

EDL Navigation Risk

During the CubeSats’ atmospheric entry phase, the absence of active EDL guidance systems introduces the risk of unstable descent or off-nominal impact. To mitigate this, a robust ADCS architecture ensures precise attitude control prior to entry, while each CubeSat is designed with a carefully balanced center of mass to enhance aerodynamic stability. Extensive pre-mission trajectory and aerodynamics simulations were conducted to verify natural attitude alignment during hypersonic descent. These measures collectively reduce the likelihood of EDL failure despite the lack of active navigation or terrain-relative systems.



I. Cost Estimate and Schedule

WBS Code	Level	Line Item Name / Description	Non-Recurring (\$M)	Design & Development (\$M)	System Test Hardware (\$M)	Flight Unit (\$M)	Recurring Production (\$M)	Non-Allocated (\$M)	Operations (\$M)	FY2024 Total (\$M)
0	1	1. MOCHA Project	\$ 454.06	-	-	-	\$ 370.88	-	\$ 166.30	\$ 991.24
1.0	2	Project Management	\$ 8.00	-	-	-	\$ 2.00	-	-	\$ 10.00
2.0	2	Systems Engineering	\$ 2.50	-	-	-	\$ 2.40	-	-	\$ 4.90
3.0	2	Safety and Mission Assurance	\$ 5.00	-	-	-	\$ 3.00	-	-	\$ 8.00
4.0	2	Science / Technology	-	-	-	-	-	-	-	-
5.0	2	Flight System / Spacecraft	\$ 201.78	-	-	-	\$ 181.74	-	-	\$ 383.52
5.01	3	Orbiter	\$ 123.00	-	-	-	\$ 64.00	-	-	\$ 187.00
5.02	4	Orbiter Management	\$ 3.64	-	-	-	\$ 5.46	-	-	\$ 9.10
5.03	4	Orbiter Systems Engineering	\$ 4.55	-	-	-	\$ 6.82	-	-	\$ 11.36
5.x	4	Orbiter Product Assurance	\$ 2.91	-	-	-	\$ 4.37	-	-	\$ 7.28
4	4	Structures & Mechanisms	\$ 2.88	-	-	-	\$ 53.00	-	-	\$ 55.88
4	4	Thermal Control	\$ 5.25	-	-	-	\$ 7.00	-	-	\$ 12.25
4	4	Electrical Power & Distribution	\$ 34.69	-	-	-	\$ 21.00	-	-	\$ 55.69
4	4	GN&C	\$ 4.42	-	-	-	\$ 4.00	-	-	\$ 8.42
4	4	Communications	\$ 9.96	-	-	-	\$ 5.00	-	-	\$ 14.96
4	4	C&DH	\$ 3.20	-	-	-	\$ 0.60	-	-	\$ 3.80
6.0	3	CubeSat 1 (Cosmos)	\$ 1.23	-	-	-	\$ 2.33	-	-	\$ 3.55
4	4	Cosmos Management	\$ 0.07	-	-	-	\$ 0.11	-	-	\$ 0.18
4	4	Cosmos Systems Engineering	\$ 0.16	-	-	-	\$ 0.24	-	-	\$ 0.40
4	4	Cosmos Product Assurance	\$ 0.08	-	-	-	\$ 0.12	-	-	\$ 0.20
6.10	4	Structures & Mechanisms	\$ 0.20	-	-	-	\$ 0.30	-	-	\$ 0.50
4	4	Thermal Control	\$ 0.07	-	-	-	\$ 0.04	-	-	\$ 0.10
4	4	Electrical Power & Distribution	\$ 0.17	-	-	-	\$ 0.20	-	-	\$ 0.37
4	4	GN&C	\$ 0.09	-	-	-	\$ 0.13	-	-	\$ 0.22
4	4	Communications	\$ 0.23	-	-	-	\$ 0.50	-	-	\$ 0.73
4	4	C&DH	\$ 0.16	-	-	-	\$ 0.70	-	-	\$ 0.86
7.0	3	Daelion CubeSats	\$ 2.42	-	-	-	\$ 2.92	-	-	\$ 5.34
4	4	Daelion Management	\$ 0.22	-	-	-	\$ 0.33	-	-	\$ 0.54
4	4	Daelion Systems Engineering	\$ 0.35	-	-	-	\$ 0.53	-	-	\$ 0.88
4	4	Daelion Product Assurance	\$ 0.20	-	-	-	\$ 0.30	-	-	\$ 0.50
4	4	Structures & Mechanisms	\$ 0.30	-	-	-	\$ 0.60	-	-	\$ 0.90
4	4	Thermal Control	\$ 0.05	-	-	-	\$ 0.03	-	-	\$ 0.08
4	4	Electrical Power & Distribution	\$ 0.89	-	-	-	\$ 0.70	-	-	\$ 1.59
4	4	GN&C	\$ 0.09	-	-	-	\$ 0.14	-	-	\$ 0.23
4	4	Communications	\$ 0.16	-	-	-	\$ 0.10	-	-	\$ 0.26
4	4	C&DH	\$ 0.16	-	-	-	\$ 0.20	-	-	\$ 0.36
8.0	2	Mission Operations System (MOS)	\$ 20.00	-	-	-	-	-	\$ 16.30	\$ 36.30
9.0	2	Launch Vehicle / Services	-	-	-	-	-	-	\$ 150.00	\$ 150.00
10.0	2	Ground System(s)	\$ 15.00	-	-	-	-	-	-	\$ 15.00
11.0	2	System Integration, Assembly, Test & Checkout	-	-	-	-	-	-	-	-
12	2	Education & Outreach	-	-	-	-	-	-	-	-
										Total Reserves \$ 991.24

Figure 28. Cost Budget

A detailed cost estimation was conducted based on a structured Work Breakdown Structure (WBS), separating non-recurring, recurring production, and operations-related expenditures. The total estimated cost amounts to **\$991.24 million**, with the majority of the budget allocated to subsystem development (\$454.06M) and recurring unit production (\$370.88M). Major cost centers include the orbiter (\$383.25M), which incorporates structural, thermal, power, and communication systems, as well as two distinct CubeSat configurations: Cosmos and Daelion. Launch services were modeled at \$150M, assuming a Falcon Heavy-class vehicle. Mission Operations System (MOS) and Ground Systems contributed \$36.3M and \$15M respectively. Each subsystem was individually itemized, allowing traceability and alignment between technical architecture and financial planning. This breakdown enabled clear cost attribution across flight hardware, systems engineering, integration, and operational phases. Remaining money will be used for extended mission.

J. Compliance Matrix

Table 38. Compliance Table

ID	Requirement Description	Explanation	Complies	Section
REQ-RFP-01	Design an integrated mission of one or more exploration assets to Mars vicinity with the primary objective to accurately characterize the atmospheric composition, detailed geographic survey, and/or determine the potential subsurface resources that may exist on Mars. (address at least one of these primary objectives: REQ-RFP-01a/b/c)	MOCHA's constellation of one main orbiter and eight 6U CubeSats, designed to carry out coordinated atmospheric, topographic, and resource-mapping investigations through four tailored science investigations.	Yes	Executive Summary (pg. 8-13)
REQ-RFP-01a	Characterization of the atmospheric composition and detailed density profile will provide mission planners the necessary data to plan and design the entry, descent, and landing system to support human exploration.	The EMCS infrared sounder, MARLI aerosol-wind lidar, and Daelion/Cosmos CubeSat in-situ sensors will profile atmospheric composition and density.	Yes	F.2 Science Instruments (pg. 28-30)
REQ-RFP-01b	Detailed geographic survey, including terrain and elevation profile of the entire Martian surface will provide mission planners the ability to pinpoint potential landing location and traverse paths for each mission to maximize the potential to achieve exploration objectives.	The LOLA laser altimeter will map global terrain and elevation with the required accuracy for future EDL planning.	Yes	F.2 Science Instruments (pg. 29-31)
REQ-RFP-01c	Investigation, identification, and quantification of potential surface and subsurface resources will enable mission planners to determine the potential of utilizing such resources in support of the human exploration activities.	The MAJIS imaging spectrometer will detect and quantify surface and subsurface mineralogical resources.	Yes	F.2 Science Instruments (pg. 30-31)
REQ-RFP-02	Provide data on at least one primary objective area with $\geq 75\%$ coverage of the entire Mars globe at the conclusion of the primary mission phase.	EMCS and MAJIS makes $\geq 75\%$ coverage for two different primary objectives.	Yes	F.2 Science Instruments (pg. 31) E.3 Science Orbit Selection (21)
REQ-RFP-03	Perform benefit-risk-cost trade studies across mission architectures (including single vs. multiple assets), launch vehicles, instruments, orbital mechanics, and subsystem designs, prioritizing flight-proven or NASA-developing technologies.	Architecture, launch-vehicle, instrument, orbital-mechanics, and subsystem trades quantify benefit, risk, and cost using heritage technologies.	Yes	D & E Vehicle Overview & Trades & Trajectory Analysis (20-24)
REQ-RFP-04	Perform mission analysis to evaluate the flight profile for the asset(s) and describe the mission profile for observation/measurement and to show how the mission provides adequate coverage.	Trajectory analysis covers cruise transfer, Mars insertion, and science orbits that satisfy the coverage and timing requirements.	Yes	E Mission & Trajectory Analysis (21-24)

REQ-RFP-05	Discuss selection of subsystem components and the values of each selection, and how the design requirements or scientific objectives drove the selection of the subsystem.	Selections of structures, propulsion, ADCS, power, communications, and thermal subsystems are justified by mass/power budgets, heritage, and linkage to the science objectives.	Yes	F Mars Orbiter Vehicle (25–56)
REQ-RFP-06	Discuss the instruments selected to address the primary objectives, and the data collection, analysis, and transmission process to address those objectives.	Each asset’s instrument section details the data path—from raw measurement through onboard processing and storage to DSN downlink—across both the orbiter and CubeSats..	Yes	F.4 Communications and Data Handling (47–57)
REQ-RFP-07	The cost for the mission and capability development in support of its activities—including development, hardware, launch, and operations through the primary phase—shall not exceed \$1.0 Billion US Dollar (in FY24).	The total mission cost is estimated at \$991.24 million (FY 2024 USD).	Yes	I Cost Estimate & Schedule (82)
REQ-RFP-08	The mission should complete deployment and primary data gathering activities no later than December 31, 2033, with the system designed to operate into the late 2030s (though operation cost past the primary mission phase will be outside the scope of this RFP).	The MOCHA mission is scheduled to launch on January 16, 2029, and science operations ending in December 2033, meeting the RFP deadline.	Yes	E Trajectory Trades (23–25)

L. APPENDIX

Appendix A: Atmospheric Entry Trajectory and Thermal Analysis Methodology

This appendix describes the methodology and fundamental formulations used to calculate the trajectory behavior, total heating, and flight duration of our Cosmos and Daelion CubeSats, during its entry into the Martian atmosphere. To ensure the passive aero-dynamic stability of our satellite, its design aims to position the center of gravity (CG) at the front of the vehicle and the center of pressure (CP) at the rear. This design approach provides natural stability to the vehicle during atmospheric entry, helping to maintain a near-zero angle of attack and supporting the assumption of a constant reference area for drag calculations. It is known that our satellite has a specific flight path angle (FPA, γ) as it descends from its extra-atmospheric orbit towards Mars (e.g., in the phase from approximately 180 km to 120 km). However, in this analysis, starting from the atmospheric entry interface, considered at an altitude of 120 km, calculations are initiated with a simplified "Zero Angle of Attack" ($\alpha = 0$) and thus an initial flight path angle $\gamma_0 = 0^\circ$ assumption. With this approach, the calculations are performed using a 3-Degrees-of-Freedom (3-DOF) trajectory simulation code developed in the Python programming language, in accordance with the formulas presented in "Chapter 9: Zero Angle of Attack Reentry" of P. Gallais's book "Atmospheric Re-Entry Vehicle Mechanics" [57].

A.1 Fundamental Assumptions and Approaches

The fundamental assumptions considered in the analysis are as follows:

- **Zero Angle of Attack ($\alpha = 0$) and Initial Flight Path Angle (γ_0):** It is assumed that our satellite has a symmetrical structure and, thanks to its passive aero-dynamic stability, the angle of attack is negligible ($\alpha \approx 0$) and the initial flight path angle is $\gamma_0 = 0^\circ$ from the atmospheric entry interface at an altitude of 120 km. This forms the basis for the "Zero Angle of Attack Reentry" scenario presented by Gallais [57].
- **Atmosphere Model:** An exponential density profile has been used for the Martian atmosphere. The atmospheric scale height (H_R) for Mars is assumed to be approximately 11.1 km (this value is based on average values found in Mars atmosphere models, e.g., NASA TM-2007-214763, "Guide to Mars Standard Atmosphere Models" [57]).
- **Trajectory Dynamics:** In our Python code, the full 3-DOF equations of motion, including the effect of gravity and a time-varying flight path angle, are numerically integrated.
- **Basic Vehicle Parameters and Approximations:** The basic vehicle parameters used in the analysis and the assumptions made regarding these parameters are as follows:
 - Mass (m): 11 kg (Constant)
 - Reference Area (S_{ref}): 0.02 m² (Constant, frontal area suitable for passive stability)
 - Lift Coefficient (C_L): 0 (Dimensionless, Constant)

- Drag Coefficient (C_D): 2.2 (Dimensionless, Approximate Value)
- Vehicle Nose Radius (R_N): 0.05 m (Approximate Value, for Worst-Case Heating Scenario)

A.2 Fundamental Formulations Used

A.2.1 Atmospheric Density (ρ)

The density of the Martian atmosphere at an altitude z is calculated using the following exponential model:

$$\rho(z) = \rho_s e^{-z/H_r}$$

Where:

- ρ_s : Atmospheric density at the surface of Mars (or at a reference altitude) (kg/m³).
- H_r : Atmospheric scale height (for Mars $\approx 11.1 \times 10^3$ m, [58]).

A.1.1 Equations of Motion (3-DOF)

The trajectory of our satellite is solved by numerical integration of the following system of three-degrees-of-freedom equations of motion using the Runge-Kutta 4th order method:

$$\begin{aligned} \frac{dV}{dt} &= -\frac{D}{m} - g \sin(\gamma) \\ \frac{d\gamma}{dt} &= \frac{1}{V} \left(\frac{L}{m} - (g - \frac{V^2}{R_p + h}) \cos(\gamma) \right) \\ \frac{dh}{dt} &= V \sin(\gamma) \\ \frac{ds}{dt} &= \frac{R_p}{R_p + h} V \cos(\gamma) \end{aligned}$$

Where V is velocity, γ is flight path angle, h is altitude, s is downrange distance, D is drag force, L is lift force (in our case $L = 0$ as $C_L = 0$), m is satellite mass, g is local gravitational acceleration, and R_p is the radius of Mars.

A.1.1 Aerodynamic Forces

The drag force (D) is calculated as follows:

$$D = \frac{1}{2} \rho V^2 S_{ref} C_D$$

Where S_{ref} is the reference area of the vehicle and C_D is the drag coefficient. The values of m , S_{ref} , C_D , C_L and other vehicle parameters used are given in Table A.1.

A.1.1 Stagnation Point Convective Heat Flux (Φ_c)

The convective heat flux at the stagnation point on the nose of our satellite during atmospheric entry is calculated using the correlation proposed by Sutton and Graves [57].

$$\Phi_c = C_{Mars} \sqrt{\frac{\rho}{R_N}} V^3 \quad [W/m^2]$$

Where:

- R_N : Nose radius of our satellite (m).
- C_{Mars} : Coefficient for the Martian atmosphere (%95 CO₂)

$$C_{Mars} = 1.89 \times 10^{-4} \quad [kg^{1/2} \cdot m^{-1}]$$

A.1 Simulation Results

The simulation code developed in Python was run using the methodology described above and the parameters given in Table A.1 to analyze the Mars atmospheric entry of our satellite. The main results obtained are summarized below, with detailed graphical representations provided in Figures A.1 through A.3.

The simulation starts at an altitude of 120 km with an initial velocity of 3.49 km/s and a flight path angle of 0 degrees. The vehicle gradually descends through the Martian atmosphere.

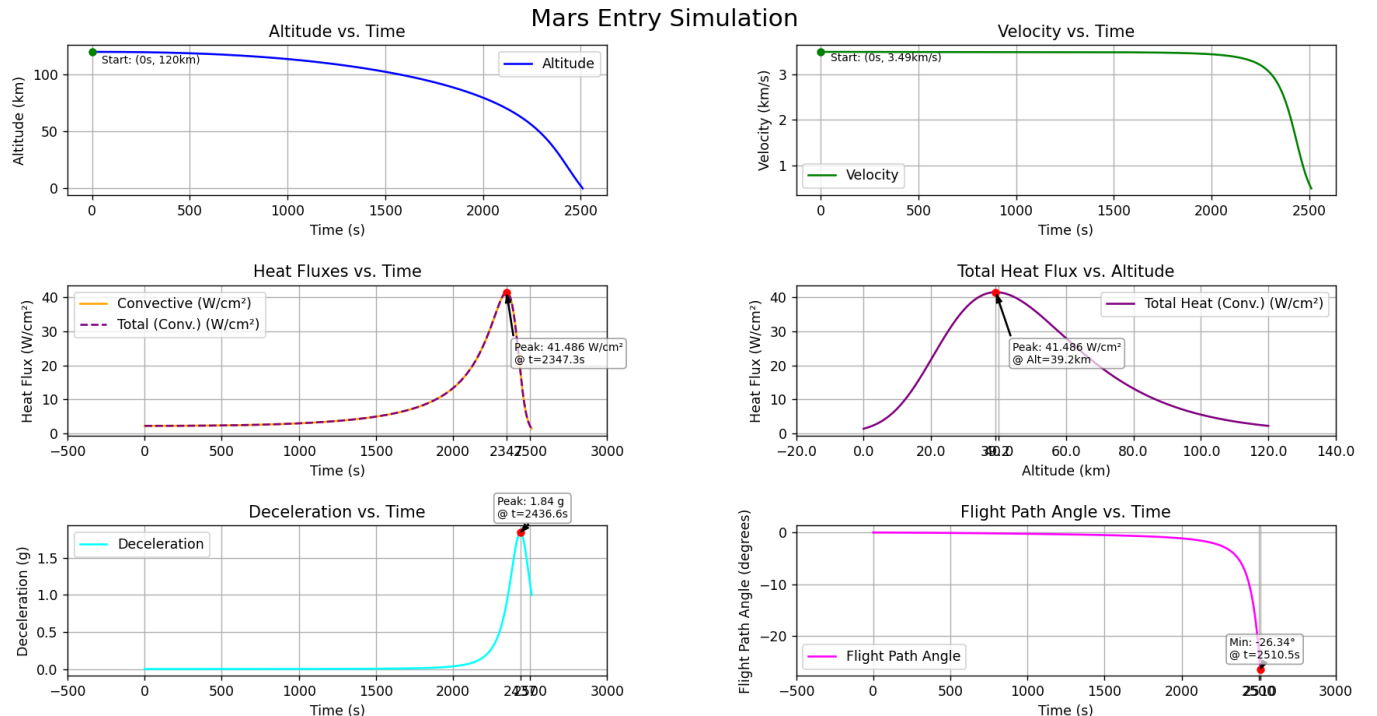


Figure 290. Mars Entry Simulation for CubeSats

Appendix A: Mission Maneuvers Calculations

All orbital mechanics formulas used in this appendix are based on standard principles found in Orbital Mechanics for Engineering Students Howard D. Curtis [59].

Interplanetary Transfer Calculations

This section presents the fundamental calculation principles and relevant formulas for the interplanetary transfer conducted from Earth to Mars. Interplanetary trajectories are typically modeled using the "Patched Conics" approach. In this approach, the spacecraft's trajectory is divided into three main segments: escape from the sphere of influence of the departure planet (hyperbolic), the Sun-centered transfer orbit (elliptical), and entry into the sphere of influence of the arrival planet (hyperbolic). The formulas you provided are particularly related to the arrival phase.

Fundamental Formulas Used (Interplanetary Transfer)

Below are listed some critical formulas used for calculations during the fundamental phases of the interplanetary transfer. Transfer orbit parameters (e.g., semi-major axis for a Hohmann transfer) depend on the distances of the departure and arrival planets from the Sun ($r_{\text{Departure}}$, r_{Arrival}) and the Sun's gravitational parameter (μ_{Sun}).

$$\rho(z) = \rho_s \cdot e - zHR$$

$$v_{\text{Sun}} = \sqrt{\mu_{\text{Sun}} \left(\frac{2}{r_{\text{Sun}}} - \frac{1}{a_{\text{Transfer}}} \right)} \quad (\text{Sun-Centered Velocity})$$

$$v_{\text{Arrival Planet Orbit}} = \sqrt{\mu_{\text{Sun}} / r_{\text{Arrival}}} \quad (\text{Arrival Planet Velocity})$$

$$v_{\infty, \text{Arrival}} = |v_{\text{Transfer, Arrival}} - v_{\text{Arrival Planet Orbit}}| \quad (\text{Arrival } v_{\infty})$$

$$v_{\text{Periareion}} = \sqrt{v_{\infty, \text{Arrival}}^2 + \frac{2\mu_{\text{Arrival}}}{r_{\text{Periareion}}}} \quad (\text{Periareion Velocity, Around Arrival Planet})$$

Here a Transfer is the semi-major axis of the Sun-centered transfer orbit. For simple transfers like the Hohmann transfer,

$a_{\text{Transfer}} = \frac{r_{\text{Departure}} + r_{\text{Arrival}}}{2}$ is used. r_{Sun} is the instantaneous distance of the vehicle from the Sun. The results of these calculations directly influence the cost of the capture and orbit adjustment maneuvers, and all maneuver details are summarized in a consolidated table under Table 39.

Mars Capture Maneuver Calculations

This appendix details the calculation methods and formulas used for Mars capture and orbit adjustment maneuvers. The capture maneuver is modeled by simulating continuous thrust with time steps, instead of an impulsive velocity change. Spacecraft mass is dynamically updated during thrust. This approach reflects a method similar to real missions that perform long-duration orbit insertion maneuvers, such as MAVEN (36-minute orbit insertion burn, 1321 Newton thrust system)[60]. The calculation of the resulting orbit, achieved through a 30-minute burn with our 1700 Newton thrust system, was performed using the fundamental formulas and numerical integration method specified below, implemented in our Python code.

Fundamental Formulas Used (Capture Simulation)

Below are listed the fundamental formulas used for calculating orbit dynamics, thrust effect, orbit elements, and the initial state in the capture simulation.

$\mu = GM$	(Gravitational Parameter)
$\dot{m} = \frac{F_T}{I_{sp}g_0}$	(Mass Flow Rate)
$m(t) = m_{initial} - \dot{m}t_{burn}$	(Instantaneous Mass)
$a_t = \frac{F_T}{m(t)}$	(Thrust Acceleration)
$\ddot{r} = -\frac{\mu}{r^3}r + a_t$	(Equation of Motion)
$y_{n+1} = y_n + \frac{\Delta t}{6}(k_1 + 2k_2 + 2k_3 + k_4)$	(RK4 Step)
$h = r \times v$	(Specific Angular Momentum)
$\mathcal{E} = \frac{v^2}{2} - \frac{\mu}{r}$	(Specific Energy)
$e = \left \frac{(v \times h)}{\mu} - \frac{r}{r} \right $	(Eccentricity)
$a = -\frac{\mu}{2\mathcal{E}}$	(Semi-major Axis)
$r_{p,a} = a(1 \mp e)$	(Apsis Distances)
$(r_0, v_0) = f(\text{Hyperbolic Parameters})$	(Initial State Vectors)

Post-Capture Orbit Adjustment Maneuver Calculations

Post-capture maneuvers aim to bring the vehicle to its final circular orbit. These maneuvers (Apoareion lowering, inclination change, circularization) are modeled as simplified, segmented burns based on classical orbit mechanics formulas. Burns were segmented with certain maximum durations to minimize orbit degradation and ensure return to the optimal orbit point (periareion or apoareion), using waiting periods (orbital periods) in between.

Fundamental Formulas Used (Post-Capture Maneuvers)

Below are listed the fundamental formulas used for planning and calculating the costs (Delta-V, fuel, duration) of these maneuvers.

$$r = \text{altitude} + R_{\text{planet}} \quad (\text{Radius}) \quad (17)$$

$$a = (r_p + r_a)/2 \quad (\text{Semi-major Axis}) \quad (18)$$

$$e = (r_a - r_p)/(r_a + rp) \quad (\text{Eccentricity, for } r_a \neq r_p) \quad (19)$$

$$T = 2\pi\sqrt{a^3/\mu} \quad (\text{Orbital Period}) \quad (20)$$

$$v = \sqrt{\mu \left(\frac{2}{r} - \frac{1}{a} \right)} \quad (\text{Vis-Viva Equation, Velocity}) \quad (21)$$

$$v_{\text{circular}} = \sqrt{\mu/r} \quad (\text{Circular Orbit Velocity}) \quad (22)$$

$$\Delta V_{\text{apsis change}} = |v_{\text{current}} - v_{\text{target}}| \quad (\text{Velocity Change at Apsis}) \quad (23)$$

$$\Delta V_{\text{inclination change}} = 2v \sin \left(\frac{\Delta i}{2} \right) \quad (\text{Plane Change}) \quad (24)$$

$$m_{\text{final}} = m_{\text{initial}} / \exp \left(\frac{\Delta V}{I_{sp}g_0} \right) \quad (\text{Tsiolkovsky Rocket Equation}) \quad (25)$$

$$\text{Fuel} = m_{\text{initial}} - m_{\text{final}} \quad (26)$$

$$t_{\text{burn, total}} = \text{Fuel}/\dot{m} \quad (\text{Total Burn Time}) \quad (27)$$

$$\text{Maneuver Duration} = (\text{Number of Burns} - 1) \times T_{\text{waiting}} + t_{\text{burn, total}} \quad (\text{Total Maneuver Duration}) \quad (28)$$

Initial/final orbit parameters, ΔV values, fuel consumption, and durations for all capture and orbit adjustment maneuvers are summarized in a detailed table under Table-39 Mission Maneuvers Calculations.

Table 39. Mission Maneuvers Calculations

	Initial Mass	Initial Orbit	Target Orbit	Burn Direction and Time	Details	Final State
Mars Orbit Insertion	Wet mass =4597.606397 kg	H _p = 400 km V _p =5.4423 km/sec i = 30.35	H _a =180000 km H _p =300 km e=~0.996672 i=30.35	Retrograde at periareion Time= ~1800 sec	Total delta-V = 772 m/s Total number of burn = 1 time Used propellant mass= 1000.3144 kg	Wet mass=3597.2920 kg Time = Arrival
Apoareion Change	Wet mass =3597.2920 kg	H _a =180000 km H _p =300 km e=~0.996672 i=30.35	H _a =90000 km H _p =300 km e= ~0.993355 i=30.35	Retrograde at periareion Burn time = ~91.30 s	Total maneuver time= 10 days Total number of burn = 1 time Total delta-V = 44.73 m/s Used propellant =50.7552 kg	Wet mass=3546.5889 kg Time= Arrival +10 days
Inclination Change	Wet mass =3546.5889 kg	H _a =90000 km H _p =300 km e= ~0.993355 i=30.35	H _a =90000 km H _p =300 km e= ~0.993355 i=77	Perpendicular to the orbiter's current velocity vector at apoareion Burn time per period = ~20 s	Total maneuver time= 56.382days Total number of burn = 15 times Total delta-V = 153.49 m/s Used propellant: 168.7784 kg	Wet mass=3377.8105 kg Total maneuver time= 56.382 days Time= Arrival +67 days
Circularization phaseA	Wet mass =3377.8105 kg	H _a =90000 km H _p =300 km e= ~0.993355 i=77	H _a =1000 km H _p =300 km e= ~0.538462 i=77	Retrograde at periareion Burn time per period= ~200 sec	Total maneuver time=33.849 days Total number of burn = 10 times Total delta-V =1173.31 m/s Used propellant =1050.9882 kg	Wet mass=2326.8223 kg Total maneuver time=33.849 days Time= Arrival +100 days
Circularization phaseB	Wet mass =2326.8223 kg	H _a =1000 km H _p =300 km e= ~0.538462 i=77	H _a =300 km H _p =300 km e=0 i=77	Retrograde at periareion Burn time per period =~20 sec	Total maneuver time= 1 day Total number of burn = 10 times Total delta-V =144.25 m/s Used propellant =104.2146 kg	Wet mass=2222.6077 kg Total maneuver time= 1 day Time= Arrival +101 days
Final Science Orbit For Orbiter	Wet mass =2222.6077 kg	H _a =300 km H _p =300 km e=0 i=77				

REFERENCE

- [1] American Institute of Aeronautics and Astronautics (AIAA). (2024). *2024–2025 AIAA Undergraduate Team Space Design Competition*. Retrieved May 17, 2025, from <https://aiaa.org/wp-content/uploads/2024/12/2024-25-aiaa-undergraduate-team-space-design-competition.pdf>
- [2] Elbert, B. (2008). *Introduction to Satellite Communication* (3rd ed.). Artech House.
- [3] NASA Goddard Space Flight Center. (2024). *LOLA Fact Sheet*. Retrieved May 17, 2025, from <https://science.nasa.gov/wp-content/uploads/2024/01/lola-fact-sheet.pdf>
- [4] Fonseca, R. M., Zorzano, M.-P., and Martín-Torres, J., “MARSWRF Prediction of Entry Descent Landing Profiles: Applications to Mars Exploration,” *Earth and Space Science*, Vol. 6, No. 8, 2019, pp. 1440–1459. <https://doi.org/10.1029/2019EA000575>.
- [5] Ho, C., Golshan, N., & Kliore, A. (2002, March). *Radio Wave Propagation Handbook for Communication on and Around Mars*. NASA JPL.
- [6] NASA Goddard Space Flight Center. (2024). *LOLA Fact Sheet*. Retrieved May 17, 2025, from <https://science.nasa.gov/wp-content/uploads/2024/01/lola-fact-sheet.pdf>
- [7] National Oceanic and Atmospheric Administration (NOAA). (n.d.). *Terrain Relative Navigation (TRN)*. Retrieved May 17, 2025, from <https://oceanexplorer.noaa.gov/okeanos/explorations/ex2102/features/trn/trn.html?utm>
- [8] Jet Propulsion Laboratory (JPL). (2022, June 6). *Deep Space Network Services Catalog (Rev. H, JPL D-19002)*. Retrieved May 17, 2025, from <https://deepspace.jpl.nasa.gov/files/820-100-H.pdf>
- [9] DHV Technology. (2017). *6U Solar Panel Datasheet – Julio v1 (Front and Back)*. Retrieved May 17, 2025, from <https://dhvtechnology.com/wp-content/uploads/2017/07/Datasheet-6U-Julio-v1-front-back.pdf>
- [10] DHV Technology. (n.d.). *Micro EPS Product Page*. Retrieved May 17, 2025, from <https://satsearch.co/products/dhv-technology-micro-eps>
- [11] Wertz, J. R., & Larson, W. J. (2005). *Space Mission Analysis and Design* (3rd ed.). Microcosm Press and Kluwer Academic Publishers.
- [12] Meghdadi, V. (2008, January). *BER Calculation*. University of Limoges. Retrieved from https://www.unilim.fr/pages_perso/vahid/notes/ber_awgn.pdf
- [13] Spectrolab. (2010). *XTJ Solar Cell Datasheet*. Retrieved from <https://www.spectrolab.com/DataSheets/cells/PV%20XTJ%20Cell%205-20-10.pdf?utm.com>
- [14] European Space Agency (ESA). (2016, February). *ExoMars 2016 TGO Solar Array Deployment [Video]*. Retrieved from https://www.esa.int/Topics/ExoMars_2016/TGO_Solar_Array_Deployment

from https://www.esa.int/esatv/Videos/2016/02/ExoMars_2016_TGO_solar_array_deployment

[15] AAC Clyde Space. (n.d.). *SmallSat PCDU Starbuck Mini*. Retrieved from <https://www.aac-clyde.space/what-we-do/space-products-components/pcdu/smallsat-pcdu-starbuck-mini>

[16]

<https://satcatalog.s3.amazonaws.com/components/458/SatCatalog - IMT - CubeSat On-Board Computer - Datasheet.pdf>

[17] <https://satcatalog.s3.amazonaws.com/components/396/SatCatalog - Space Micro - Proton2x-Box - Datasheet.pdf>

[18] Taylor, J., Lee, D. K., & Shambayati, S. (2006). *Mars Reconnaissance Orbiter Telecommunications*. DESCANSO Design and Performance Summary Series, Article [12] Jet Propulsion Laboratory, California Institute of Technology.

[19] L3Harris Technologies. (2024, August). *CTT-600 Software Defined Radio*. Retrieved from <https://www.l3harris.com/sites/default/files/2024-08/l3harris-ctt-600-software-defined-radio.pdf>.

[20] Mars Antennas. (2018, April). *Ultra-Wideband Antenna (MA-WO-UWB-1)*. Retrieved from <https://mars-antennas.com/wp-content/uploads/2018/04/MA-WO-UWB-1.pdf>.

[21] Space Propulsion, "Apogee Motors," [Online]. Available: <https://www.space-propulsion.com/spacecraft-propulsion/apogee-motors/>

[22] NASA Mars Exploration Program, "Mars Facts," NASA, 2023. Available: <https://science.nasa.gov/mars/facts/>.

[23] <https://satsearch.co/products/dhv-technology-micro-eps>

[24] J. Schofield, "Mars Climate and Atmosphere Studies," Mars Climate Modeling Workshop, Paris, 2011. Available: https://www-mars.lmd.jussieu.fr/paris2011/abstracts/schofield_paris2011.pdf

[25] J. Abshire, "MARLI - Mars Direct-Detection Wind and Aerosol Lidar," presented at the Mars Atmospheric Science Workshop, Paris, 2022. Available: https://www-mars.lmd.jussieu.fr/paris2022/abstracts/poster_Abshire_James_MARLI.pdf.

[26] <https://www.aac-clyde.space/wp-content/uploads/2021/11/ANT-100.pdf>

[27] <https://25796913.fs1.hubspotusercontent-eu1.net/hubfs/25796913/Anywaves-Datasheets-2024/Anywaves-S-Band-TT&C-Antenna.pdf>

[28] https://www.spacemanic.com/files/datasheet/SM-MRG-DS-0001_1.0_DataSheet.pdf

[29] https://www.skylabs.si/wp-content/uploads/2023/11/skylabs_nanolink_boost_2.pdf

[30] Finckenor, M. M., and Dooling, D., "Multilayer Insulation Material Guidelines," NASA Technical Publication NASA/TP-1999-209263, Marshall Space Flight Center, AL, Apr. 1999. Available: <https://ntrs.nasa.gov/api/citations/19990047691/downloads/19990047691.pdf>

[32] SpaceX, "Falcon User's Guide," September 2021. [Online]. Available: <https://www.spacex.com/media/falcon-users-guide-2021-09.pdf>. [Accessed 29 November 2023].

[33] United Launch Alliance. (2010). *Atlas V launch services user's guide*. Retrieved from https://www.ulalaunch.com/docs/default-source/rockets/atlasvusersguide2010a.pdf?sfvrsn=f84bb59e_2

[34] ArianeGroup. (2021, March). *Ariane 6 user's manual* (Issue 2, Revision 0). Retrieved from https://ariane.group/app/uploads/sites/4/2024/10/Mua-6_Issue-2_Revision-0_March-2021.pdf

[35] China Great Wall Industry Corporation. (n.d.). *LM-5*, from <https://www.cgwic.com/Launchservice/LM5.html>

- [36] Ehlmann, B. L., & Edwards, C. S. (2014). Mineralogy of the Martian surface. *Annual Review of Earth and Planetary Sciences*, 42(1), 291–315. <https://doi.org/10.1146/annurev-earth-060313-055024>
- [37] Cremons, D. R., Abshire, J. B., Sun, X., Allan, G., Riris, H., Smith, M. D., Guzewich, S., Yu, A., and Hovis, F., “Design of a Direct-Detection Wind and Aerosol Lidar for Mars Orbit,” *CEAS Space Journal*, Vol. 13, No. 3, 2021, pp. 487–506. <https://doi.org/10.1007/s12567-020-00301-z>
- [38] Piccioni, G., Bini, A., Bugetti, G., Guerri, I., Rossi, M., Tommasi, L., Langevin, Y., Filacchione, G., Tosi, F., Grassi, D., Poulet, F., Dumesnil, C., & Degalarreta, C. R. (2019). Scientific goals and technical challenges of the MAJIS imaging spectrometer for the JUICE mission. *2022 IEEE 9th International Workshop on Metrology for AeroSpace (MetroAeroSpace)*, 318–323. <https://doi.org/10.1109/metroaerospace.2019.8869566>
- [39] Poulet, F., Piccioni, G., Langevin, Y., Dumesnil, C., Tommasi, L., Carlier, V., Filacchione, G., Amoroso, M., Arondel, A., D’Aversa, E., Barbis, A., Bini, A., Bolsée, D., Bousquet, P., Caprini, C., Carter, J., Dubois, J., Condamin, M., Couturier, S., . . . Snels, M. (2024b). Moons and Jupiter Imaging Spectrometer (MAJIS) on Jupiter Icy Moons Explorer (JUICE). *Space Science Reviews*, 220(3). <https://doi.org/10.1007/s11214-024-01057-2>
- [40] Akbari, H., Nilsson, H., Stenberg Wieser, G., Eriksson, A. I., Slapak, R., Ramstad, R., . . . & Futaana, Y. (2019). Ambipolar electric field in the Martian ionosphere: MAVEN measurements. *Journal of Geophysical Research: Space Physics*, 124(6), 4518–4524. <https://doi.org/10.1029/2018JA026325>
- [41] Rafkin, S. C. R., & Barth, E. L. (2010). Environmental constraints on the survival of meteoroids during atmospheric entry: Implications for the Martian surface. *Advances in Space Research*, 45(10), 1221–1231. <https://doi.org/10.1016/j.asr.2009.11.018>
- [42] Sakraker, I., Umit, E., Scholz, T., Testani, P., Baillet, G., & Van der Haegen, V. (2015, March). *QARMAN: An atmospheric entry experiment on CubeSat platform*. Presented at the Envisat Symposium, European Space Agency. Retrieved from [https://www.researchgate.net/publication/277891078_QARMAN_AN_ATMOSPHERIC_ENTRY_EXPERIMENT_ON_CU_BESAT_PLATFORM:contentReference\[oaicite:0\]{index=0}](https://www.researchgate.net/publication/277891078_QARMAN_AN_ATMOSPHERIC_ENTRY_EXPERIMENT_ON_CU_BESAT_PLATFORM:contentReference[oaicite:0]{index=0}).
- [43] Calle, C. I., Mackey, P. J., Johansen, M. R., Hogue, M. D., Phillips, J. III, & Cox, R. E. (2016, November 3). *The electrostatic environment of Mars: Atmospheric discharges* [Presentation]. Minta Martin Seminar, Department of Aerospace Engineering, University of Maryland. NASA Kennedy Space Center.
- [44] Gallais, P. (2007). *Atmospheric Re-Entry Vehicle Mechanics*. Springer. <https://doi.org/10.1007/978-3-540-73647-9>
- [45] Justus, C. G., & Braun, R. D. (2007). *Atmospheric Environments for Entry, Descent and Landing (EDL)* (NASA/TM-2007-214763). National Aeronautics and Space Administration. <https://ntrs.nasa.gov/citations/20070032693>
- [46] Orbital Mechanics for Engineering Students Howard D. Curtis, <https://www.sciencedirect.com/book/9780080977478/orbital-mechanics-for-engineering-students>

- [47] West, T. K., IV, & Brandis, A. M. (2020). *Updated stagnation point aeroheating correlations for Mars entry* (NASA Report No. NF1676L-28692; NTRS Document ID 20200002354). National Aeronautics and Space Administration. <https://ntrs.nasa.gov/citations/20200002354>
- [48] “NASA CEARUN Program,” ,1984. URL <https://cearun.grc.nasa.gov/>.
- [49] Musielak, D. (2025). Liquid Propellant Rocket Engines. In: Introduction to Rocket Propulsion for Astronautics. Synthesis Lectures on Engineering, Science, and Technology. Springer, Cham. https://doi.org/10.1007/978-3-031-86141-3_4
- [50] <https://nssdc.gsfc.nasa.gov/planetary/factsheet/marsfact.html>